

Degradation mechanism of biomass in subcritical water and applications of the remained solid char

Wei Yang

Graduate School of Environmental and Life Science, Okayama University

March 2015

Contents

| | |
|---|----|
| Chapter 1 General Introduction | 1 |
| 1.1 Biomass..... | 1 |
| 1.1.1 Cellulose | 2 |
| 1.1.2 Hemicellulose | 2 |
| 1.1.3 Lignin..... | 4 |
| 1.2 Biomass conversion methods..... | 4 |
| 1.2.1 Prolysis..... | 4 |
| 1.2.2 Gasification | 5 |
| 1.2.3 Acid hydrolysis | 5 |
| 1.2.4 Enzymatic hydrolysis..... | 6 |
| 1.2.5 Subcritical water treatment | 6 |
| 1.3 Objective and strategy of this study..... | 9 |
| References..... | 10 |
| | |
| Chapter 2 Investigation of the degradation kinetic parameters and structure changes of microcrystalline cellulose (MCC) in subcritical water | 16 |
| 2.1 Introduction..... | 16 |
| 2.2 Materials and Methods..... | 17 |
| 2.2.1 Materials | 17 |
| 2.2.2 Subcritical water treatment | 17 |
| 2.2.3 Analysis of extracts..... | 18 |
| 2.2.4 Determination of kinetic parameters of MCC in subcritical water..... | 19 |
| 2.2.5 Characterization of MCC and MCC residue..... | 20 |
| 2.3 Results and Discussion | 21 |
| 2.3.1 Degradation of MCC in subcritical water and the concentrations of glucose and HMF in the extract..... | 21 |
| 2.3.2 Determination of kinetic parameters of MCC in subcritical water..... | 23 |
| 2.3.3 FTIR spectra of MCC and MCC residues..... | 24 |
| 2.3.4 SEM images of the MCC and MCC residues | 26 |
| 2.3.5 X-ray diffraction patterns of the MCC and MCC residues..... | 28 |
| 2.3.6 The proposed degradation mechanism of MCC in subcritical water..... | 30 |
| 2.4 Conclusions..... | 30 |
| References..... | 31 |

| | |
|---|----|
| Chapter 3 Preparation of the biodegradable foam from walnut shell treated by subcritical water | 35 |
| 3.1 Introduction..... | 35 |
| 3.2 Materials and Methods..... | 36 |
| 3.2.1 Materials | 36 |
| 3.2.2 Subcritical water treatment of walnut shell | 36 |
| 3.2.3 Analysis of the carbohydrate content in the extract..... | 36 |
| 3.2.4 Analysis of the components in the walnut shell and solid char | 36 |
| 3.2.5 Preparation of biodegradable foam..... | 38 |
| 3.2.6 Morphology of prepared foam | 38 |
| 3.2.7 Measurement of mechanical properties of prepared foam..... | 39 |
| 3.3 Results and Discussion | 39 |
| 3.3.1 Total carbohydrate content in the extract..... | 39 |
| 3.3.2 The components in walnut shells and solid char | 40 |
| 3.3.3 Optical scans and density of prepared foam | 41 |
| 3.3.4 SEM observation of prepared foam | 43 |
| 3.3.5 Mechanical properties of prepared foam | 44 |
| 3.4 Conclusions..... | 46 |
| References..... | 46 |

| | |
|---|----|
| Chapter 4 Characterization of surface properties of woody thin boards composed of commercially available lignin and cellulose: Relationship between the orientation of lignin and water repellency | 49 |
| 4.1 Introduction..... | 49 |
| 4.2. Materials and Methods..... | 50 |
| 4.2.1 Materials | 50 |
| 4.2.2 Preparation of woody thin boards by the compression molding method..... | 50 |
| 4.2.3 Measurement of contact angle | 51 |
| 4.2.4 Dielectric measurement | 51 |
| 4.2.5 ATR-FTIR..... | 51 |
| 4.2.6 X-ray diffraction measurement | 51 |
| 4.2.7 Scanning electron microscopic observation | 52 |
| 4.2.8 Atomic force microscopic observation | 52 |
| 4.2.8.1 Observation..... | 52 |
| 4.2.8.2 Estimation of surface roughness | 52 |

| | |
|---|-----------|
| 4.3 Results and Discussion | 53 |
| 4.3.1 Screening of the woody thin boards preparation using lignin/cellulose/water system.... | 53 |
| 4.3.2 Surface properties of woody thin boards | 56 |
| 4.3.2.1 Macroscopic surface properties of woody thin boards | 56 |
| 4.3.2.2 Chemical composition of the surface of woody thin boards as microscopic | |
| property | 58 |
| 4.3.2.3 X-ray diffraction (XRD) study of woody thin boards | 61 |
| 4.3.2.4 Surface state of woody thin boards..... | 63 |
| 4.3.3 Microscopic surface structure of woody thin boards..... | 65 |
| 4.3.4 Possible interpretation of water repellency, hydrophobicity and surface roughness for | |
| woody thin boards | 66 |
| 4.4 Conclusions..... | 66 |
| References..... | 66 |
| | |
| Chapter 5 Characterization of fuel properties of solid chars obtained from subcritical | |
| water treatment of various biomasses..... | 70 |
| 5.1 Introduction..... | 70 |
| 5.2 Materials and Methods..... | 71 |
| 5.2.1 Materials | 71 |
| 5.2.2 Subcritical water treatment | 71 |
| 5.2.3 Characterization of solid char | 71 |
| 5.3 Results and Discussion | 72 |
| 5.3.1 The solid char yield..... | 72 |
| 5.3.2 The components of biomasses and solid chars | 73 |
| 5.3.3 Elemental analysis of biomasses and solid chars..... | 75 |
| 5.3.4 The hydrophobicity of biomasses and solid chars | 80 |
| 5.3.5 The SEM topography of biomasses and solid chars | 80 |
| 5.4 Conclusions..... | 81 |
| References..... | 82 |
| | |
| Chapter 6 Conclusions..... | 84 |
| | |
| Acknowledgement | 86 |
| List of publications..... | 87 |

Appendix-1.....88
Appendix-2.....98
Appendix-3.....110

Chapter 1

General Introduction

1.1 Biomass

With the increasing concerns about energy security, environmental pollution and climate change, utilization of renewable energy resources has attracted more and more interest in the recent years. Solar, wind, hydro, geothermal, wave and biomass are the most important renewable energy source. Among these renewable energy sources, biomass is considered as a promising candidate to replace fossil fuels and it is also the only one that holds the potential to produce liquid and gas fuels for transportation in the near future [1]. Comparing with solar, wind and hydroelectric systems, the biomass conversion system could be set up in virtually any location where plants could be grown and it needs no energy storage system [2]. Besides, biomass is a carbon neutral fuel with the annual net CO₂ fixation of 5.6×10^{10} tons and emits less sulfur compared with the fossil fuels during combustion [3].

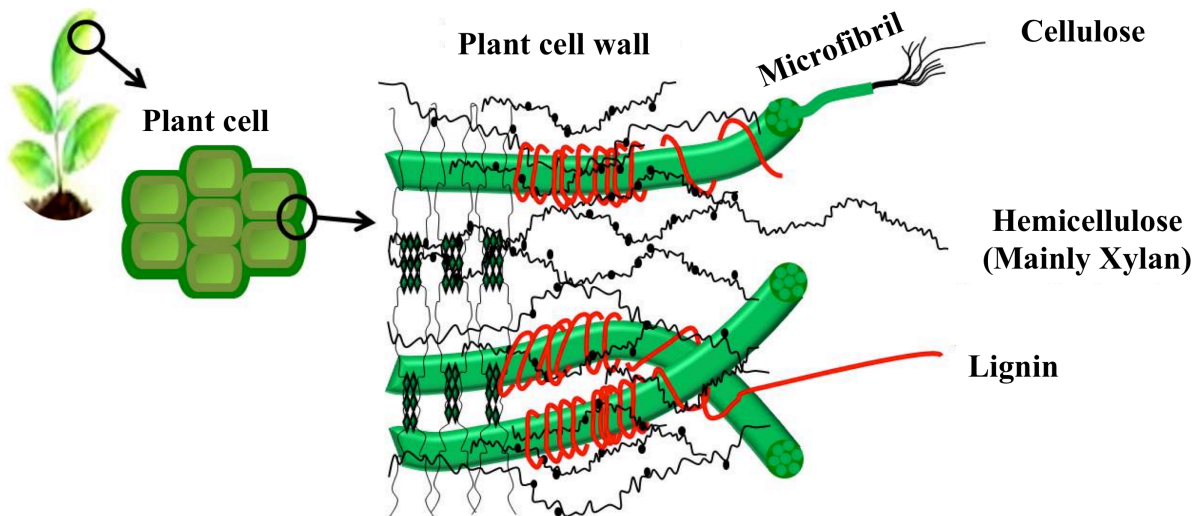


Figure 1-1. The structure of biomass (The figure is adopted from reference 5).

The annual world production of biomass by biosynthesis is estimated at 146 billion tons and only one-eighth of the total biomass produced every year could provide all the energy for human consumption [4]. As shown in Fig. 1-1, the primary components of biomass are cellulose, hemicellulose and heterogeneous phenolic polymer lignin that composed the biomass cell walls [5]. The components proportions depend on the type, the species and the source of biomass [3, 6], but the typical biomass, wood and grass plants, are roughly composed of 50% cellulose, 25% hemicellulose and 20% lignin [7].

1.1.1 Cellulose

Cellulose, with the annual production of 1.5×10^{12} tons by biosynthesis, is the most abundant natural polymer in the world [8]. Cellulose is a polysaccharide composed of linear glucan chains linked by β -1,4-glycosidic bonds with cellobiose residues as the repeating unit at different degrees of polymerization that depending on resource (Fig. 1-2). These long chains that also called elemental fibrils are grounded together to form microfibrils that bundle together to form cellulose fibers through covalent bonds, hydrogen bonds and Van der Waals forces [5]. The cellulose also appears in the forms of crystalline and amorphous that are due to the introduction of highly ordered and disordered cellulose chains into the structure of cellulose, respectively. The rigid structure and extensive hydrogen bond network make cellulose hard to be degraded and insoluble in water as well as most of the organic solvent. Cellulose could be degraded to monomeric sugars that are building-block compounds for both energy and valuable chemicals through acid hydrolysis, enzymatic degradation etc. [6, 9].

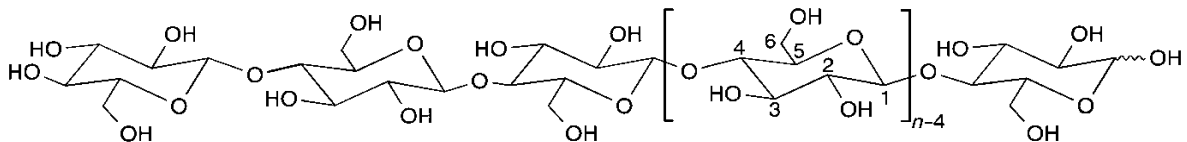


Figure 1-2. The structure of cellulose (The figure is adopted from reference 8).

1.1.2 Hemicellulose

Hemicellulose is the second most abundant polymers next to cellulose. It consists of D-xylose, D-mannose, D-galactose, D-glucose, L-arabinose and acetylated sugars that are linked together by β -1,4- and occasionally β -1,3- glycosidic bonds (Fig. 1-3) [6]. In many plants, the principle component is glucuronoxylan whereas glucomannan is predominant of softwood. Comparing with cellulose, hemicellulose has amorphous structure and branches with short lateral chains consisted of different sugars that make it easy to be hydrolyzed and have little strength. Hemicellulose bounds to the cellulose microfibrils via hydrogen bound and covalently attaches to lignin that form the highly complex structure of plant cell wall. Hemicellulose is easily hydrolyzed by dilute acid, base and myriad hemicellulose enzymes to monomeric sugars and other valuable chemicals [10, 11].

1.1.3 Lignin

Lignin that confers a rigid structure, impermeable property and resistance against microbial attack and oxidative stress on the plants is the third most abundant nature polymer next to cellulose and hemicellulose. Lignin has a complex network that is consisted of polymerization of phenyl propane units and constitutes the most abundant non-polysaccharide fraction in lignocelluloses [12]. The main monomers in lignin are *p*-coumaryl alcohol, coniferyl alcohol and sinapyl alcohol, which are joined by alkyl-aryl, alkyl-alkyl and aryl-aryl ether bonds (Fig. 1-4). Lignin offers a protection of cellulose against microbial and enzymatic degradation by embedded into cellulose. It is also able to form covalent bonds with hemicellulose. For instance, the lignin carbohydrate complexes are formed between lignin and arabinose or galactose side groups in xylans and mannans.

1.2 Biomass conversion methods

As aforementioned, biomass has many advantages compared with other renewable resources and it is a promising candidate to take place of fossil fuels in the future. However, biomass dose not seem to be suit for direct combustion with fossil fuels because the drawbacks of low caloric value, low energy density, high volatile content and high hydrophobicity make biomass defined as a low-grade fuel. Therefore, the biomass needs a pretreatment to upgrade its fuel properties or convert to other valuable chemicals, such as bio-crude and biogases that have high fuel qualities before utilization [13]. Up to now, various methods including pyrolysis, gasification, acid hydrolysis, enzymatic hydrolysis and subcritical water treatment etc., have been used to upgrade the fuel quantities of biomass or convert biomass and their main components to bio-fuels as well as valuable chemicals. [14-29].

1.2.1 Pyrolysis

Pyrolysis is a type of thermolysis process that converts biomass into liquid (termed bio-oil or bio-crude), solid and gaseous fractions by heating the biomass to the temperature around 500 °C in an inert atmosphere [30]. The solid charcoal is favored if pyrolysis is carried out at the lower temperature and longer residence time. In contrast, higher gas yield could be obtained at higher temperature and longer residence time, whereas liquids are preferred in the conditions of moderate temperature and short residence time [31]. Pyrolysis is classified into slow, mild and fast pyrolysis according to the heating rate during pyrolysis. Among these three pyrolysis processes, fast pyrolysis can directly convert biomass to bio-crude with the yield as high as 80% that could be applied as bio-fuel [32]. The bio-crude was of great interest

because the bio-crude could be further used for energy, chemicals or as energy carrier that can be stored and transported. The process had the advantages of improved efficiency, environmental acceptability and virtually any type of biomass. However, the biomass needed a pre-dry process before pyrolysis and the liquid products had poor thermal stability, high corrosion to the equipment. Besides, fuel properties of bio-crude should be improved before application by the means of lowering the oxygen content, hydrogenation and catalytic cracking.

1.2.2 Gasification

Gasification is a process that converts biomass into combustible gas mixture (synthesis gas or syngas) under the controlled conditions of limited amount of oxygen at the temperature higher than 700 °C [33, 34]. The gas mixture can be combusted directly, or used as a fuel for gas engines and gas turbines or as a feedstock for chemicals production [30]. The gas mixture is mainly composed of hydrogen, carbon monoxide, light hydrocarbons, non-combustible gas (carbon dioxide, water vapour and nitrogen) and some of impurities, such as char, ash and soot [35]. The components of the gas mixture significantly depended on the operating conditions, such as temperature and operating pressure, type of feed store and the fuel moisture content. Besides, the gas quality was affected by the type of gasifier, residence time and heating rate [36]. Gasification is considered as one of the most efficient biomass conversion processes and one of the best alternatives for reusing waste solids [37], but it also has some disadvantages due to the type of gasifier. For instance, the fixed bed and moving bed gasifiers generated large amount of tar and char that were due to the low and non-uniform heat and mass transfer between solid biomass and gasifying agent with the reactor [38, 39]. Besides, the gasification needed high-energy input and the biomass needed a pre-dry process before gasification.

1.2.3 Acid hydrolysis

Acid hydrolysis that is a traditional biomass treatment process and it can be classified into concentrated acid hydrolysis and diluted acid hydrolysis [40]. The concentrated acid process for production of fermentable sugars has a long history. The ability to dissolve and hydrolyze native cellulose in cotton by concentrated sulfuric acid was reported in the literature as early as 1883 [41]. The concentrated acids, such as H₂SO₄ and HCl, were always employed to disrupt the hydrogen bonds between cellulose chains and converted the crystalline structures in cellulose to the amorphous structure, forming a homogenous gelatin with the acid. The gelatin was then diluted with water at modest temperatures where the

decrystallized cellulose could be completely and rapidly hydrolyzed to glucose with little degradation of glucose. This process can achieve the theoretical glucose yield of 90%, but the concentrated acids employed were toxic and hazardous and had strong corrosiveness to the reactor. The corrosiveness made the process very expensive [42]. Besides, a large amount of waste stream of gypsum was generated during neutralization of the acid with limestone.

Diluted acid hydrolysis that was much economically feasible than concentrated acid hydrolysis has been well developed for the pretreatment of biomass and it significantly elevated the efficiency of the enzymatic hydrolysis step. This process was always carried out at the acid concentration of 2%~5% with high temperature (160 °C) and pressure (~10 atm) in order to improve the glucose yield [43, 44]. The main advantages of this process were that the acid recovery was not required and that there was no significant loss of acid. However, it also has many drawbacks, such as requirement of corrosion resistance equipment, low concentration of sugar, formation of inhibitory by-product and requirement of a pH neutralization process.

1.2.4 Enzymatic hydrolysis

Enzymatic hydrolysis is one of the unit operations on the biomass conversion process that utilization of enzymes or microorganisms to depolymerize biomass to produce reducing sugars or other value-added chemicals [45]. The enzymes used in this process have highly specific and the process is always conducted at mild conditions with the pH of 4.8 and temperature range from 45 to 50 °C [46]. Fungi, known as good source for enzymes, are the well-know microorganisms having the capability to degrade biomass. For instance, *Trichoderma reesei* produces two *cellobiohydrolases*, five *endoglucanases* and two β -glucosidases. Several of them have shown the synergetic manner by either hydrolyzing different ends of the cellulose chain or exhibiting different affinities for different sites of attack [42]. The main advantage of this process is that it does not create a corrosion problem to the equipment compared with that of acid hydrolysis [47]. However, this process requires a long retention time for hydrolysis and biomass pretreatment, enzyme production as well as enzyme recovery makes this process economically unfeasible [48]. Besides, the final products of enzymatic hydrolysis should be removed as soon as they are formed because they inhabited the activity of enzyme, which further leads to the low efficiency of hydrolysis process [42].

1.2.5 Subcritical water treatment

Subcritical water treatment is considered as a promising method to hydrolyze biomass and other wastes such as marine waste. Water that remains its liquid states at the temperature

range from 100 to 374 °C under pressurized conditions is called subcritical water (Fig. 1-5). Such water has two unique properties including a higher ion product and a lower relative dielectric constant compared with the water at ambient condition. For instance, when the temperature increased from ambient temperature to 250 °C, the relative dielectric constant of water decreases from 80 to nearly 27, which is similar to those of acetone and methanol at ambient temperature [49-52]. Meanwhile, the value of ion product increases to about 10^{-11} , which means that subcritical water can act as an acidic catalyst to catalyze chemical reactions, such as hydrolysis and degradation without any additional catalyst (Fig. 1-6) [52, 53]. This treatment was always conducted at the temperature higher than 150 °C with various treatment temperatures for extraction of value-added chemicals from biomass [54, 55], hydrolysis of cellulose and hemicellulose [56-58], gasification of biomass [59] and conversion of lipids (fatty acid and glycerin) and protein [60-63]. Among them, the most common application of subcritical water was to degrade biomass or its main components to obtain fermentable sugars or other chemicals such as 5-(hydroxymethyl)furfural. For instance, Winboonsirikul *et al.* had successfully extracted functional substances (e.g. carbohydrates, protein) from rice bran and found that the optimum conditions for getting maximum extract yield was at 200 °C for the treatment time of 5 min [27]. As for the main components of biomass, Sasaki *et al.* [64, 65] had detailly studied the hydrolysis of cellulose and the further degradation of the main product glucose in subcritical water. They pointed out that the main products for glucose were C3-C6 sugars, aldehydes and furans. The glucose degradation rate was higher than that from hydrolysis of cellulose at the temperature under 350 °C, whereas it was slower than that of cellulose above 350 °C. Mok and Antal found that nearly 100% of the hemicellulose in various wood and herbaceous biomass could be hydrolyzed at 230 °C for 2 min under the pressure of 34.5 MPa [66]. Sasaki *et al.* showed that the retro-aldol condensation of D-xylose was the dominant reaction during degradation of D-xylose in subcritical and supercritical water and the contribution of dehydration was small in subcritical water. The main degradation products were glycolaldehyde, glyceraldehyde and dihydroxyacetone [67]. Lignin was difficult to be hydrolyzed in subcritical water and the main products were catechol, phenols, cresols and methyl dehydroabietate when it was hydrolyzed at the temperature range from 350 °C to 400 °C [68, 69]. The hydrolysis products of cellulose, hemicellulose and lignin were different during subcritical water treatment, but the basic reaction mechanisms can be described as follows [70, 71]:

- (1) Depolymerization of the biomass.
- (2) Cleavage, dehydration, decarboxylation and deamination of biomass monomers.
- (3) Recombination of reactive fragments.

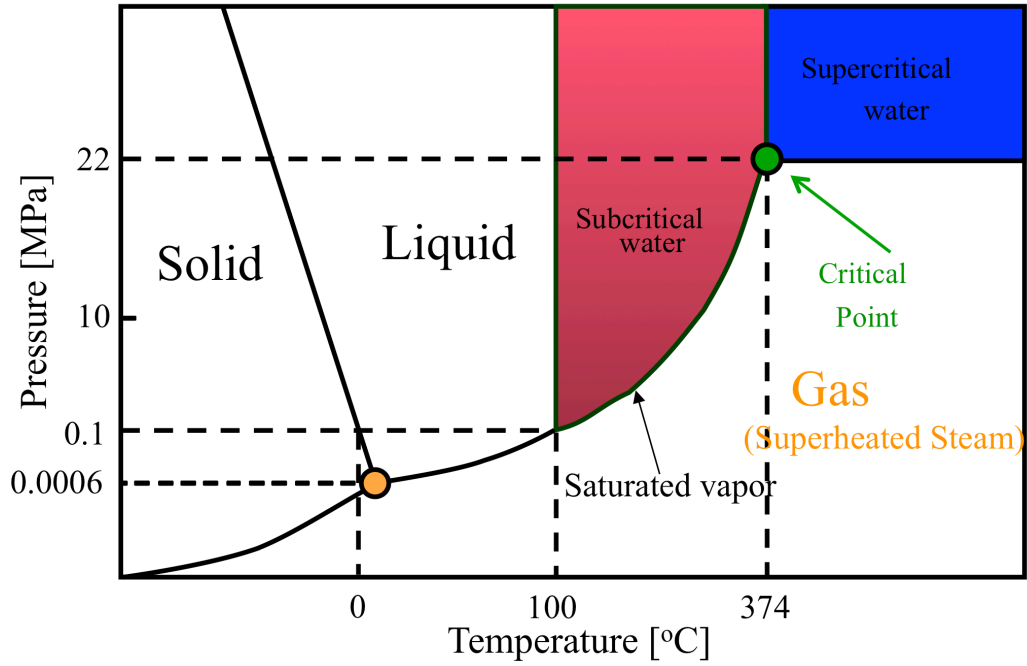


Figure 1-5. The phase of water under various temperatures and pressures.

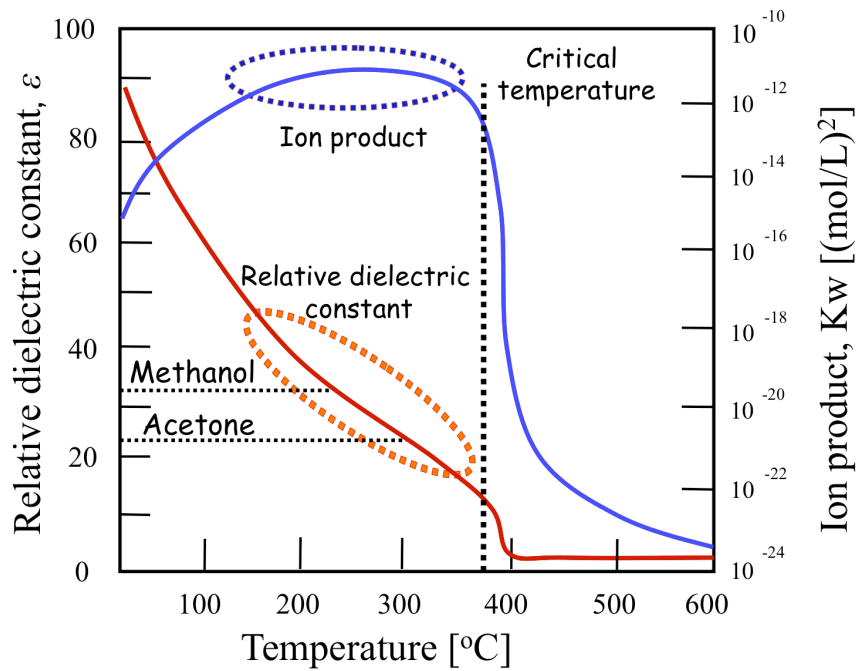


Figure 1-6. Physical properties of subcritical water at different temperatures and pressures.

1.3 Objective and strategy of this study

Hydrolysis of biomass by subcritical water has attracted more and more attention in recent years, because this treatment only uses water as a solvent that results low impact to the environment. Additionally, subcritical water also shows some advantages compared with traditional methods aforementioned: (1) there is no necessary for pre-drying of biomass since water was used as the solvent; (2) this process is always employed at lower temperature than those of pyrolysis, gasification and flash carbonization [72] and (3) the generated gases, such as CO_2 , NO_x and SO_x are dissolving in water, forming the corresponding acids and/or salts that make further treatment for air pollution possibly unnecessary [73]. The main products obtained after subcritical water treatment of biomass were liquid extract and solid char. Up to now, many researches have been done about subcritical water liquefaction of biomass to obtain valuable chemicals, such as carbohydrates, protein and phenolic compounds [27-30, 70, 74, 75]. However, the degradation mechanism of biomass in subcritical water was still

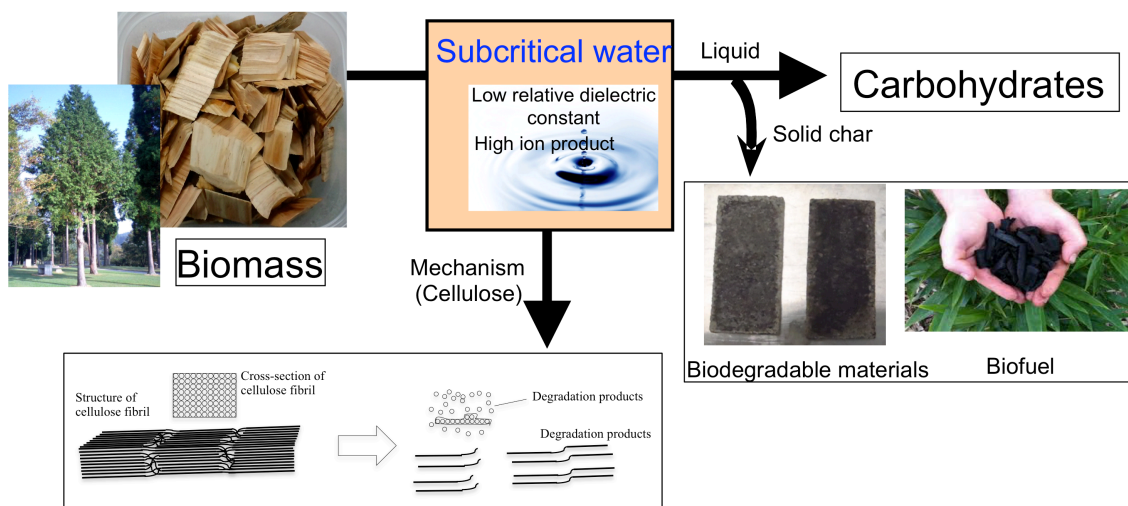


Figure 1-7. The research strategy of the present study.

remaining unclear, and few researchers have considered the utilization of solid char remained after subcritical water. Knowing the degradation mechanisms of biomass components would give a theoretic support for subcritical water liquefaction of biomass to obtain target products. However, it was difficult to investigate the degradation mechanisms of biomass components at the same time. Because among these three components, hemicellulose was degraded at relatively lower temperature and the hemicellulose structure was affected by biomass species (grass hemicellulose: rich in xylane; woody hemicellulose: rich in glucose, galactose and mannose) [76]; the decomposition of lignin was always carried out at near- and supercritical conditions [68, 77]; only cellulose, the most contained component in common biomass was degraded in the whole subcritical water condition. We considered that investigation of the

degradation mechanism of cellulose would be the key knowledge for understanding the biomass degradation mechanism in subcritical water. Hemicellulose and a portion of cellulose were degraded after subcritical water liquefaction of biomass. The solid char remained after subcritical water liquefaction of biomass would be rich in cellulose and lignin and it might have the potential to be applied as a new resource.

Therefore, the degradation mechanism of cellulose that served as model of biomass in subcritical water and the potential applications of solid char were considered in the present research. The research strategy is shown in Fig. 1-7. First of all, the degradation mechanism of cellulose that was one of the main components in biomass was investigated to provide a theoretical supplement for the determination of optimum conditions for obtaining the valuable chemicals in liquid extract and the solid char. Secondly, the solid char was applied to prepare biodegradable foams and woody thin board that are promising candidates for replacing of plastic products by a compression-molding method. Finally, the fuel properties of obtained solid char were characterized as the solid char could also been used as a bio-fuel. The results obtained in the present research should give a theoretic support to determine the optimum conditions for subcritical water liquefaction of biomass to gain liquid products or solid char, and stimulate the novel applications of solid char as well as effective utilization of all the products obtained from subcritical water liquefaction of biomass.

References

- [1] Neill, R., Proceeding of the international symposium on hydrogen produced from renewable energy. Honolulu, May 24-25, 1984, p. 260.
- [2] Ozcomen, D.; Ersoy-Mericboyu, A., Characterization of biochar and bio-oil samples obtained from carbonization of various biomass materials. *Renew. Energ.* 2010, 35, 1319-1324.
- [3] Pauly, M.; Keegstra, K., Cell wall carbohydrates and their modification as a resource for biofuels. *Plant J.* 2008, 54, 559-568.
- [4] Asghari, F. S.; Yoshida, H., Conversion of Japanese red pine wood (*Pinus densiflora*) into valuable chemicals under subcritical water conditions. *Carbohydr. Res.* 2010, 345, 124-131.
- [5] Tomme, P.; Warren, R. A. J.; Gilkes, N. R., Cellulose hydrolysis by bacteria and fungi. Academic Press, London, 1995, p. 1-81.
- [6] Perez, J.; Munoz-Dorado, J.; De-la-Rubia, T.; Martinez, J., Biodegradation and biological treatments of cellulose, hemicellulose and lignin: an overview. *Int. Microbiol.* 2002, 5, 53-63.
- [7] Bobleter, O., Hydrothermal degradation of polymers derived from plants. *Prog. Polym. Sci.* 1994, 19, 797-841.

- [8] Klemm, D.; Heublein, B.; Fink, H.; Bohn, A., Cellulose: Fascinating biopolymer and sustainable raw material. *Annew. Chem. Int. Ed.* 2005, *44*, 3358-3393.
- [9] Martinez, A.; Rodrigues, M. Z.; York S. W.; Preston J. F.; Ingram L. O., Use of UV absorbance to monitor furans in dilute acid hydrolysates of biomass. *Biotechno. Pro.* 2000, *16*, 637-641.
- [10] Dutta, S.; De, S.; Saha, B.; Alam, Md. I., Advances in conversion of hemicellulosic biomass to furfural and upgrading biofuels. *Catal. Sci. Technol.* 2012, *2*, 2025-2036.
- [11] Kirk, K.; Cullen, D., Enzymology and molecular genetics of wood degradation by white rot fungi. Wiley Press, New York, 1998, p. 273-307.
- [12] Sanchez, C., Lignocellulosic residues: Biodegradation and bioconversion by fungi. *Biotechnol. Adv.* 2009, *27*, 185-194.
- [13] Wannapeera, J.; Worasuwannarak, N., Upgrading of woody biomass by torrefaction under pressure. *J. Ana. Appl. Pyrol.*, 2012, *96*, 173-180.
- [14] Becidan, M.; Sjreberg, Ø.; Hustad, J. E., Products distribution and gas release in pyrolysis of thermally thick biomass residues samples. *J. Ana. Appl. Pyrolysis* 2007, *78*, 207-213.
- [15] Mahinpey, N.; Murugan, P.; Mani, T.; Raina, R., Analysis of bio-oil, bio-gas and bio-char from pressurized pyrolysis of wheat straw using a tubular reactor. *Energy Fuels* 2009, *23*, 2736-2742.
- [16] Tushar, M. S. H. K.; Mahinpey, N.; Murugan, P.; Mani, T., Analysis of gaseous and liquid products from pressurized pyrolysis of flax straw in a fixed bed reactor. *Ind. Eng. Chem. Res.* 2010, *49*, 4627-4632.
- [17] Mani, T.; Murugan, P.; Mahinpey, N., Pyrolysis of oat straw and the comparison of the product yield to wheat and flax straw pyrolysis. *Energy Fuels*, 2011, *25*, 2803-2807.
- [18] Christodoulou, Chr.; Grimekis, D.; Panopoulos, K. D.; Vamvuka, D.; Karellas, S.; Kakaras, E., Circulating fluidized bed gasification tests of seed cakes residues after oil extraction and comparison with wood. *Fuel* 2014, *132*, 71-81.
- [19] Kramb, J.; Konttinen, J.; Gomez-Barea, A.; Moilanen, A.; Umeki, K., Modeling biomass char gasification kinetics for improving prediction of carbon conversion in a fluidized bed gasifier. *Fuel* 2014, *132*, 107-115.
- [20] At Naw, S. M.; Sulaiman, S. A.; Yusup, S., Syngas production from downdraft gasification of oil palm fronds. *Energy* 2013, *61*, 491-501.
- [21] Taufiq-Yap, Y. H.; Wong, P.; Marliza, T. S.; Nurul Suziana, N. M.; Tang, L. H.; Sivasangar, S., Hydrogen production from wood gasification promoted by waste eggshell catalyst. *Int. J. Energ. Res.* 2013, *37*, 1866-1871.

- [22] Danon, B.; Hongsiri, W.; Van der Aa, L.; Jong, W. de, Kinetic study on homogeneously catalyzed xylose dehydration to furfural in the presence of arabinose and glucose. *Biomass Bioenerg.* 2014, *66*, 364-370.
- [23] Zhang, H. D.; Wu, S. B., Dilute ammonia pretreatment of sugarcane bagasse followed by enzymatic hydrolysis to sugars. *Cellulose* 2014, *21*, 1327-1340.
- [24] Esteghlalian, A.; Hasimoto, A. G.; Fenske, J. J.; Penner, M. H., Modeling and optimization of the dilute-sulfuric-acid pretreatment of corn stover, poplar and switchgrass. *Bioresource Technol.* 1997, *59*, 129-136.
- [25] Lenihan, P.; Orozco, A.; O'Neill, E.; Ahmad, M. N. M.; Rooney, D. W.; Walker, G. M., Dilute acid hydrolysis of lignocellulosic biomass. *Chem. Eng. J.* 2010, *156*, 395-403.
- [26] Chen, W. S.; Chen, Y. C.; Lin, J. G., Study of chemical pretreatment and enzymatic saccharification for producing fermentable sugars from rice straw. *Bioproc. Biosyst. Eng.* 2014, *37*, 1337-1344.
- [27] Wiboonsirikui, J.; Kimura, Y.; Kanaya, Y.; Tusno, T.; Adachi, S., Production and characterization of functional substances from a by-product of rice bran oil and protein production by a compressed hot water treatment. *Biosci. Biotechnol. Biochem.* 2008, *72*, 384-392.
- [28] Liu, Z. G.; Quek, A. Hoekman, S. K.; Balasubramanian, R., Production of solid biochar fuel waster biomass by hydrothermal carbonization. *Fuel* 2013, *103*, 943-949.
- [29] Hata, S.; Wiboonsirikul, J.; Maeda, A.; Kimura, Y.; Adachi, S., Extraction of defatted rice bran by subcritical water treatment. *Biochem. Eng. J.* 2008, *40*, 44-53.
- [30] Mckendry, P., Energy production from biomass (part 2): conversion technologies. *Bioresource Technol.* 2002, *83*, 47-54.
- [31] Bridgwater, A. V., Fast pyrolysis of biomass for energy and fuels. RSC Press, UK, 2010, p. 46-187.
- [32] Czernik, S.; Bridgwater, A. V., Overview of application of biomass fast pyrolysis oils. *Energy Fuels* 2004, *18*, 590-598.
- [33] Mohammed, M. A. A.; Salmiaton, A.; Azlina, W. W.; Mohammad Amran, M. S.; Fakhrul-Razi, A.; Taufiq-Yap, Y. H., Hydrogen rich gas from oil palm biomass as a potential source of renewable energy in Malaysia. *Renew. Sustain. Energ. Rev.* 2011, *15*, 1258-1270.
- [34] Mohammed, M. A. A.; Salmiaton, A.; Azlina, W. W.; Mohammad Amran, M. S.; Fakhrul-Razi, A., Air gasification of empty fruit bunch for hydrogen-rich gas production in a fluidized-bed reactor. *Energ. Convers. Manage.* 2011, *52*, 1555-1561.
- [35] Chhiti, Y.; Kemiha, M., Thermal conversion of biomass, pyrolysis and gasification: A review. *Int. J. Eng. Sci.* 2013, *2*, 75-85.

- [36] Basu, P., Combustion and gasification in fluidized beds. CRC press Taylor and Francis group, 2006, p. 1-496.
- [37] Alauddin, Z. A. B. Z.; Lahijani, P.; Mohammadi, M.; Mohamed, A. R., Gasification of lignocellulosic biomass in fluidized beds for renewable energy development: A review. *Renew. Sust. Energ. Rev.* 2010, *14*, 2852-2862.
- [38] Xu, G.; Murakami, T.; Suda, T.; Matsuzaw, Y.; Tani, H., Two-stage dual fluidized bed gasification: its conception and application to biomass. *Fuel Process Technol.* 2009, *90*, 137-144.
- [39] Warnecke, R., Gasification of biomass: comparison of fixed bed and fluidized bed gasifier. *Biomass Bioenerg.* 2000, *18*, 489-497.
- [40] Sun, Y.; Cheng, J. Y., Hydrolysis of lignocellulosic materials for ethanol production: a review. *Bioresour. Technol.* 2002, *83*, 1-11.
- [41] Harris, E. E., Wood saccharification advances in carbohydrate chemistry. Academic Press, New York, 1949, p. 153-188.
- [42] Binod. P.; Janu, K. U.; Sindhu, R.; Pandey, A., Hydrolysis of lignocellulosic biomass for bioethanol production. Academic Press, Burlington, 2011, p. 229-250.
- [43] Broder, J. D.; Barrier, J. W.; Lee, K. P.; Bulls, M. M., Biofuels system economics. *World Resource Re.* 1995, *7*, 560-569.
- [44] Patrick Lee, K. C.; Bulls, M.; Holmes, J.; Barrier, J. W., Hybrid process for conversion of lignocellulosic materials. *Appl. Biochem. Biotechnol.* 1997, *66*, 1-23.
- [45] Modenbach, A. A.; Nokes, S. E., Enzymatic hydrolysis of biomass at high-solids loading-A review. *Biomass Bioenerg.* 2013, *56*, 526-544.
- [46] Duff, S. J. B.; Murray, W. D., Bioconversion of forest products industry waste cellulose to fuel ethanol: a review, *Bioresour. Technol.* 1996, *55*, 1-33.
- [47] Duff, S. J. B.; Murray, W. D., Bioconversion of forest products industry waste cellulose to fuel ethanol: a review. *Bioresour. Technol.* 1996, *55*, 1-33.
- [48] Iranmahboob, J.; Nadim, F.; Monemi, S., Optimizing acid-hydrolysis: a critical step for production of ethanol from mixed wood chips. *Biomass Bioenerg.* 2002, *22*, 401-404.
- [49] Clifford, T., Fundamentals of supercritical fluids. Oxford University Press, New York, 1998, p. 22-23.
- [50] Ayala, R. S.; Castro, L., Continuous subcritical water extraction as a useful tool for isolation of edible essential oils. *Food Chem.* 2001, *75*, 109-113.
- [51] Herrero, M.; Cifuentes, A.; Ibanez, E., Sub- and supercritical fluid extraction of functional ingredients from different natural sources: plants, food by-products, algae and microalgae. *Food Chem.* 2001, *98*, 136-148.

- [52] Rogalinski, T.; Herrmann, S.; Brunner, G., Production of amino acids from bovine serumalbumin by continuous sub-critical water hydrolysis. *J. Supercrit. Fluids* 2005, 36, 49-58.
- [53] Haghghat Khajavi S.; Ota, S.; Kimura, Y.; Adachi, S., Kinetics of maltooligosaccharide hydrolysis in subcritical water. *J. Agric. Food Chem.* 2006, 54, 3663-3667.
- [54] Pourali, O.; Asghari, F. S.; Yoshida, H., Production of phenolic compounds from rice bran biomass under subcritical water conditions. *Chem. Eng. J.* 2010, 160, 259-266.
- [55] Iqbal, S.; Bhangar, M. I.; Anwar, F., Antioxidant properties and components of some commercially available varieties of rice bran in Pakistan. *Food Chem.* 2005, 93, 265-272.
- [56] Moller, M.; Harnisch, F.; Schroder, U., Hydrothermal liquefaction of cellulose in subcritical water-the role of crystalline on the cellulose reactivity. *RSC Adv.* 2013, 3, 11035-11044.
- [57] Sasaki, M.; Kabyemela, B.; Malaluan, R.; Hirose, S.; Takeda, N.; Adschiri, T.; Arai, K., Cellulose hydrolysis in subcritical and supercritical water. *J. Supercrit. Fluids* 1998, 13, 261-268.
- [58] Pinkowska, H.; Wolak, P.; Zlocinska, A., Hydrothermal decomposition of xylan as a model substance for plant biomass waste-Hydrothermalysis in subcritical water. *Biomass Bioenerg.* 2011, 35, 3902-3912.
- [59] Molino, A.; Migliori, M.; Nanna, F.; Tarquini, P.; Braccio, G., Semi-continuous biomass gasification with water under subcritical conditions. *Fuel* 2013, 112, 249-253.
- [60] Lehr, V.; Sarlea, M.; Ott, L.; Vogel, H., Catalytic dehydration of biomass-derived polyols in sub- and supercritical water. *Catal. Today* 2007, 121, 121-129.
- [61] Buhler, W.; Dinjus, E.; Ederer, H. J.; Kruse, A.; Mas, C., Ionic reactions and pyrolysis of glycerol as competing reaction pathways in near- and supercritical catalytic dehydration of biomass-derived polyols in sub- and supercritical water. *J. supercrit. Fluids.* 2002, 22, 37-53.
- [62] Watanabe, M.; Iida, T.; Inomata, H., Decomposition of long chain saturated fatty acid with some additives in hot compressed water. *Energ. Convers. Manage.* 2006, 47, 3344-3350.
- [63] Khuwijitjaru, P.; Fuji, T.; Adachi, S.; Kimura, Y., Matsuno, R., Kinetic on the hydrolysis of fatty acid esters in subcritical water. *Chem. Eng. J.* 2004, 99, 1-4.
- [64] Sasaki, M.; Adschiri, T.; Arai, K., Kinetics of cellulose conversion at 25 MPa in sub- and supercritical water. *AIChE J.* 2004, 50, 192-202.
- [65] Sasaki, M.; Fang, Z.; Fukushima, Y.; Adschiri, T.; Arai, K., Dissolution and hydrolysis of cellulose in subcritical and supercritical water. *Ind. Eng. Chem. Res.* 2000, 39, 2883-2890.
- [66] Mok, W. S. L.; Anatal, M. J., Uncatalyzed solvolysis of whole biomass hemicellulose by hot compressed liquid water. *Ind. Eng. Chem. Res.* 1992, 31, 57-61.

- [67] Sasaki, M.; Hayakawa, T.; Arai, K.; Adichiri, T., Measurement of the rate of retro-aldol condensation of D-xylose in subcritical and supercritical water. Proceeding of the 7th international symposium on hydrothermal reactions. 2003, p. 169-176.
- [68] Wahyudiono, Kanetake, T.; Sasaki, M.; Moto, M., Decomposition of a lignin model compound under hydrothermal conditions. *Chem. Eng. Technol.* 2007, 30, 1113-1122.
- [69] Zhang, B.; Huang, H. J.; Ramaswamy, S., Reaction kinetics of the hydrothermal treatment of lignin. *Appl. Biochem. Biotechnol.* 2008, 147, 119-131.
- [70] Peterson, A. A.; Vogel, F.; Lachance, R. P.; Froling, M.; Antal, M. J.; Tester, J. M., Thermochemical biofuel production in hydrothermal media: a review of sub- and supercritical water technologies. *Energ. Environ. Sci.* 2008, 1, 32-65.
- [71] Demirbas, A., Mechanisms of liquefaction and pyrolysis reactions of biomass. *Energ. Convers. Manage.* 2000, 41, 633-646.
- [72] Meyer, S.; Glaser, B.; Quicher, P., Technical, economical and climate-related aspects of biochar production technologies: a literature review. *Environ. Sci. Technol.* 2011, 45, 9473-9483.
- [73] Kang, S. M.; Li, X. L.; Fan, J.; Chang, J., Characterization of hydrochars produced by hydrothermal carbonization of lignin, cellulose, D-xylose, and wood meal. *Ind. Eng. Chem. Res.* 2012, 51, 9023-9031.
- [74] Libra, J. A.; Ro, K. S. Kammann, C.; Funke, A.; Berge, N. D.; Neubauer, Y.; Titirici, M. M.; Fuhner, C.; Bens, O.; Kern, J.; Emmerich, K. H., Hydrothermal carbonization of biomass residuals: A comparative review of the chemistry, process and applications of wet and dry pyrolysis. *Biofuels* 2011, 2, 71-106.
- [75] Funke, A.; Ziegler, F., Hydrothermal carbonization of biomass: A summary and discussion of chemical mechanisms for process engineering. *Biofuels Bioprod. Biorefin.* 2010, 4, 160-177.
- [76] Toor, S. S.; Rosendahl, L.; Rudolf, A., Hydrothermal liquefaction of biomass: A review of subcritical water technologies. *Energy* 2011, 36, 2328-2342.
- [77] Wahyudiono; Sasaki, M.; Gato, M., Conversion of biomass model compound under hydrothermal conditions using batch reactor. *Fuel* 2009, 88, 1656-1664.

Chapter 2

Investigation of the degradation kinetic parameters and structure changes of microcrystalline cellulose in subcritical water

2.1 Introduction

With the increased problems of global warming and energy deficiency, production of clean and sustainable power from sustainable resources has attracted more and more interest in recent years. Biomass is the most abundant and cheap resource in the world. The advantages of its renewable ability, carbon neutrality, and low sulfur emission during combustion make biomass a promising candidate to replace fossil fuels for producing fuels, sustainable biomaterials, and value-added chemicals [1-5].

Subcritical water treatment is proposed as an environmentally friendly method to liquefy biomass. Up to now, many studies have focused on conversion of biomass to valuable chemicals or biofuel by subcritical water treatment in the past decade [1, 4, 5, 6-10]. However, the conversion mechanisms of its main components (cellulose, hemicellulose, and lignin) in subcritical water that serve as fundamental research are still not fully understood. The typical biomass (wood and grass plants) is roughly composed of 50% cellulose, 25% hemicellulose, and 20% lignin that are hydrolyzable polymers built from glucosan, xylan, mannan, and galactan (cellulose and hemicellulose) or aromatic alcohols (lignin) [11, 12]. Among these three components, hemicellulose was degraded at low temperature. It was reported that nearly 100% of hemicellulose can be degraded and solubilized by treatment for 0 to 15min in subcritical water at temperatures from 200 to 230 °C, respectively [13, 14]. The degradation of lignin was always carried out at near- and supercritical water conditions [15, 16]. Cellulose, the most abundant natural polymer and most contained component in biomass, was degraded at the temperature higher than 200 °C [17, 18]. The degradation temperatures of cellulose almost covered the whole subcritical water region. We thus considered that investigation of the degradation mechanism for cellulose in subcritical water was very important and was the key knowledge for understanding the degradation mechanism of biomass in subcritical water. For the degradation kinetics of cellulose in subcritical water, Schwald and Bobleter reported that the hydrolysis of cellulose at 200-300 °C was a heterogeneous and pseudo-first-order

reaction, and other researchers also used this model to express the degradation kinetics of cellulose in subcritical water and on an ionic-liquid-based catalyst [17-20]. Sasaki *et al.* suggested that the degradation kinetics of cellulose in subcritical water could be expressed by a grain model and a surface reaction rate model [21, 22]. They also pointed out that the crystallinity of the cellulose residue was not affected by subcritical water treatment. However, to the knowledge of the authors, only a few studies [19, 23, 24] have investigated the structure changes of cellulose in subcritical water besides Sasaki *et al.* and no researcher has evaluated the degradation order of cellulose in subcritical water. Investigation of the relationship between structure changes and kinetic parameters of cellulose was crucial for a better understanding of the cellulose degradation mechanism and biomass conversion process in subcritical water. Therefore, the structure changes and degradation kinetic parameters of cellulose (activation energy, pre-exponential factor, and order of reaction) in subcritical water that served as fundamental research were investigated in the present research.

2.2 Materials and Methods

2.2.1 Materials

5-hydroxymethyl-2-furaldehyde (HMF) and microcrystalline cellulose powder (MCC) with the size of 20 μm , were purchased from Sigma-Aldrich (St. Louis, Missouri, USA). The glucose, acetone and methanol were purchased from Wako Pure Chemical Industries (Osaka, Japan).

2.2.2 Subcritical water treatment

The degradation behavior of MCC in subcritical water was investigated in a SUS 316 stainless steel batch reactor (Taiatsu, Osaka, Japan) with the working volume of 10 mL. The experimental scheme for subcritical water treatment of biomass is shown in Fig. 2-1. A weight of 300 mg of MCC combined with 7 mL of Mill-Q water was charged into the batch reactor and then the reactor was tightly closed. The reactor was set into a ceramic furnace (ARF-40K, Asahi-Rika, Chiba, Japan) with a digital temperature controller (TXN-700, AS ONE, Osaka, Japan). The temperature inside the reactor was monitored by a thermocouple inserted into a tube installed in the middle of the reactor. It took 4.25 min to make the temperature inside the reactor reached to 100 $^{\circ}\text{C}$ and this time point was defined as the residence time of 0 s. The reactor was treated for 0 to 680 s with 10 s intervals and temperature inside reactor versus residence time was shown in Fig. 2-2. The heating rate inside reactor was 19.1 $^{\circ}\text{C}/\text{min}$ that was calculated by linear fitting of the experimental data.

After the specified residence time had elapsed, the reactor was rapidly immersed in an ice bath to stop the reaction. The mixture in the reactor was filtered by a G-4 glass filter (Vidtec, Fukuoka, Japan). The extract was stored in a fridge until it was needed. The MCC residue was dried at 110 °C until the weight reached to a constant value.

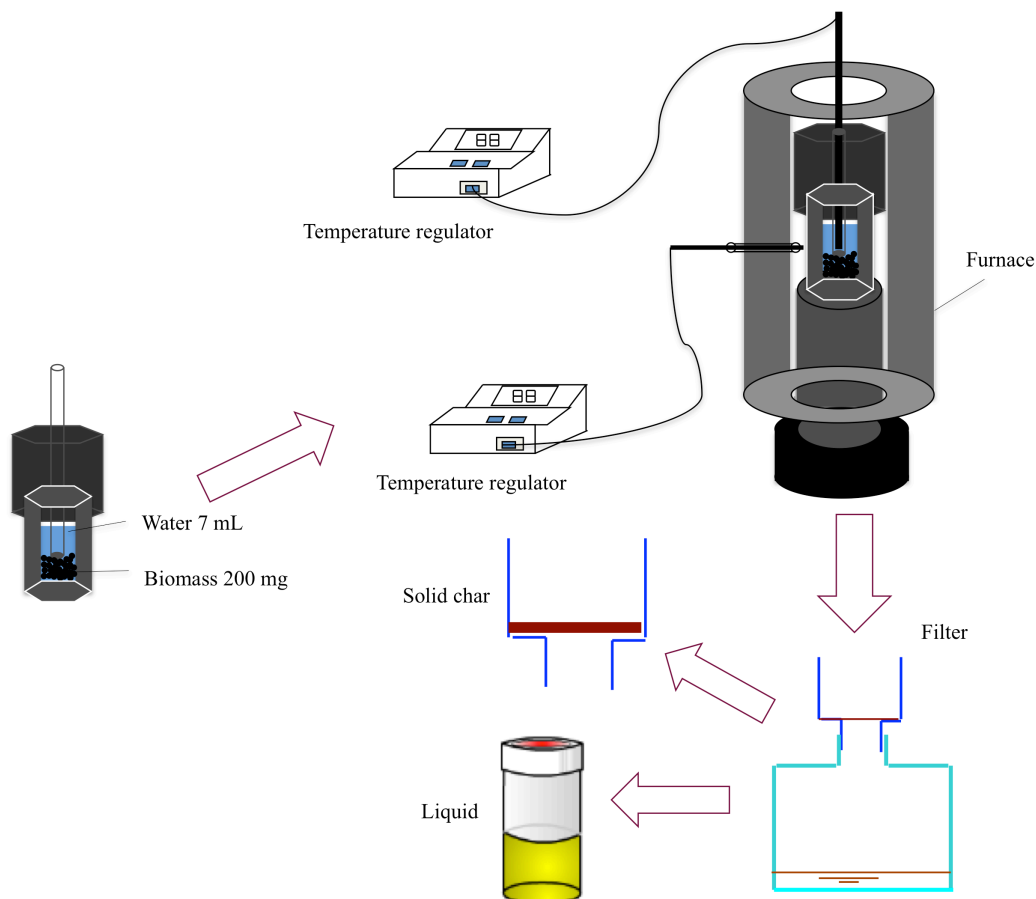


Figure 2-1. The experimental scheme for subcritical water treatment of biomass.

2.2.3 Analysis of extracts

The concentration of glucose in extract was analyzed by a high performance liquid chromatography (HPLC) combined with a LC-20AD pump (Shimadzu, Kyoto, Japan), a refractometer (RI-800, Tosoh, Tokyo, Japan), a Cosmosil Sugar-D Packed column (4.6 mm I.D. × 250 mm) and a Cosmosil Sugar-D guide column (4.6 mm I.D. × 10 mm; Nacalai Tesque, Kyoto, Japan). The elution was a mixture of acetone and water (1:4 by vol.) at 1.6 mL/min. The sample injection volume was 25 μ L. The HMF concentration in the extract was evaluated by HPLC with an ultraviolet detector (UV-8010, Tosoh, Tokyo, Japan), an ODS-5C₁₈-AR-II column (4.6 mm I. D. × 250 mm) and ODS-5C₁₈-AR-II guide column (4.6 mm I. D. × 10 mm; Nacalai Tesque, Kyoto, Japan). The elution was a mixture of methane and water with the volume ratio of 1:4 at 1 mL/min. The sample injection volume was 5 μ L.

The yields of glucose and HMF were calculated as follows:

$$\text{Glucose or HMF yield (\%)} = 100 \times CV/M_{\text{MCC}} \quad (2-1)$$

where C , V and M_{MCC} are the concentration of glucose or HMF in the extract with the unit of kg/m^3 , volume of the extract (m^3) and weight of the original MCC (kg), respectively.

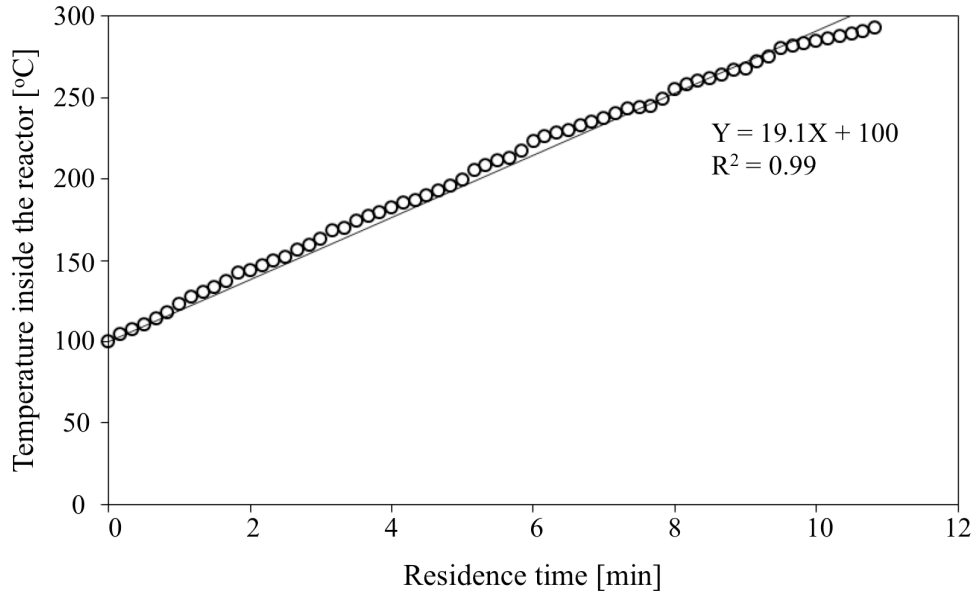


Figure 2-2. The temperatures inside the reactor at various residence times.

2.2.4 Determination of kinetic parameters of MCC in subcritical water

The determination of kinetic parameters of MCC was based on the modified form of Arrhenius equation that was used for determining the kinetic parameters of biomass from thermogravimetric analysis technique [25-28].

Global kinetic of the devolatilization reaction can be expressed as follows:

$$-dX/dt = kX^n \quad (2-2)$$

The Arrhenius equation can be written as

$$k = Ae^{-E/RT} \quad (2-3)$$

Substituting the value of k in Eq. (2) and taking Napierian logarithm (ln) on both sides

$$\ln(-dX/dt) = \ln A - E/RT + n \ln X \quad (2-4)$$

The X can be written as

$$X = (w_t - w_f)/(w_0 - w_f) \quad (2-5)$$

The Eq. (4) can be converted to

$$\ln[-1/(w_0 - w_f) dw_t/dt] = \ln A - (E/RT) + n \ln [(w_t - w_f)/(w_0 - w_f)] \quad (2-6)$$

The dw_t/dt in Eq. (6) is defined as the variation of w during $t \sim t+10$, and it was written as

$$dw_t/dt = (w_{t+10} - w_t)/10 \quad (2-7)$$

The Eq. (6) is in the form of

$$y = B + Cx + Dz \quad (2-8)$$

where y , x , z , B , C and D in Eq. (8) are defined as follows:

$$y = \ln [-1/(w_0 - w_f) dw_t/dt]$$

$$x = 1/RT$$

$$z = \ln [(w_t - w_f)/(w_0 - w_f)]$$

$$B = \ln A$$

$$C = -E$$

$$D = n$$

The X , t , k , n , A , E , R , T , w_0 , w_f , w_t and w_{t+10} in Eq. (2)~(7) were defined as follows:

X Weight ratio of MCC undergoing reaction (-)

t Residence time (s)

k The degradation rate (s^{-1})

n Order of reaction (-)

A Pre-exponential factor (s^{-1})

E Activation energy of degradation reaction (kJ mol^{-1})

R Universal gas constant ($\text{kJ mol}^{-1} \text{K}^{-1}$)

T Absolute temperature (K)

w_0 Initial weight of MCC residue in the particular zone (not the whole reaction) (kg)

w_f Final weight of MCC residue in the particular zone (not the whole reaction) (kg)

w_t Weight of MCC residue at time t (kg)

w_{t+10} Weight of MCC residue at time $t + 10$ (kg)

The constants B , C and D in Eq. (8) that stood for $\ln A$, $-E$ and n , respectively, were estimated by multi-linear regression of the experimental data using the Linest Function in Microsoft Excel Sheet.

2.2.5 Characterization of MCC and MCC residues

The functional groups on MCC and MCC residue were measured by a Jasco 4100 Fourier transform infrared spectroscopy (FTIR; Jasco, Tokyo, Japan). The morphologies were observed by a Hitachi S-4700 scanning electron microscope (SEM; Hitachi High-Technology, Tokyo, Japan) where the samples were sputter-coated with Pt. The crystalline changes were analyzed by powder X-ray diffraction (XRD) with monochromated $\text{CuK}\alpha$ radiation, using Rigaku Geiger flex RAD-C and RINT2000 diffractometers (Tokyo, Japan). The crystallinity index (CI) was calculated from the raw data of XRD by the peak-height method using the following equation [29, 30]:

$$\text{CI (\%)} = 100 \times (I_{200} - I_{\text{am}})/I_{200} \quad (2-9)$$

where I_{200} is the peak intensity corresponding to the (200) lattice plane of cellulose I Beta crystal, and I_{am} is the peak intensity of amorphous cellulose.

2.3 Results and Discussion

2.3.1 Degradation of MCC in subcritical water and the concentrations of glucose and HMF in the extract

As temperature is one of the most important parameters that influence the degradation of MCC in subcritical water, the degradation behavior of MCC was evaluated at the temperature range from 100 to 300 °C. As shown in Fig. 2-3, the MCC began to be degraded slowly at 205 °C and the MCC residue yield steeply decreased at above 245 °C. The lowest yield of MCC residue (10.8%) was obtained at the temperature of 275 °C. Meanwhile, the color of MCC residue abruptly changed from white to yellow and then to black, which indicated that various chemical reactions dramatically occurred during subcritical water treatment (data not shown). However, the MCC yield gradually increased with the increasing of temperature at the temperature above 275 °C and it reached to 22.2% at 300 °C. The results described above were similar to those reported by Fang *et al.* [12]. The significant change of MCC residue yield was due to the pyrolytic depolymerization of MCC [22]. The increase of MCC residue yield was due to the further decomposition of tar (monomer and hydrolysable oligomer) that was from pyrolysis of non-dissolved compounds to glucose char and the degradation of linked oligosaccharides to form aromatic linked polymer char [12, 31, 32].

Glucose and HMF are the main goal products during conversion of biomass or cellulose. As shown in Fig. 2-4, no glucose was detected below 245 °C although a portion of MCC was decomposed (Fig. 2-3). It was due to the high degradation rate of glucose at the temperature above 200 °C [33]. The glucose yield was then increased with increasing of temperature until it reached the maximum yield of 18.1% at 275 °C where the minimum yield of MCC was obtained (Fig. 2-3). Finally, the glucose yield showed a reduction at the temperature above 275 °C and decreased to zero at 300 °C. Meanwhile, the yield of HMF increased with increasing of treatment temperature below 289 °C and then reduced at higher temperature. The glucose (18.1%) and HMF (5.5%) yields obtained at 275 °C were much higher than those of 6.7% (glucose) and 0% (HMF) from hydrolysis of cellulose catalyzed by H_3PO_4 at 270 °C for 5 min [34]. The yield of HMF (10.8%) obtained at 289 °C could be comparable with those of HMF obtained by hydrolysis of cellulose in the acid ionic liquids of $(C_4SO_3Hmin)Cl$ (18%) and $(C_4SO_3Hmin)HSO_4$ (12%) at 100 °C for 1 h [35].

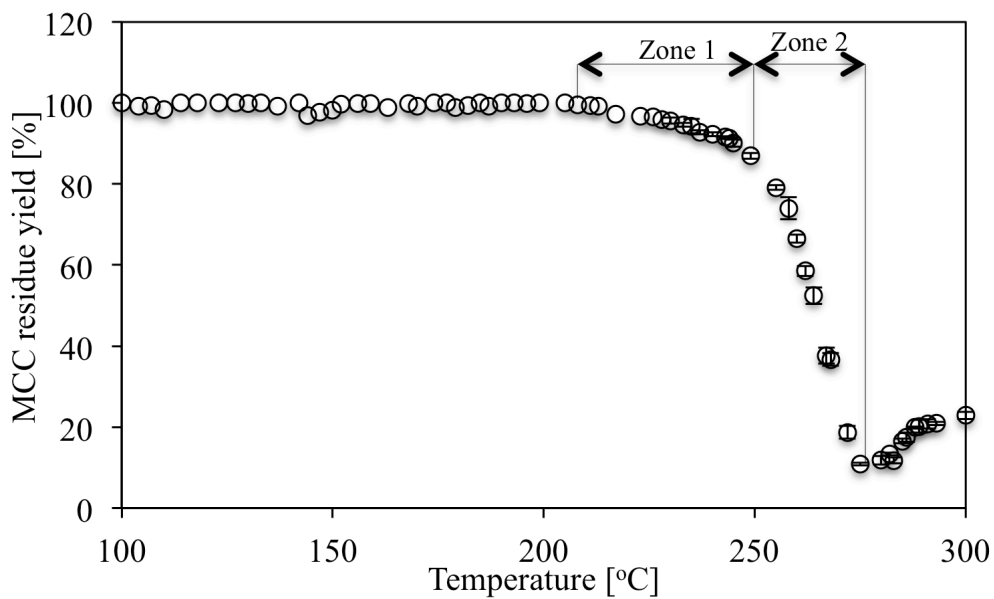


Figure 2-3. Effect of temperature on the yield of MCC residue (100 °C~200 °C: N = 1, 205 °C~300 °C: N = 3).

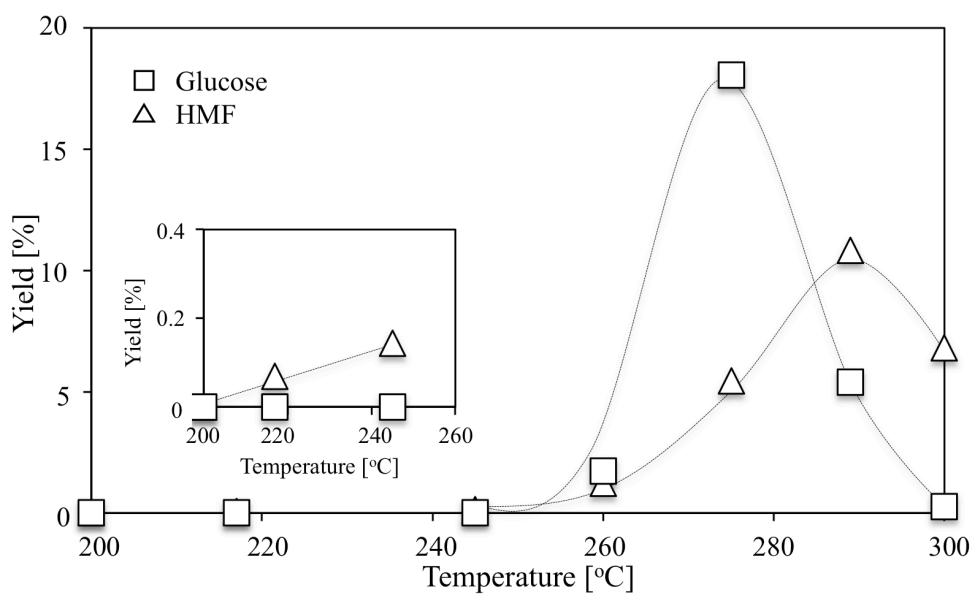


Figure 2-4. Effect of temperature on the yields of (□) glucose and (△) HMF analyzed by HPLC.

Table 2-1 Temperature range and kinetic parameters of each zone.

| Zone | Temperature range (°C) | Activation energy E (kJ mol ⁻¹) | Pre-exponential factor A (s ⁻¹) | Order of reaction n (-) |
|------|---------------------------|--|--|------------------------------|
| 1 | 205~245 | 226.5 | 2.3×10^{23} | 0.6 |
| 2 | 245~275 | 423.1 | 9.0×10^{40} | 0.5 |

2.3.2 Determination of kinetic parameters of MCC in subcritical water

According to the yield changes of MCC residue (Fig. 2-3), it was found that the chemical reactions occurred during MCC degradation at 245 to 275 °C were more temperature sensitive than those occurred at the temperature between 205 to 245 °C. The kinetic parameters might be different in these two temperature ranges. The MCC residue yield was increased at the temperature range from 275 to 300 °C. In this temperature range, the kinetic parameters were difficult to be determined. Therefore, the MCC degradation area between 205 and 275 °C was separated into two degradation zones (Fig. 2-3) with the temperature of 245 °C as a boundary. The kinetic parameters were determined by multi-linear regression of the experimental data at each degradation zone.

The calculated kinetic parameters of MCC are shown on Table 2-1 and the coefficients of determination in zone 1 and zone 2 were 0.99 and 0.93, respectively. The activation energy in zone 1 was 226.5 kJ mol⁻¹. In contrast, the activation energy (423.1 kJ mol⁻¹) in zone 2 was much higher than that in zone 1. This result indicated that the hydrolytic reaction was not the only controlling resistance during MCC degradation process because the same Arrhenius plot could not be applied at the whole temperature range, and the breaking point for Arrhenius plot in this study was at 245 °C. Xiang *et al.* had reported the similar observation that the reaction rates exhibited a sudden departure of the rate constants from normal Arrhenius pattern with a breaking point at the near 215 °C during acid hydrolysis of α -cellulose [36]. They pointed out that both the hydrolytic reaction and physical state of substrate affected the kinetic behavior of cellulose. Sasaki *et al.* also reported a similar result during hydrolysis of cellulose in subcritical and supercritical water [21, 37]. They reported that the cellulose decomposition rate at 300~320 °C was much higher than that at 260~280 °C.

The pre-exponential factors in this study were 2.3×10^{23} for zone 1 and 9×10^{40} for zone 2. They were much higher than reported by Sasaki *et al.* where the pre-exponential factors were $10^{11.9 \pm 0.4}$ below 370 °C and $10^{44.6 \pm 2.2}$ above 370 °C [22]. The MCC degradation orders determined in this study were 0.6 in the zone 1 and 0.5 in the zone 2 and these results indicated that the degradation reactions in zone 1 and zone 2 were heterogeneous. However, most of the researches assumed first-order reactions for their investigation of the cellulose

degradation kinetics in subcritical water [19, 20, 36]. Duvvuri *et al.* had reported that the kinetic order for cellulose was 1.2~1.4 during pyrolysis process [26].

In this study, there were two zones that gave the different activation energy as same as those showed by Xiang *et al.* and Sasaki *et al.* [21, 36, 37]. However, most researchers estimated the activation energy under the assumption that the reaction obeyed first-order kinetics ($n = 1$) during investigation of the cellulose degradation kinetics. They showed the values using various types of reactors. For example, the activation energy was 71.4, 164 and 145 kJ mol⁻¹ when the cellulose was degraded at the temperature range from 230 to 270 °C by a semi-flow reactor [38], 250 to 310 °C by a flow-type reactor [39] and 320 to 400 °C by a continuous-flow-type microreactor [22], respectively. Tolonen *et al.* also showed the activation energy (225 kJ mol⁻¹), which was comparable with that of this study during degradation of cellulose at the temperature range from 245 to 319 °C by a flow rate reactor [19]. Like these, there was a large variation in the values of activation energies including the Tolonen's value, which was comparable with that in zone 1 in the present study. Additionally even using a diluted acid catalyst, which could decrease the value of activation energy, some values in activation energy were compatible, i.e. 100 and 144 kJ mol⁻¹ at the temperature range from 190 to 250 °C and 190 to 227 °C, respectively [40]. We could not give a clear explanation for these differences in activation energy, however, the reasons were considered to be as follows: (1) the degradation methods and treatment conditions were variously defined among the different researches, and (2) concerned with the evaluation of the kinetic parameters, the other researchers assumed that the degradation of MCC obeyed the first-order kinetic while we estimated all of the kinetic parameters (kinetic order, activation energy and pre-exponential factor) in the present study. This accurate estimation could induce to such a high value of activation energy.

2.3.3 FTIR spectra of MCC and MCC residues

FTIR is a technique that is possible to follow the functional group changes in MCC during subcritical water treatment. Therefore, the FTIR spectra of MCC as well as MCC residues obtained at 200 °C, 217 °C, 260 °C, 275 °C, 289 °C and 300 °C were evaluated in the present study. As shown in Fig. 2-5, the peak around 3300 cm⁻¹, which attributed to the hydrogen-bonded O–H groups in intermolecular and intramolecular cellulose, became weaker with the increasing of treatment temperature and it disappeared at the temperature above 275 °C. The loss of O–H group was due to the dehydration of cellulose during subcritical water and it could improve the hydrophobicity of cellulose residue or the torrefied biomass [38]. The peaks at 2900 (aliphatic C–H stretching), 1100 (ether bond C–O–C in cellulose) and

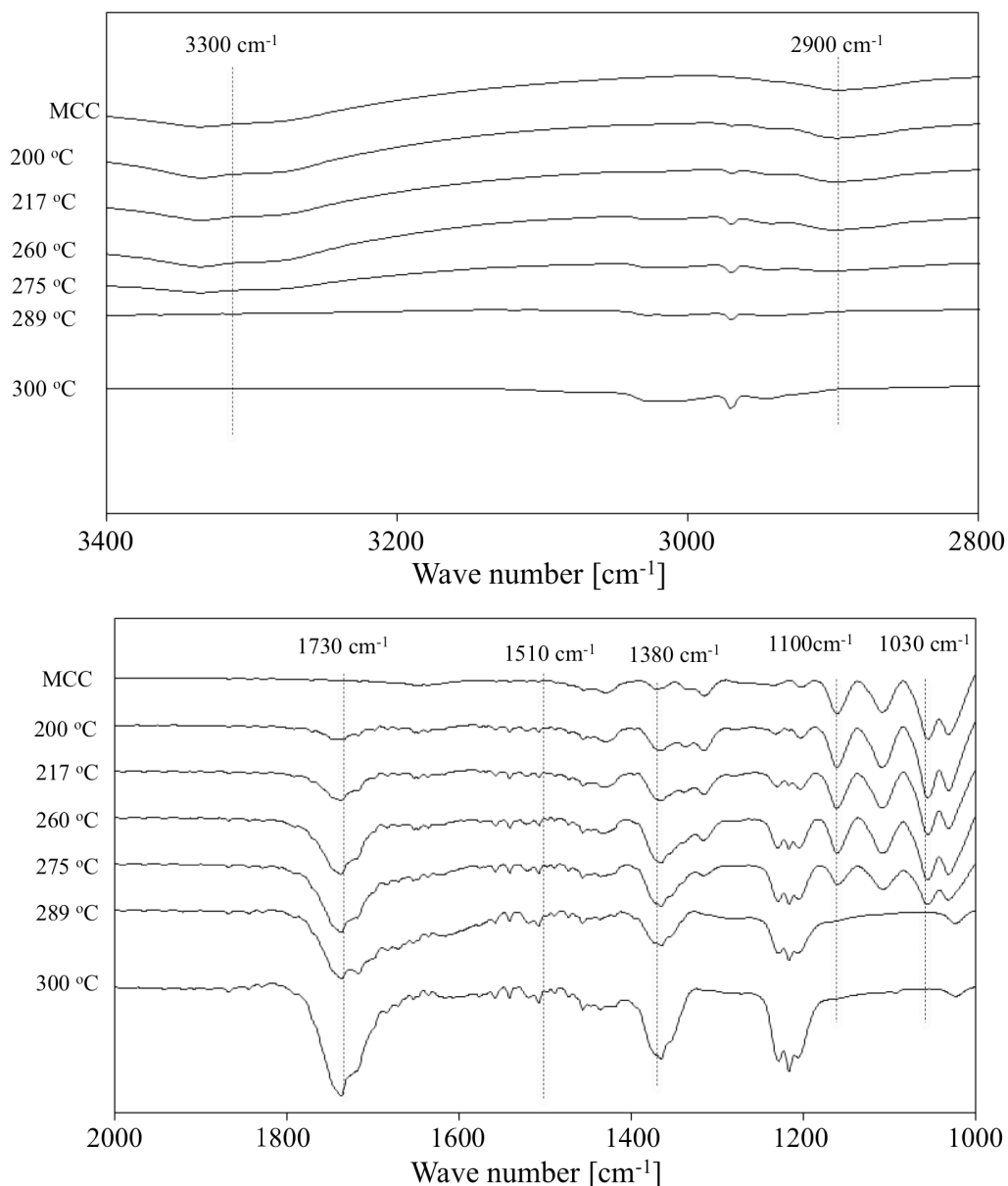


Figure 2-5. FTIR spectra of original MCC and MCC residues obtained at 200 °C, 217 °C, 260 °C, 275 °C, 289 °C and 300 °C, respectively.

1030 cm⁻¹ (C–O stretch) also showed the same phenomenon to the O–H group. Besides, the CH₂ bending at 1380 cm⁻¹ became stronger with increasing of treatment temperature and it was due to the O–H bending during subcritical water treatment. Two new bands at 1510 and 1730 cm⁻¹ appeared and they became stronger at higher treatment temperature. These two peaks were assigned to C=C stretching and C=O stretching, respectively. The C=O presented here may be a carboxyl group and/or carbonyl groups derived from hydroxyl group through dehydration because the cellulose body was rich in carboxyl groups. The presence of C=C stretching indicated that aromatic polymer was generated during subcritical water treatment. The aromatic polymer generated here might also be due to aromatization and cross-linking

reactions of cellulose during subcritical water treatment besides the reasons aforementioned [41]. Therefore, it was considered that the cellulose surface functional groups were significantly destroyed during subcritical water treatment.

2.3.4 SEM images of the MCC and MCC residues

Using the SEM, it was possible to observe the surface morphology change that could indirectly reflect the extent of reaction on MCC surface. The SEM images of MCC and MCC residues obtained at 217 °C, 260 °C, 275 °C, 289 °C and 300 °C are shown in Fig. 2-6. The average diameter of original MCC fiber was approximately 20 μm and the length of MCC fiber was between 20 to 80 μm (Fig.2-6a). The morphology of MCC had no significant change below 260 °C except the slightly decreasing of the diameter and length of MCC fiber (Fig. 2-6b and 6c). However, the surface of MCC residue was completely destroyed and the MCC residue trended to agglomerate above 260 °C (Fig. 2-6d, 6e and 6f). Meanwhile, MCC residues with strong pore structures were obtained at 289 and 300 °C (Fig. 2-6e and 6f). The agglomeration of MCC residue was due to the dehydration of acid catalyzed intermolecular surface among microfibrils [42]. The pore structure on MCC residue was probably due to coverage of glucose char and aromatic linked polymer char on the MCC residue surface as aforementioned.

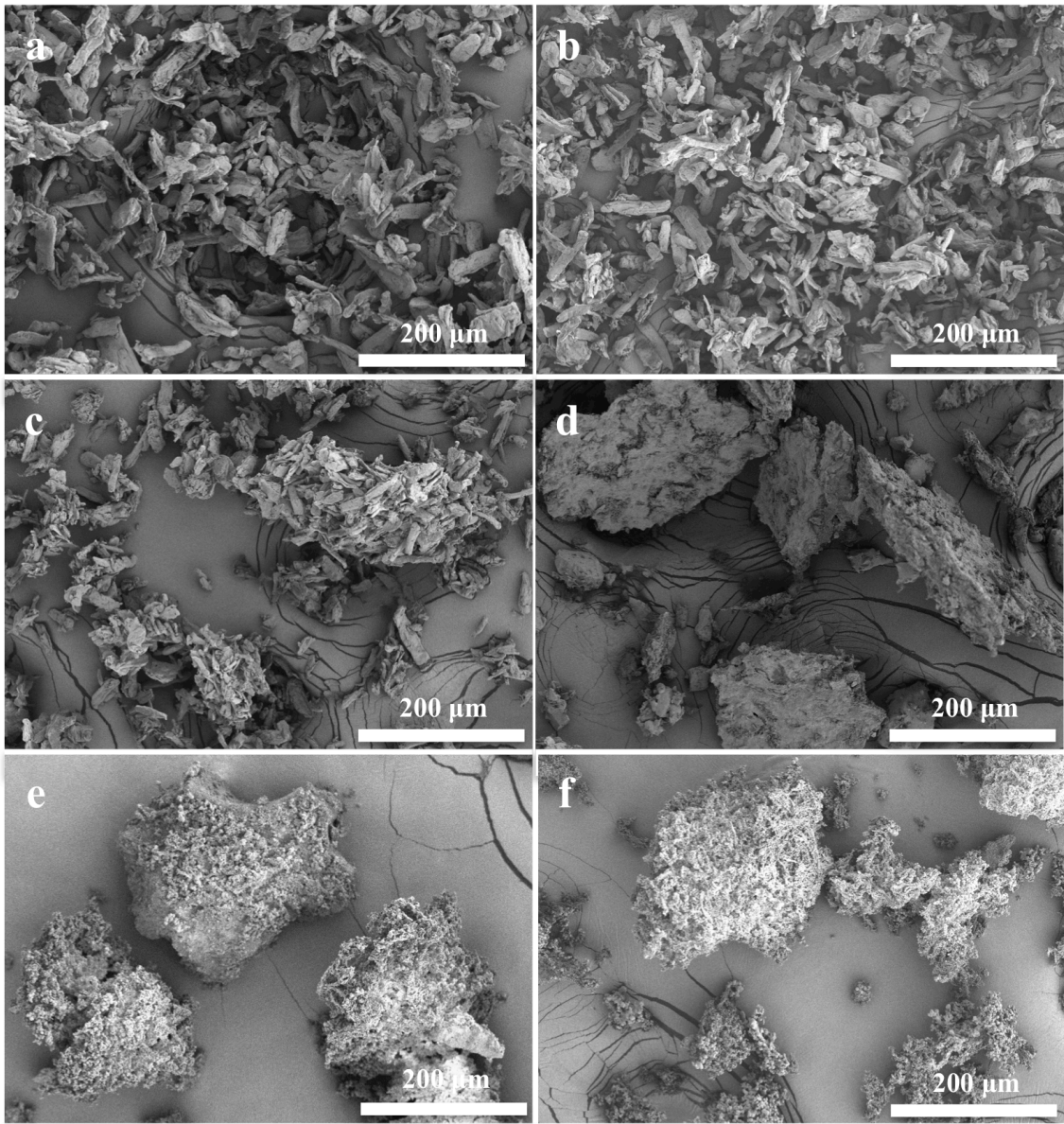


Figure 2-6. SEM images of (a) original MCC and MCC residues obtained at (b) 217 °C, (c) 260 °C, (d) 275 °C, (e) 289 °C and (f) 300 °C, respectively.

2.3.5 X-ray diffraction patterns of the MCC and MCC residues

The MCC and MCC residues were analyzed by X-ray diffraction in order to investigate the crystalline changes of them. The X-ray diffraction spectra and CI of MCC as well as MCC residues obtained at 200 °C, 217 °C, 260 °C, 275 °C, 289 °C and 300 °C were shown in Fig. 2-7 and 2-8, respectively. The XRD patterns showed that the crystalline peaks on the MCC residues were not disrupted at the temperature range from 200 to 275 °C compared with those of original MCC, although 89.2% of MCC was decomposed and the surface morphology of MCC was completely destroyed at 275 °C (Fig. 2-3 and Fig. 2-6d). Meanwhile, the CI of MCC showed a decrease of 10.7%, which meant a portion of cellulose crystalline was destroyed compared with that of the original MCC at 275 °C (Fig. 2-8). Sasaki *et al.* had reported that the hydrolysis of cellulose in subcritical water was consisted with surface peeling at relatively low temperature followed by homogeneous swelling and dissolution at the temperature higher than 350 °C at the pressure of 25 MPa in a flow reactor [22]. However, no cellulose II structure that was due to the swelling of cellulose was observed in this study. Therefore, it is probably that only the surface of MCC was peeled and its internal structure remained intact at the temperature below 275 °C. In contrast, the crystalline peaks of MCC residues dramatically reduced, resulting a steeply reduction of CI at the temperatures of 289 and 300 °C. It meant that the internal crystalline structure was damaged at these temperatures. Therefore, it was considered that the pore structure on the MCC residue described above could also be the result of destruction of internal crystalline structure of MCC.

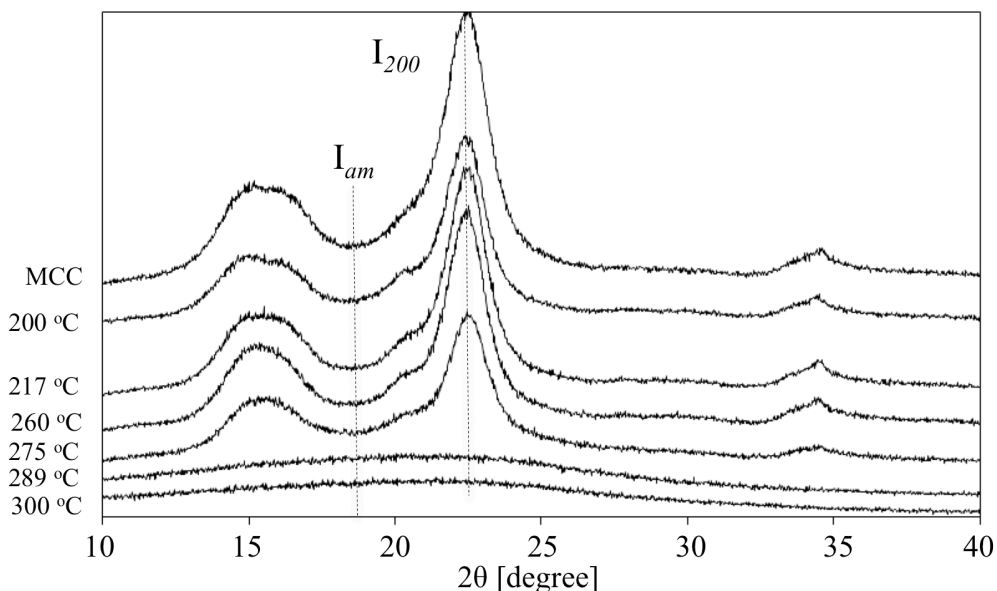


Figure 2-7. XRD patterns of original MCC and MCC residues obtained at 200 °C, 217 °C, 260 °C, 275 °C, 289 °C and 300 °C, respectively.

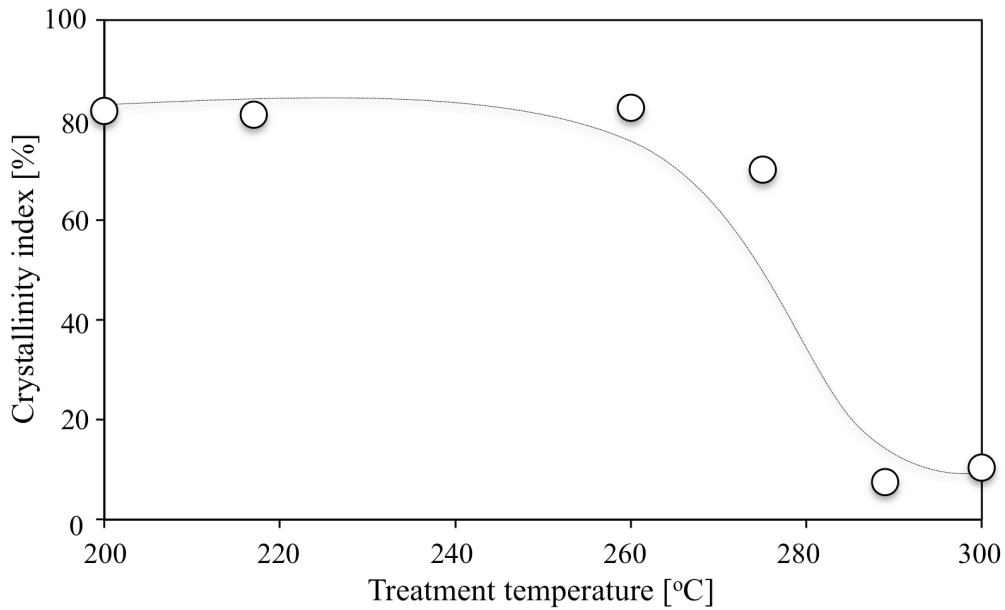


Figure 2-8. The crystalline index of MCC residues obtained at 200 °C, 217 °C, 260 °C, 275 °C, 289 °C and 300 °C, respectively.

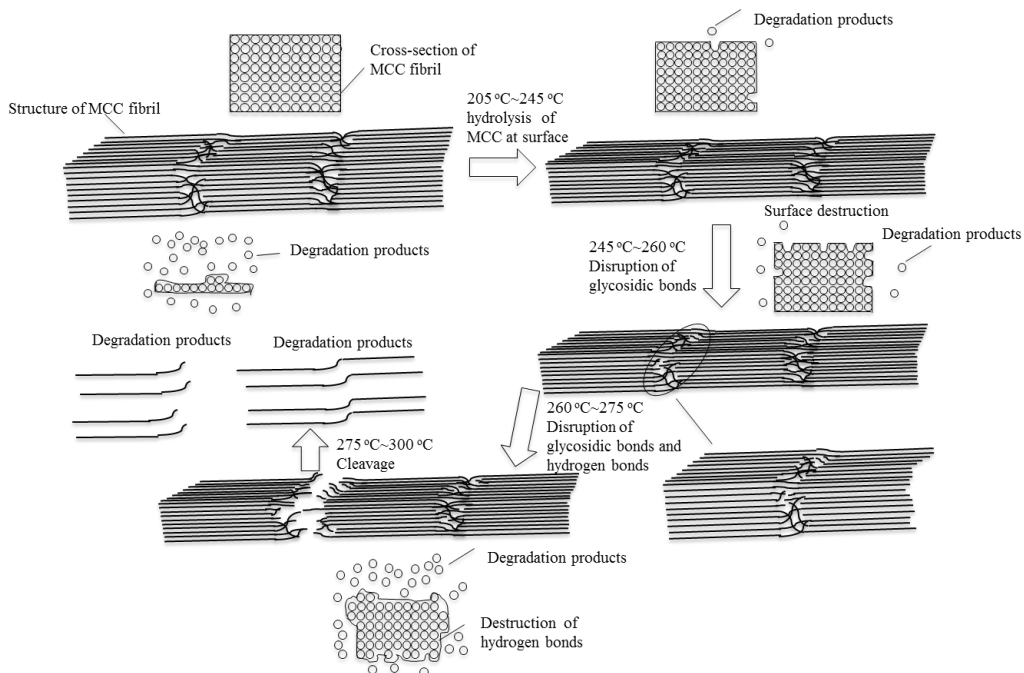


Figure 2-9. The proposed degradation mechanism of MCC at the temperature range from 205 °C~300 °C. The MCC structure was referred from reference 15.

2.3.6 The proposed degradation mechanism of MCC in subcritical water

Considering all the experimental and analytical results described above, the degradation mechanism of MCC at the temperature range from 205 °C~300 °C was proposed in Fig. 2-9. At zone 1 (205 °C~245 °C), the degradation of MCC took place slowly on the MCC surface region without swelling because no cellulose II was observed (Fig. 2-7). Therefore, the surface morphology and XRD patterns of MCC had no significant change (Fig.2-6b and Fig. 2-7). In contrast, the hydrogen bonds and the glycosidic bonds began to be destroyed, resulting the dramatic change of MCC surface morphology and reduction of CI at zone 2 with the temperature range from 245 °C to 275 °C (Fig. 2-6c and 6d and Fig. 2-8). The degradation reactions were heterogeneous at zone 1 and zone 2, because the orders of reaction were fraction (Table 2-1). The activation energy in zone 2 was 423.1 kJ mol⁻¹ and it was much higher than 226.5 kJ mol⁻¹ in zone 1 (Table 2-1). It was because that only a few of the glycosidic bonds on MCC fibrils surface were destroyed while the glycosidic bonds and hydrogen bonds on the interior of the MCC fibrils were remained unabridged in zone 1; however, these glycosidic and hydrogen bonds on the interior MCC fibrils began to be destroyed in zone 2 and it resulted in the higher activation energy than that in zone 1. Meanwhile, the pre-exponential factor became much larger because the MCC surface was destroyed through degradation, resulting the high surface area on MCC surface. At for the temperature above 275 °C, the hydrogen bonds and glycosidic bonds on the interior of MCC fibrils continuously destroyed that led to the significant reduction of CI, and the generated oligomer and monomer, further degraded to glucose char, aromatic linked char and other chemicals.

2.4 Conclusions

The degradation behavior of MCC was evaluated at the temperature range from 100 to 300 °C. The MCC began to be degraded slowly at 205 °C and became faster above 245 °C. The lowest yield of MCC residue was obtained at 275 °C and it showed an increase at higher temperature. The highest yields of glucose and HMF yields were obtained at 275 °C and 289 °C with the value of 18.1% and 10.8%, respectively. The degradation area (205 °C~275 °C) of MCC was separated into two zones with 245 °C as a boundary. The activation energy (E), pre-exponential factor (A) and reaction order (n) of MCC in zone 1 and zone 2 were 226.5 kJ mol⁻¹, 2.3×10^{23} s⁻¹ and 0.6 and 423.1 kJ mol⁻¹, 9.0×10^{40} and 0.5, respectively. The hydrolytic reaction was not the only controlling resistance during MCC degradation process and there showed a breaking point of Arrhenius plot at the temperature of 245 °C. The surface morphology of MCC had no significant change before 260 °C, as

indicated by SEM images. However, it was completely destroyed at the temperature higher than 275 °C and MCC residues with pore structures were obtained at 289 °C and 300 °C. The crystalline peaks and CI of MCC had no dramatic changed before 275 °C although 89.2% of MCC was decomposed at 275 °C and then it was steeply reduced, as shown by XRD patterns. The degradation mechanism of MCC at 205 °C to 300 °C was proposed as follows: (1) degradation of MCC at surface at 205 °C~245 °C; (2) destruction of hydrogen bonds and glycosidic bonds of MCC at the temperature range from 245 °C to 275 °C and (3) further degradation of MCC as well as generated oligomer and monomer at the temperature above 275 °C.

Reference

- [1] Xu, C. B.; Lad, N., Production of heavy oils with high caloric values by direct liquefaction of woody biomass in sub/near-critical water. *Energy Fuels* 2008, 22, 635-642.
- [2] Ragauskas, A. J.; Williams, C. K.; Davison, B. H.; Britovsek, G.; Cairney, J.; Eckert, C. A.; Frederick Jr., W. J.; Hallett, J. P.; Leak, D. J.; Liotta, C. L.; Mielenz, J. R.; Murphy, R.; Templer, R.; Tschaplinski, T., The path forward for biofuels and biomaterial. *Science* 2006, 27, 484-489.
- [3] Rostrup-Nielsen, J. R., Making fuels from biomass. *Science* 2005, 3, 1421-1422.
- [4] Rodrigues-Meizoso, L.; Marin, F. R.; Herrero, M.; Senorans, F. J.; Reglero, G.; Cifuentes, A.; Ibanez, E., Subcritical water extraction of nutraceuticals with antioxidant activity from oregano. Chemical and functional characterization. *J. Pharm. Biomed. Anal.* 2006, 5, 1560-1565.
- [5] Pourali, O.; Asghari, F. S.; Yoshida, H., Production of phenolic compounds from rice bran biomass under subcritical water conditions. *Chem. Eng. J.* 2010, 160, 259-266.
- [6] Wiboonsirikui, J.; Kimura, Y.; Kanaya, Y.; Tusno, T.; Adachi, S., Production and characterization of functional substances from a by-product of rice bran oil and protein production by a compressed hot water treatment. *Biosci. Biotechnol. Biochem.* 2008, 72(2), 384-392.
- [7] Liu, Z. G.; Quek, A. Hoekman, S. K.; Balasubramanian, R., Production of solid biochar fuel waster biomass by hydrothermal carbonization. *Fuel* 2013, 103, 943-949.
- [8] Hata, S.; Wiboonsirikul, J.; Maeda, A.; Kimura, Y. Adachi, S., Extraction of defatted rice bran by subcritical water treatment. *Biochem. Eng. J.* 2008, 40, 44-53.
- [9] Lü, X.; Saka, S., Hydrolysis of Japanese beech by batch and semi-flow water under subcritical temperatures and pressures. *Biomass Bioenerg.* 2010, 34, 1089-1097.
- [10] Asghari, F. S.; Yoshida, H., Conversion of Japanese red pine wood (*Pinus densiflora*)

into valuable chemicals under subcritical water conditions. *Carbohydr. Res.* 2010, *345*, 124-131.

[11] Bobleter, O., Hydrothermal degradation of polymers derived from plants. *Prog. Polym. Sci.* 1994, *19*, 797-841.

[12] Fang, Z.; Minowa, T.; Smith, Jr., R. L.; Ogi, T.; Kozinski, J. A., Liquefaction and gasification of cellulose with Na₂CO₃ and Ni in subcritical water at 350 °C. *Ind. Eng. Chem. Res.* 2004, *43*, 2454-2463.

[13] Lynam, J. C.; Coronella, C. J.; Yan, W.; Reza, M. T.; Vasques, V. R., Acetic acid and lithium chloride effect on hydrothermal carbonization of lignocellulosic biomass. *Bioresource Technol.* 2011, *102*, 6192-6199.

[14] Mok, W. S. L.; Antal, M. J., Uncatalyzed solvolysis of whole biomass hemicellulose by hot compressed liquid water. *Ind. Eng. Chem. Res.* 1992, *31*, 1157-1161.

[15] Wahyudiono, Kanetake, T.; Sasaki, M.; Moto, M., Decomposition of a lignin model compound under hydrothermal conditions. *Chem. Eng. Technol.* 2007, *30*, 1113-1122.

[16] Wahyudiono; Sasaki, M.; Gato, M., Conversion of biomass model compound under hydrothermal conditions using batch reactor. *Fuel* 2009, *88*, 1656-1664.

[17] Bobleter, O., Hydrothermal degradation of polymers derived from plants. *Prog. Polym. Sci.* 1994, *19*, 797-841.

[18] Schwald, W.; Bobleter, O., Hydrothermolysis of cellulose under static and dynamic conditions at high temperatures. *J. Carbohydr. Chem.* 1989, *8*(4), 565-578.

[19] Tolonen, L. K.; Zuckerstatter, G.; Penttila, P. A.; Milacher, W.; Habicht, W.; Serimaa, R.; Andrea, K.; Sixta, H., Structural changes in microcrystalline cellulose in subcritical water treatment. *Biomacromolecules* 2011, *12*, 2544-2551.

[20] Gaikward, A.; Chakraborty, S., Mixing and temperature effects on the kinetics of alkali metal catalyzed ionic liquid base batch conversion of cellulose to fuel products. *Chem. Eng. J.* 2014, *240*, 109-115.

[21] Sasaki, M.; Kabyemela, B.; Malaluan, R.; Hirose, S.; Takeda, N.; Adschiri, T.; Arai, K., Cellulose hydrolysis in subcritical and supercritical water. *J. Supercrit. Fluids* 1998, *13*, 261-268.

[22] Sasaki, M.; Adschiri, T.; Arai, K., Kinetics of cellulose conversion at 25 MPa in sub- and supercritical water. *AIChE J.* 2004, *50*, 192-202

[23] Moller, M.; Harnisch, F.; Schroder, U., Hydrothermal liquefaction of cellulose in subcritical water-the role of crystallinity on the cellulose reactivity. *RSC Adv.* 2013, *3*, 11035-11044.

[24] Kumar, S.; Gupta, R.; Lee Y. Y.; Gupta, R. B., Cellulose pretreatment in subcritical

water: Effect of temperature on molecular structure and enzymatic reactivity. *Bioresour. Technol.* 2010, *101*, 1337-1347.

[25] Goldfrab, J.; Guchuan, I. R.; Meeks, A. C., Kinetic analysis of thermogravimetry, Part , Programmed temperature, Report NO. ARML-TR-68-181. Air Force Laboratory, Wright-Patterson AFB, Ohio, 1968.

[26] Duvvuri, M. S.; Muhlenkamp, S. P.; Iqbal, K. Z.; Welker, J. R., The pyrolysis of natural fuels. *J. Fire Flammabil.* 1975, *6*, 468-477.

[27] Mansaray, K. G.; Ghaly, A. E., Determination of kinetic parameters of rice husks in oxygen using thermogravimetric analysis. *Biomass Bioenerg.* 1999, *17*, 19-31.

[28] Parthasaeathy, P.; Narayanan, S. K., Determination of kinetic parameters of biomass samples using thermogravimetric analysis. *Environ. Prog. Sustain.* 2014, *33*, 256-266.

[29] Segal, L.; Creely, J. J.; Martin Jr, A. E.; Conrad, C. M., An empirical method for estimating the degree of crystallinity of native cellulose using the X-ray diffractometer. *Text Res. J.* 1959, *29*, 786-794.

[30] Park, S.; Baker, J. O.; Himmel, M. E.; Parilla, P. A.; Johnson, D. K., Cellulose crystallinity index: measurement techniques and their impact on the interpreting cellulose performance. *Biotechnol. Biofuels* 2010, *3*, 10.

[31] Shafizadeh, F., Industrial pyrolysis of cellulosic materials. *Appl. Polym. Symp.* 1975, *28*, 153-174.

[32] Boon, J. J.; Pastorova, I.; Botto, R. E.; Arisz, P. W., Structural studies on cellulose pyrolysis and cellulose char by PYMS, PYGVMS, FTIR, NMR and by wet chemical techniques. *Biomass Bioenerg.* 1994, *7*(1-6), 25-32.

[33] Khajavi, S. H.; Kimura, Y.; Oomori, T.; Matsuno, R. Adachi, S., Degradation kinetics of monosaccharides in subcritical water. *J. Food Eng.* 2005, *68*, 309-313.

[34] Daorattanachai, P.; Namuangruk, S.; Viriya-empilul, N.; Laosiripojana, N., 5-hydroxymethylfurfural production from sugars and cellulose in acid- and base-catalyzed conditions under hot compressed water. *J. Ind. Eng. Chem.* 2012, *18*, 1893-1901.

[35] Jiang, F.; Zhu, Q. J.; Ma, D.; Liu, X. M.; Han, X. W., Direct conversion and NMR observation of cellulose to glucose and 5-hydroxymethylfurfural (HMF) catalyzed by the acidic ionic liquids. *J. Mol. Catal. A-Chem.* 2011, *334*, 8-12.

[36] Xiang, Q.; Lee, Y. Y.; Pettersson, P. O.; Torget, R. W., Heterogeneous aspects of acid hydrolysis of α -cellulose. *Appl. Biochem. Biotech.* 2003, *107*, 505-514.

[37] Sasaki, M.; Fang, Z.; Fukushima, Y.; Adschiri, T.; Arai, K., Dissolution and hydrolysis of cellulose in subcritical and supercritical water. *Ind. Eng. Chem. Res.* 2000, *39*, 2883-2890.

[38] Abdullah, R.; Ueda, K.; Saka, S., Hydrothermal decomposition of various crystalline

- celluloses as treated by semi-flow hot-compressed water. *J. Wood Sci.* 2014, *60*, 278-286.
- [39] Schacht, C.; Zetzl, C.; Brunner, G., From plant materials to ethanol by means of supercritical fluid technology. *J. Supercrit. Fluids* 2008, *46*, 299-321.
- [40] Mok, W. S.; Antal, M. J.; Varhegyi, G., Productive and parasitic pathways in diluted acid-catalyzed hydrolysis of cellulose. *Ind. Eng. Chem.* 1992, *31*, 94-100.
- [41] Agrawal, K. R., Kinetics of reactions involved in pyrolysis of cellulose. I. The three reaction model. *Can. J. Chem. Eng.* 1988, *66*, 403-412.
- [42] Zhao, H. B.; Kwak, J. H.; Zhang, Z. C.; Brown, H. M.; Arey, B. W.; Holladay, J. E., Studying cellulose fiber structure by SEM, XRD, NMR and acid hydrolysis. *Carbohydr. Polym.* 2007, *68*, 235-241.

Chapter 3

Preparation of biodegradable foam from walnut shell treated by subcritical water

3.1 Introduction

According to the results obtained in Chapter 2, less than 30% of cellulose was degraded under the temperature of 260 °C. Generally, hemicellulose was much more reactive than cellulose and lignin was degraded at near- and supercritical conditions [1]. For example, it was reported that nearly 100% of hemicellulose could be decomposed and solubilized by treatment for 0 to 15 min in subcritical water at temperatures from 200 to 230 °C [2, 3]. We thus speculated that the solid char remained after subcritical water treatment would be rich in lignin and cellulose and had the potential to be applied as a new resource, although few researchers have focused on the application of solid char.

There have been various studies on the use of pure lignin and cellulose, such as preparation of starch-lignin films, starch-lignin foams and starch-cellulose foams [4-6]. It was reported that the addition of lignin and cellulose (<15%) could reinforce the mechanical properties of starch foam. Probably, the solid char that was rich in cellulose and lignin could play the roles of pure lignin and cellulose to reinforce the mechanical properties of starch foam.

Therefore, in this study, solid char remained after subcritical water liquefaction of biomass was used to prepare biodegradable foams by compounding with corn starch. Walnut shell (WS) from *Carya cathayensis* Sarg was employed as a model waste biomass. Roughly 10000 tons of this biomass are generated annually in Lin'an city, China, and an effective treatment method for this resource has been anticipated. The purpose of this study was to investigate the effect of solid char on the mechanical properties of biodegradable foam. Major applications of the prepared foams would be as disposable food containers for single or short-term use, which would decrease the use of foamed polystyrene.

3.2 Materials and Methods

3.2.1 Materials

The WS was produced in Lin'an city, China. The WS was milled and screened (diameter less than 0.3 mm) using a milling machine (WB-1, Osaka Chemical Corporation, Osaka, Japan). Before the experiments, the WS was dried at 105 °C for 24 h. The reagents used i.e., sodium hydroxide (99%), acetic acid (99%), sulfuric acid (95%), sodium carbonate (99%), sodium chlorite (80%), corn starch, potassium acetate (99%), magnesium nitrate hexahydrate (99%), magnesium stearate and acetic acid (99%) were all purchased from Wako Pure Chemical Industries (Osaka, Japan). Calcium sulfate was obtained from Nakarai Tesque (Kyoto, Japan).

3.2.2 Subcritical water treatment of walnut shell

The subcritical water treatment of WS was carried out in the same equipment as described in Chapter 2. Actually, 100 mg of WS and 7 mL of water was used. The reactor was treated at the temperature range from 160 to 260 °C with the treatment time of 15 to 60 min. After treatment the mixture in the reactor was filtered and the extract and solid char were recycled.

3.2.3 Analysis of the carbohydrate content in the extract

The carbohydrate content in the extract was evaluated using a modified phenol-sulfuric acid method [7]. A 75% (w/w) aqueous phenol solution (0.25 mL) and 2.5 mL of sulfuric acid were added to 1 mL of extract, which was previously diluted by ultrapure water for 5 times, or glucose solution as a standard and then well mixed. The mixture was kept at ambient temperature for 20 min. The carbohydrate content in the extract was analyzed using a UV-1200 spectrophotometer (Shimadzu, Kyoto, Japan) at 490 nm versus water as a blank. The measurements were conducted in triplicate.

3.2.4 Analysis of the components in the walnut shells and solid char

The holocellulose and cellulose contents in the biomass were analyzed by the method described by Yokoyama *et al.* [8]. 100 mg of biomass and 4 mL of Mill-Q water were set in to a 20 mL flask, and then reacted with 200 mg of 80% sodium chlorite as well as 0.8 mL acetic acid at 90 °C for 1 h. After reaction, the flask was cooled in an ice bath and the suspension in the flask was filtered by a G-4 glass filter (Vidtec, Fukuoka, Japan) and washed

by Mill-Q water for 3 times (3×50 mL). The remained solid was dried at $105\text{ }^{\circ}\text{C}$ for 24 h and the yield of holocellulose was determined.

For the determination of cellulose, 50 mg of dried holocellulose as well as 4 mL of 17.5% sodium hydroxide were charged into a 20 mL sample bottle and left reacting for 30 min at room temperature. Then, 4 mL of Mill-Q water was added and left for another 30 min. After the total reaction time of 60 min had elapsed, the suspension was filtered by a G-4 glass filter and washed by Mill-Q water (3×30 mL). The remained solid was soaked in 1.0 mol/L acetic acid for 5 min. The neutralized solid was filtered and washed by water in the same manner as aforementioned. The cellulose yield was determined after the neutralized solid was dried at $105\text{ }^{\circ}\text{C}$ for 24 h.

The hemicellulose was calculated by the weight difference between holocellulose and hemicellulose.

The lignin content of biomass was determined using 72% sulfuric acid method, with some modifications [9]. 100 mg of biomass was treated by 1.5 mL of 72% sulfuric acid for 2 h at room temperature to hydrolyze and solubilize the carbohydrates. Then, the suspension was diluted with Mill-Q water (56 mL) to reduce the sulfuric acid to 3 wt% and boiled for 4 h. After treatment, the boiled suspension was filtered by a G-4 glass filter and washed by hot water until reached to a neutral pH. The remained solid was dried at $105\text{ }^{\circ}\text{C}$ for 24 h and the lignin yield was determined.

2. The protein content was determined by the Dumas method and calculated using the following equation [10]:

$$\text{Protein content (\%)} = N \times 6.25 \quad (3-1)$$

where N is the nitrogen content of WS expressed on a dry mass percentage and 6.25 is the nitrogen conversion factor.

The ash content was evaluated by combustion of the biomass in a furnace at $550\text{ }^{\circ}\text{C}$ for 4 h. A weight of 1.0 g of biomass was loaded into a platinum cell and the cell was set into an electric furnace (Super100, Shirota Electric Furnace Co. LTD, Tokyo, Japan). The furnace was then heated to $550\text{ }^{\circ}\text{C}$ and kept for 4 h. The weight of ash in biomass was measured after the combusted biomass cooling to the ambient temperature.

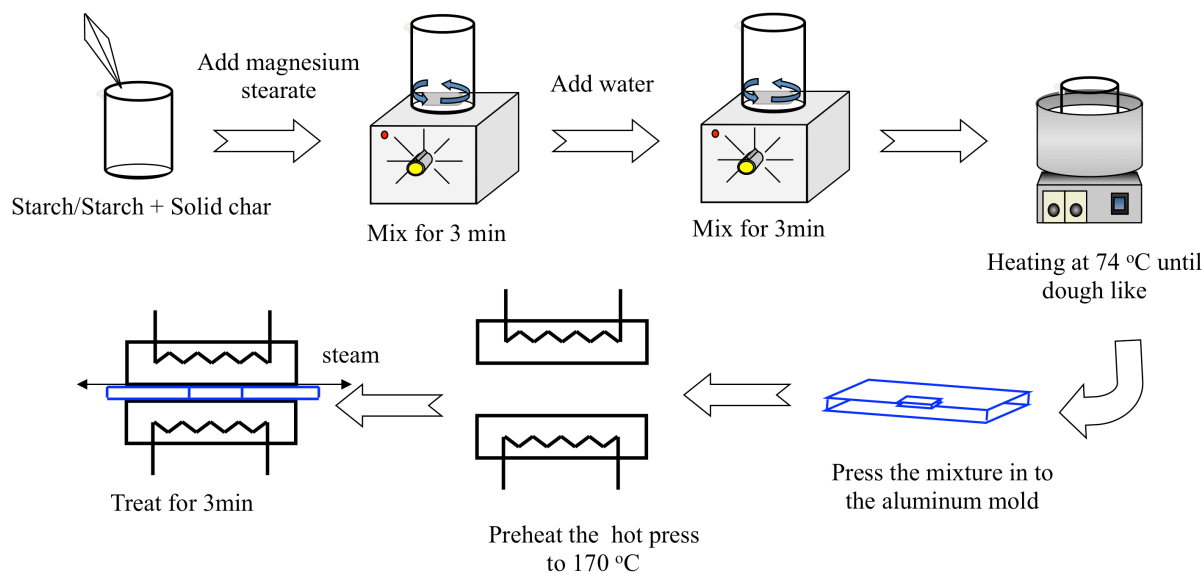


Figure 3-1. The experimental scheme for preparation of biodegradable foam by a modified compression-molding method.

3.2.5 Preparation of biodegradable foam

The solid char after subcritical water treatment was used for the preparation of biodegradable foams. The foams were prepared using a modified compression-molding method [5]. Before usage, the water content of the corn starch was measured by drying it in an oven at 105 °C for 24 h and the water content of corn starch was 12.6%. To make the starch foam, 1.0 g dry weight of corn starch was used. Part of the corn starch was replaced by 5%, 10%, 15% and 20% of solid char, respectively. Magnesium stearate was used as a releasing agent, at a level of 2.0% of the corn starch content by dry weight.

As shown in Fig. 3-1, corn starch, with or without the solid char, was mixed for 3 min by magnetic stirring. Then water was added; the ratio of the weight of water (added water + water contained in corn starch) to dry corn starch or to dry corn starch plus the solid char was kept at 1.0. The mixture was mixed for another 3 min and placed in a water bath at 74 °C until the mixture had thickened to a dough-like consistency. Then the dough-like mixture was transferred to an aluminum mold (50 mm × 20 mm × 3 mm) and the foam was prepared in a hot press (AH-2001, AS ONE, Osaka, Japan), which was preheated to 170 °C at a pressure of 2 MPa for 3 min. The density of the prepared foam was determined by weighting the foam and calculating the volume from the dimensions.

3.2.6 Morphology of prepared foam

For scanning electron microscopy (SEM) measurements, the foams were sputter-coated with Pt and examined with a Hitachi S-4700 scanning electron microscope.

3.2.7 Measurement of mechanical properties of prepared foam

Starch foam and foam containing 20% solid char were conditioned under different relative humidities (RH) before mechanical tests. The foams were conditioned in containers that contained anhydrous CaSO₄ (0% RH), or saturated salt solutions of CH₃COOK (23% RH) or Mg (NO₃)₂ (53% RH) at 50 °C for 3 d. The foams were cut into specimens of dimensions 50 mm × 10 mm × 3 mm after condition. Three-point bending tests were carried out to measure the flexural modulus E , flexural stress σ , and flexural strain ε of the prepared specimen. The flexural modulus was calculated using equations (3-2):

$$E = mL^3/4bh^3 \quad (3-2)$$

where E is the flexural modulus of the specimen; m is the slope of the tangent to the initial straight-line portion of the load-deflection line, L is the support span; and b and h are the width and height of the foam, respectively.

The flexural stress was calculated using equation (3-3):

$$\sigma = 3PL/2bh^2 \quad (3-3)$$

where σ is the stress at the midpoint of the specimen; P is the load at a given point on the load-deflection curve; and L , b and h are the same as in equation (3-2).

Flexural strain was calculated using equation (3-4):

$$\varepsilon = 6h\delta/L^2 \quad (3-4)$$

where ε is the strain in the outer surface at the midpoint of the specimen; δ is the maximum deflection of the center of the specimen; and L and h are as in equation (3-2).

3.3 Results and Discussion

3.3.1 Total carbohydrate content in the extract

The carbohydrate in the extract was the main target product during subcritical water liquefaction of biomass. We thus measured the carbohydrate content in the extract and the results are shown in Fig. 3-2. Fig. 3-2a shows the carbohydrate contents in the extracts treated at temperatures from 160 to 260 °C for 15 min. The carbohydrate content increased with the increasing of treatment temperature from 160 to 200 °C, and decreased significantly at temperatures higher than 200 °C. The decrease in carbohydrate content from 200 to 260 °C was ascribed to hydrolysis of poly- or oligo-saccharides and higher decomposition rate of monosaccharides as a result of the high ion product of water at these temperatures [11, 12]. The carbohydrate content decreased when treated for longer time at 200 °C (Fig. 3-2b).

These results showed that subcritical water treatment at 200 °C for 15 min was the optimum condition for obtaining carbohydrates. The carbohydrates obtained here were the

starting substances for producing bioethanol and effective derivatives such as 2, 5-furandicarboxylic acid. In this content, this extract solution could give their highest quantities. If the residue in this condition could be effective for preparing biodegradable foam, we can use all of WS effectively. Therefore, the residue obtained at this condition was used for preparing biodegradable foam.

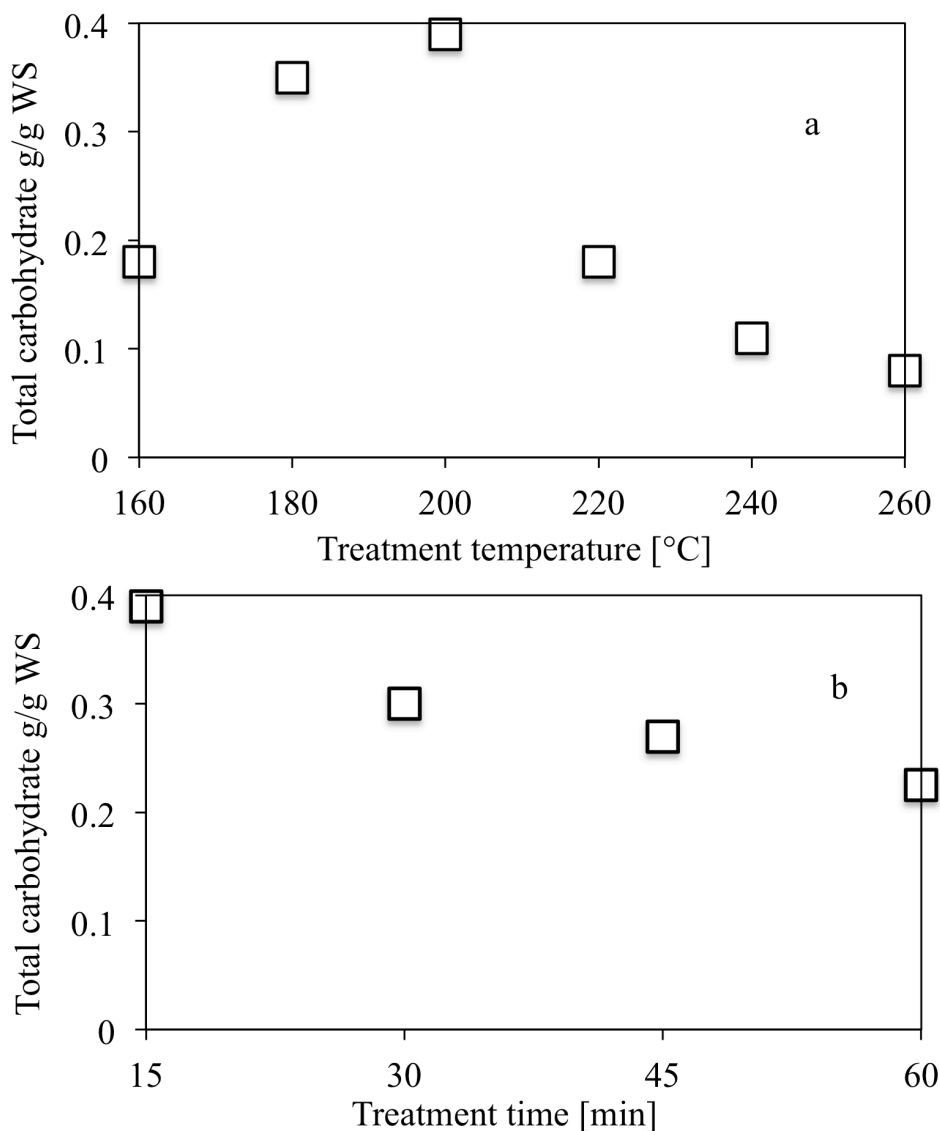


Figure 3-2. Changes in total carbohydrate content of walnut shells prepared
 (a) at the temperature range from 160 to 260 °C for 15 min and
 (b) at 200 °C for the treatment time of 15 to 60 min.

3.3.2 The components in walnut shells and solid char

The weight of the solid char was 54 mg when 100 mg of WS was treated at 200 °C for 15 min. Table 3-1 shows the contents and weights (calculated) of cellulose, hemicellulose,

lignin, protein and ash in WS and the solid char after treatment of the WS at 200 °C for 15 min (denoted by SC200). The cellulose, hemicellulose and lignin weights in 100 mg of original WS were 27.9, 30.2 and 39.1 mg, respectively. A percentage of 95.4% of hemicellulose (28.2 mg) had been degraded after the subcritical water treatment. The carbohydrates described above would be the mainly degradation products of hemicellulose and 10.4% of cellulose (2.9 mg) and 30.2% of lignin (11.8 mg) were hydrolyzed at the same time.

Table 3-1. WS and SC200 components (% wt), and mass balances based on the treatment of 100 mg of WS.

| Composition | WS (100 mg) | | SC200 (54.0 mg) | |
|---------------|-------------|---------|-----------------|---------|
| Cellulose | 27.9% | 27.9 mg | 46.3% | 25.0 mg |
| Hemicellulose | 30.2% | 30.2 mg | 2.6% | 1.4 mg |
| Lignin | 39.1% | 39.1 mg | 50.6% | 27.3 mg |
| Protein | 5.1% | 5.1 mg | N/A | N/A |
| Ash | 1.3% | 1.3 mg | N/A | N/A |

N/A: data not available

3.3.3 Optical scans and density of prepared foam

Optical scans of the prepared foams are shown in Fig. 3-3. The dimensions of the prepared foams were 48 mm × 19 mm × 3 mm. Replacing 20% of the corn starch by SC200 did not prevent formation of a foam plate. However, when the residue content was over 20%, the prepared foam was not plate-shaped. The color of the resulting foam became darker as the residue content increased.

Table 3-2 shows the densities of prepared foams. SC200 had little effect on the density of the prepared foams. The average density of the prepared foams was 346.6 kg/m³ and they were comparable to those of starch-lignin foams prepared using a similar method [5]. The starch foam density is known to depend on the starch source, water content, heating time, and heating temperature [13, 14]. However, here the similar densities of prepared foams were probably due to the mold size and total dry weight of corn starch or corn starch plus SC200, which were fixed at 48 mm × 19 mm × 3 mm and 1.0 g, respectively.

Foam densities for commercial use were approximately 20 kg/m³ [15], lower than that of the foam prepared here. However, starch foams prepared by extrusion had densities of approximately 60-70 kg/m³, which were comparable to those of commercial starch foams [16]. So, it was probably that solid char-containing foams with lower densities could be obtained if extrusion method was used in this study. Because the bulk density of starch foam was affected by the shear viscosity and the screw configurations of the extruder and lower bulk density could be obtained by changing the extrusion shear rates and screw configurations [17, 18].



Figure 3-3. Optical scans of foams (SC200 content from left to right: 0%, 5%, 10% and 20%).

Table 3-2. Densities of prepared foams.

| SC200 content (%) | Density (kg/m ³) |
|-------------------|------------------------------|
| 0 | 363 |
| 5 | 339 |
| 10 | 347 |
| 15 | 343 |
| 20 | 341 |

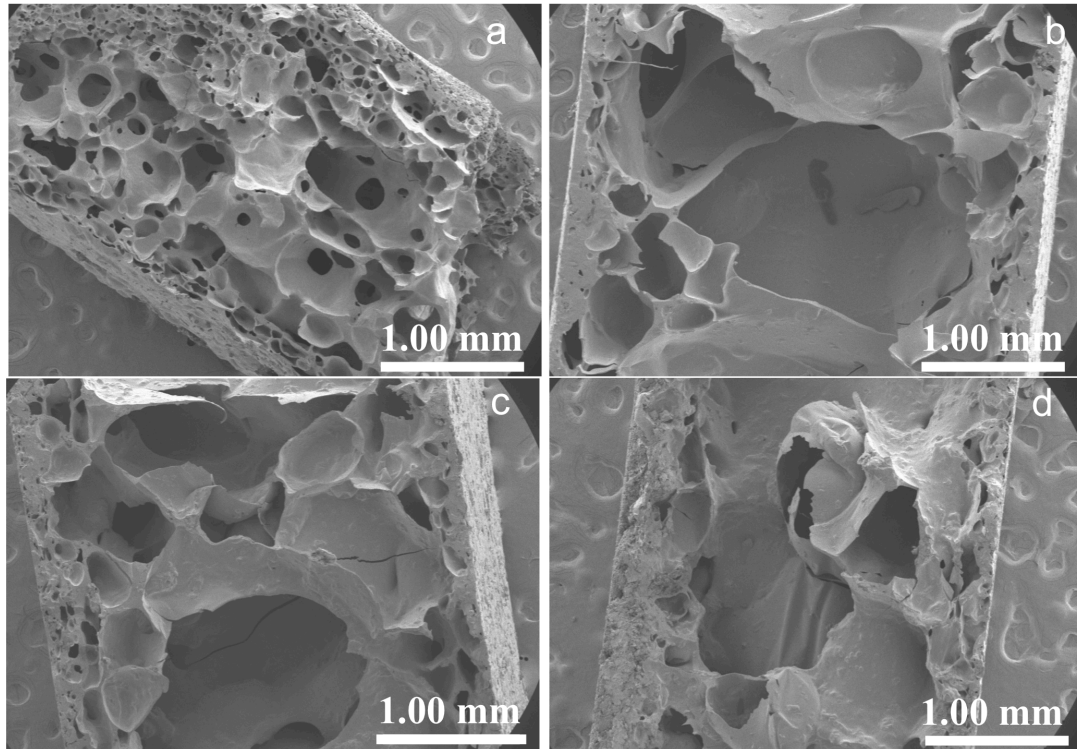


Figure 3-4. SEM images of prepared foams with SC200 contents of (a) 0%, (b) 5%, (c) 15% and (d) 20%.

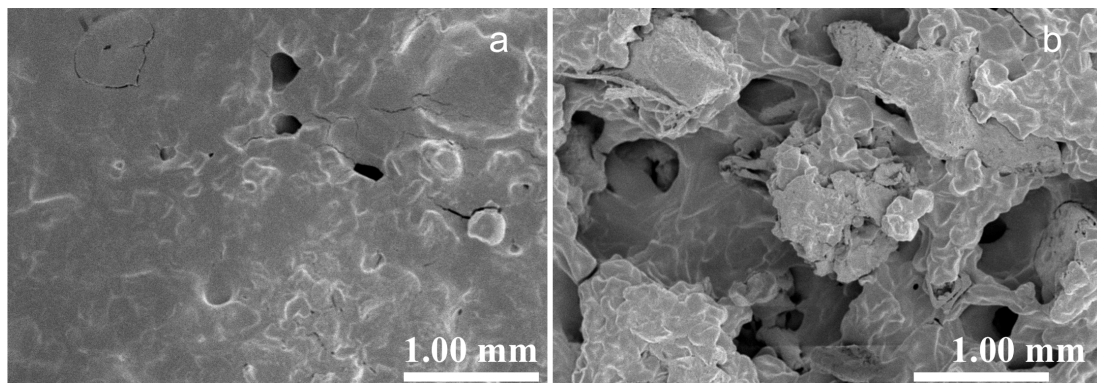


Figure 3-5. SEM images of prepared foams surface with SC200 contents of (a) 0% and (b) 20%.

3.3.4 SEM observation of prepared foam

Figure 3-4 shows the SEM images of prepared foams containing 0%, 5%, 15% and 20% of SC200, respectively. The micrograph of a cross-section of the starch foam (Fig. 3-4a) showed that the prepared foam had a sandwich-type structure. The outer skin, containing some small cells, comprised the surface of the prepared foam. The outer skin was denser than the interior. This was because the outer skin was close to the sheet of the hot press when the foam was prepared, so the water in the starch paste dried rapidly and the outer side of the

[5]. It was also reported that the starch foam combined with higher fiber content would lead to lower foam strength that directly affected the flexural modulus [20, 21]. However, the SC200 used in this study contained cellulose and lignin. So it was different from pure lignin and cellulose. There was a possibility that at the SC200 content of 10%, the ratio of cellulose and lignin contents could affect the flexural modulus. The detailed research will be done in the future. The flexural modulus of the prepared foam containing 20% SC200 was 1.5 times stronger than that of the starch foam. This indicated that SC200, which was prepared by a simple method, could effectively elevate the mechanical properties of corn starch foam.

The flexural stresses of the prepared foams containing 5%, 10% and 15% SC200 were similar to that of the starch foam. However, the flexural stress was 1.7 times stronger than that of starch foam when the SC200 content was increased to 20%. Replacing 20% of the corn starch by SC200 had little effect on the flexural strain of the prepared foam.

For comparison, the values of the mechanical properties of foamed polystyrene are as follows: flexural modulus, 105 MPa; flexural stress, 1.3 MPa; and the flexural strain, 1.7% [14]. Therefore, the flexural strains of the prepared foams in this study were similar to that of foamed polystyrene, and the flexural modulus and flexural stresses of the prepared foams were stronger.

Table 3-4. Effects of RH on mechanical properties of prepared foams.

| SC200 content (%) | Flexural modulus (MPa) | Flexural stress (MPa) | Flexural strain (%) |
|---|------------------------|-----------------------|---------------------|
| 0 | 209±6 | 3.1±1.1 | 1.6±0.5 |
| 5 | 220±17 | 2.4±0 | 1.1±0.1 |
| 10 | 186±16 | 3.1±0.5 | 1.7±0.4 |
| 15 | 226±8 | 2.6±0.8 | 1.2±0.2 |
| 20 | 322±0.1 | 5.5±0.3 | 1.8±0.1 |
| The values after ± show the standard deviations | | | N = 3 |

Table 3-4 shows the effect of RH on the mechanical properties of the prepared foams after condition at various RHs. It was clear that the maximum values of the flexural modulus for all the foam specimens investigated were obtained at 23% RH, and decreased at both lower and higher RHs. The reason for the weaker flexural modulus and strain was probably that at 0% RH, the cell structure of the starch-based foams was so brittle that cracks could form and propagate, and at 53% RH, the high amount of absorbed moisture weakened the cell structure appreciably [22]. The flexural modulus (156 MPa) of prepared foam containing 20%

SC200 conditioned at 53% RH was lower than the reported flexural modulus (395 MPa) for foams prepared using a similar method at a 1:1 (starch + 20% pure lignin): water composition [5]. The lower flexural modulus in this study was probable due to cellulose fiber in the SC200 [20, 21].

The flexural stress and flexural strain of the starch foam specimen increased with increasing of RH. However, as for the foam specimens containing 20% SC200, the highest values of flexural stress and flexural strain were obtained at the RH of 23% and lower values of them were obtained at the RHs of 0% and 53%.

Although the values of the mechanical properties for all the foam specimens investigated were lower than those before conditioning at various RHs (Table 3-3), they were still comparable to the values of the foamed polystyrene described above.

3.4 Conclusions

The solid char obtained at 200 °C for the treatment of 15 min was used to prepared biodegradable foam by a modified compression-molding method. It was found that SC200 could efficiently elevate the mechanical properties of corn starch foam. Replacing 20% of the corn starch by SC200 had no deleterious effects on density and morphology. The foams prepared by the present method had the similar flexural strains to that of foamed polystyrene, and larger flexural modulus and flexural stresses. This result suggested that the prepared foam could be a good candidate to take place of foamed polystyrene in the future.

Reference

- [1] Song, C. C.; Hu, H. Q.; Zhu, S. W.; Wang, G.; Chen, G. H., Nonisothermal catalytic liquefaction of corn stalk in subcritical and supercritical water. *Energy Fuels* 2004, *18*, 90-106.
- [2] Lynam, J. G.; Coronella, C. J, Yan, W.; Reza, M. T.; Vasques, V. R., Acetic acid and lithium chloride effect on hydrothermal carbonization of lignocellulosic biomass. *Bioresour. Technol.* 2011, *102*, 6192-6199.
- [3] Mok, W. S. L.; Antal, M. J., Uncatalyzed solvolysis of whole biomass hemicellulose by hot compressed liquid water. *Ind. Eng. Chem. Res.* 1992, *31*, 1157-1161.
- [4] Baumberger, S.; Lapiere, C.; Monties, B.; Dalla, V. G., Use of kraft lignin as filler for starch films. *Polym. Degrad. Stab.* 1998, *59*, 273-277.
- [5] Stevens, E. S.; Klamczynski, A.; Glenn, G. M., Starch-lignin foams. *Express. Polym. Lett.* 2010, *4*, 311-320.
- [6] Guan, J. J.; Eskridge, K. M.; Hanna, M. A., Functional properties of extruded acetylated

- starch-cellulose foams. *J. Polym. Environ.* 2004, 12, 113-121.
- [7] Dubois, M.; Gilles, K. A.; Hamilton, J. K.; Rebers, P. A.; Smith, F., Colorimetric method for determination of sugars and related substances. *Anal. Chem.* 1956, 28, 350-356.
- [8] Yokoyama, T.; Kadla, J. F.; Cheng, H. M., Microanalytical method for the characterization of fiber components and morphology of woody plants. *J. Agric. Food Chem.* 2002, 50, 1040-1044.
- [9] Carrier, M.; Loppinet-Serani, A.; Denux, D.; Lasnier, J.M.; Ham-Pichavant, F.; Cansell, F.; Aymonier, C., Thermogravimetric analysis as a new method to determine the lignocellulosic composition of biomass. *Biomass Bioenerg.* 2011, 35, 298-307.
- [10] Jung, S.; Rickert, D. A.; Deak, N. A.; Aldin, E. D.; Recknor, J.; Johnson, L. A.; Murphy, P. A., Comparison of Kjeldahl and Dumas methods for determining protein contents of soybeans products. *J. Am. Oil. Chem. Soc.* 2003, 80, 1169-1173.
- [11] Haghghat, K.; Kimura, Y.; Oomori, T.; Matsuno, R.; Adachi, S., Degradation kinetics of monosaccharides in subcritical water. *J. Food Eng.* 2005, 69, 309-313.
- [12] Sasaki, M.; Kabymela, B.; Malaluan, R.; Hirose, S.; Takeda, N.; Adschiri, T.; Arai, K.; Cellulose hydrolysis in subcritical and supercritical water. *J. Supercrit. Fluids* 1998, 13, 261-268.
- [13] Shogren, R. L.; Lowton, J. W.; Doane, W. M.; Tiefenbacher, K., Structure and morphology of baked starch foams. *Polymer* 1998, 39, 6649-6655.
- [14] Glenn, G. M.; Orts, W. J.; Nobes, G. A. R., Starch, fiber and CaCO₃ effects on the physical properties of foams made by a baking process. *Ind. Crop. Prod.* 2001, 14, 201-212.
- [15] Tatarka, P. D.; Cunningham, R. L., Properties of protective loose-fill foams. *J. Appl. Polym. Sci.* 1998, 67, 1157-1176.
- [16] Willet, J. L.; Shogren, R. L., Processing and properties of extruded starch/polymer foams. *Polymer* 2002, 43, 5935-5947.
- [17] Fletcher, S. I.; McMaster, T. J.; Richmond, P.; Smith, A. C., Rheology and extrusion of maize grits. *Chem. Eng. Commun.* 1985, 32, 239-262.
- [18] Nabar, Y.; Narayan, R.; Schindler, M., Twin-screw extrusion production and characterization of starch foam products for use in cushioning and insulation applications. *Polym. Eng. Sci.* 2006, 46(4), 438-451.
- [19] Lowton, J. W.; Shogren, R. L.; Doane, W. M.; Tiefenbacher, K. F., Effect of batter solids and starch type on the structure of baked starch foams. *Cereal Chem.* 1999, 76, 682-687.
- [20] Carr, L. G.; Parra, D. F.; Ponce, P.; Lugao, A. B.; Buchler, P. M., Influence of fibers on the mechanical properties of cassava starch foams. *J. Polym. Environ.* 2006, 14, 179-183.
- [21] Cinelli, P.; Chiellini, E.; Lawton, J. W.; Imam, S. H., Foamed articles based on potato

starch, corn fiber and poly (vinyl alcohol). *Polym. Degrad. Stab.* 2006, *91*, 1147-1155.

[22] Preechawong, D.; Peesan, M.; Supaphol, P.; Rujiravanit, R., Characterization of starch/poly(ϵ -caprolactone) hybrid foams. *Polym. Testing* 2004, *23*, 651-657.

Chapter 4

Characterization of surface properties of woody thin boards composed of commercially available lignin and cellulose: Relationship between the orientation of lignin and water repellency

4.1 Introduction

In chapter 3, the biodegradable foams whose mechanical properties could be comparable with those of the commercial foamed polystyrene were prepared. However, the corn starch used here is the most common carbohydrate in human diets and the source material of many sugars. Moreover, the biodegradable foam prepared showed a hydrophilic property that limited its application. Therefore, we needed to improve the hydrophobicity of the prepared foam.

Wood plastic composites (WPCs) that are produced by thoroughly mixing wood particles and waste plastic are a promising material to resolve the manager probable of waste plastic. In the past decades, many kinds of WPCs, i.e., polypropylene or high-density polyethylene or polycarbonate or polystyrene or polyvinyl chloride/wood flour compositions, were prepared by various processing methods [1-9]. They have become prevalent in many building applications, such as decking dock, landscaping timbers and fencing [10-13]. However, the highly hydrophilic characters of lignocellulosic biomass make them incompatible with thermoplastics that are highly hydrophobic. Such incompatibility produces poor interfacial adhesion between matrix and filler, which results in poor mechanical property because stress could not be transferred properly from the matrix to the fibers [14,15]. Besides, the highly hydrophilic characters also made lignocellulosic biomass vulnerable to attack by fungi and termites, resulting in the loss of dimensional stability, greater decay susceptibility and low durability [16]. Therefore, it was important to improve the water repellency of lignocellulosic biomass before preparation of WPCs.

Up to now, the water repellency has mainly been improved by the microscopic roughness of the surface [17] and the chemical approach [18] whereas few researchers focused on improving the hydrophobicity of lignocellulosic biomass through removal of the

hydrophilic component in lignocellulosic biomass [14]. The hydrophilic of lignocellulosic biomass was due to the hydroxyl groups in cellulose and hemicellulose. The solid char that was obtained after subcritical water treatment of lignocellulosic biomass always had higher water repellency and higher lignin and cellulose contents compared with those of original lignocellulosic biomass [19]. Therefore, the solid char would be good source for preparation of WPC, or in other words, the waste plastic was a good candidate to replace corn starch for improving the hydrophobicity of starch foam prepared in Chapter 3.

Before preparation of WPC, clarification of the surface property of WPC composed of only woody materials would be helpful to understand the surface modification and discuss the standard property. Meanwhile, conventional WPCs are prepared by materials such as lignin, cellulose, and other chemicals. This complex composition is easily an obstacle for elucidating the method to design the surface of WPCs with the desired properties. The investigations using the purified woody materials could give the coarse and essential findings.

Therefore, woody thin boards that served as a precursor of WPC were prepared by mixing purified lignin, cellulose (model substances for solid char) and water through compression molding method. The composition region where thin boards were obtainable was revealed on the ternary lignin/cellulose/water system. Thereafter, we characterized the physicochemical properties of woody thin boards, such as the contact angle, relative permittivity, chemical composition at the surface, and surface structure. The orientation of lignin was thereby discussed. As a result, we discussed the relationship between the water repellency and the orientation of lignin within woody thin boards.

4.2 Materials and Methods

4.2.1 Materials

Purified lignin and cellulose (crystalline cellulose I) were purchased from Wako Pure Chemical Ltd. (Osaka, Japan).

4.2.2 Preparation of woody thin boards by the compression molding method

Lignin and cellulose were mixed within a certain composition ratio for 20 min. Water (0~40 mg) was thereafter added to the mixture (30 mg) and mixed for 2 min. The above mixture was injected into the aluminum mold and the woody thin board was prepared by a hot press (AH-2001, AS ONE, Osaka, Japan) that was preheated to 180 °C with the pressure of 25 MPa for 10 min. Afterwards, the mold was considerably cooled down to recover woody

thin board. The dimensions of recovered woody thin boards were 10 mm × 10 mm × 0.3 mm.

4.2.3 Measurement of contact angle

The contact angle of water on the sample was measured by using an auto-contact angle/surface tensiometer (DSA 10, Krüss, Switzerland). The image of the water drop was recorded and analyzed with data acquisition software after 1 min. Then, the contact angle was measured by drawing a line at the edge of the water drop.

4.2.4 Dielectric measurement

To measure the frequency dependency of capacitance and conductance, we used an Agilent 4291B Impedance Analyzer (Agilent Technologies, Palo Alto, CA) with a homemade cell. The instrument was calibrated using air and a calibrated short and load circuit. Woody samples were loaded into the measuring cell, and its capacitance (C_p) was measured at frequencies from 1 MHz to 700 MHz to determine the relative permittivity (ϵ') by using the following equation:

$$\epsilon' = C_p/C_0, \quad (4-1)$$

where C_0 represents the cell constant. To minimize the errors that arise in calculation, the accuracy of our experimental data on three calibration samples (water, ethanol, and methanol) was checked to obtain the difference in permittivity from the published data [20]. It was within 4% of relative error in all cases. Finally, we determined the ϵ' value at $f = 0$ Hz by extrapolating the ϵ' value to 0 Hz.

4.2.5 ATR-FTIR

The infrared (IR) spectroscopy was performed to detect the surface of woody thin boards with an FT/IR-4300ST equipped with an attenuated total reflectometry (ATR) unit (ZnSe crystal) (Nihon Bunko Co., Ltd., Tokyo, Japan). The resolution was 4 cm⁻¹. The subtraction of spectra in the buffer was carried out to remove the contribution from water bands. The accuracy of the frequency reading was better than ±0.4 cm⁻¹. ZnSe crystal can give the analytical space with 100 nm in depth from the surface.

4.2.6 X-ray diffraction measurement

The crystalline of woody thin boards was examined using a powder X-ray diffraction (XRD) with monochromated CuK α radiation, using Rigaku Geiger flex RAD-C and RINT2000 diffractometers (Tokyo, Japan). The diffraction patterns were measured from $2\theta = 8$ -60 degree with scan speed of 0.1 degree/min at 40 kV and 30 mA.

Relative crystallinity index (CI) of the cellulose I was calculated by the following equation [21]:

$$CI (\%) = 100 \times (I_{(200)} - I_{am}) / I_{(200)} \quad (4-2)$$

where $I_{(200)}$ and I_{am} represent intensities at $2\theta = 18.5^\circ$ (amorphous state) and 22.5° (crystalline I state), respectively.

4.2.7 Scanning electron microscopic observation

The morphology of woody thin boards was observed by using a scanning electron microscope (SEM) (S-4700, Hitachi Ltd., Tokyo, Japan). Woody thin boards were mounted on metal stubs by double-faced tap and images were taken. Prior to imaging samples were coated with Pt in a sputter coater (E1030 Sputter, Hitachi Ltd.).

4.2.8 Atomic force microscopic observation

4.2.8.1 Observation

The surface of woody thin board was imaged by using the scanning probe microscope, SPM 9600 (Shimadzu Co., Kyoto, Japan). The atomic force microscopic (AFM) measurements were carried out at ambient conditions (25 °C) using dynamic mode with constant amplitude. A silicon cantilever OMCL-AC200TS (OLYMPUS, Japan), having a tetrahedral shape with a spring constant of 9 N/m and an oscillation frequency of 150 kHz, was used to scan the surface of woody thin boards. The scan rate was 1 Hz and the resolution was 512 samples per line. Scanning was performed at 3 different positions of each sample and representative images have been shown here.

4.2.8.2 Estimation of surface roughness

The digital data for profile y_i along the line in the scanned area by AFM was acquired. The equipped software of AFM automatically gave the several types of roughness by using the digital data for the scanned area. Thereafter, we used three different definitions on the roughness. The first roughness is the arithmetic average, R_a , of the absolute values of the roughness profile y_i in ordinates. The value was calculated by the equation: $R_a = \sum |y_i| / n$. The second roughness is the root mean square average, R_{rms} . The value was calculated by using the equation:

$$R_{rms} = (\sum y_i^2 / n)^{1/2} \quad (4-3)$$

Both R_a and R_{rms} are characterized by ISO 4287 standard (1997) [22]. The third is the Japanese industrial standard (JIS), R_{jis} [23]. The R_{jis} value is calculated based on the ten

highest peaks and lowest valleys over the entire sampling length:

$$R_{jis} = \sum(y_{pi} - y_{vi})/10 \quad (4-4)$$

where y_{pi} and y_{vi} are the i -th highest peak and lowest valley, respectively.

4.3 Results and Discussion

4.3.1 Screening of the woody thin boards preparation using lignin/cellulose/water system

In the first series of experiments, we prepared the woody thin boards in the variety of composition of lignin, cellulose, and water, by the compression-molding method (180 °C, 25 MPa for 10 min).

Figure 4-1 shows the relationship between the preparation of woody thin boards and their composition. In the case of the water content greater than 55%, samples in the powder-like aggregates including much moisture were obtained nevertheless to the ratio of lignin and cellulose. The treatment of hot press for 10 min at 180 °C was obviously not enough to achieve the dewatering. In the case of 35~55% of water content, woody thin boards were obtainable at the composition ratios of 4:6, 3:7, and 2:8 for lignin/cellulose. When the water content was less than 35%, the obtained samples were in powdered-state, not in thin board-state. The same was true for the compression molding without water. Apart from that, thin board-like plates that apparently had similar architecture to woody thin boards were obtained in the specific composition (triangles in Fig. 4-1). Meanwhile, thin board-like plates including moisture were subjected to be disaggregated, which was probably due to the insufficient dewatering.

It was then revealed that the region where woody thin boards were obtainable was limited (the area described by opened circles in Fig. 4-1). It was likely that the adequate initial water content and composition ratio of lignin and cellulose were required for the formation of woody thin boards. Their compositions in the condition used here were summarized in Table 4-1. Those surface properties were investigated in the following.

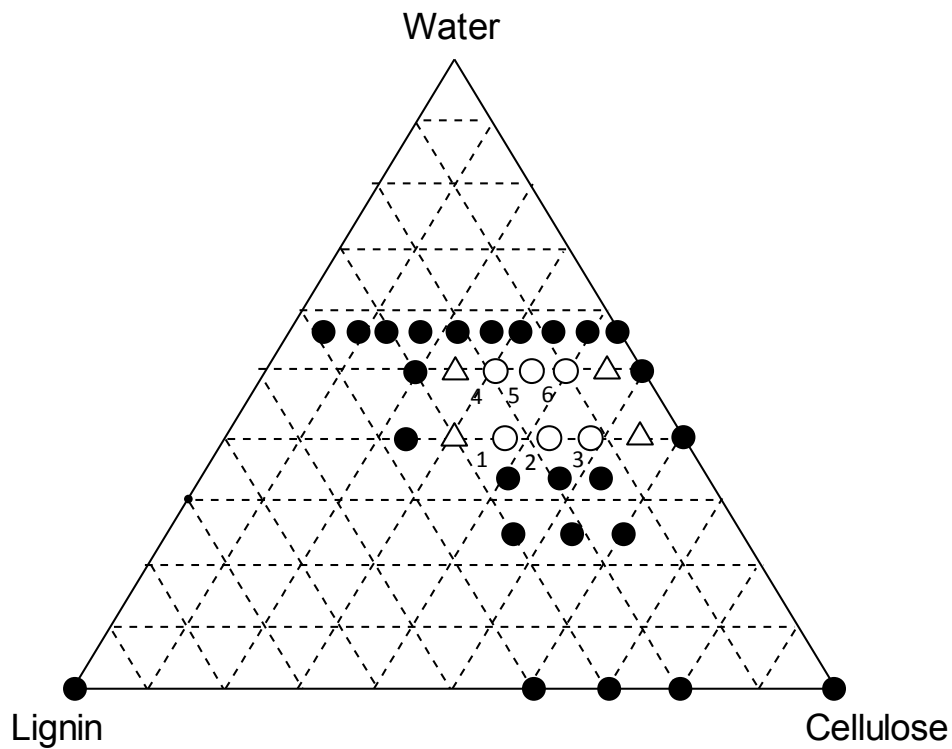


Figure 4-1 Lignin/cellulose/water ternary system for the preparation of woody thin boards. Open circle: thin boards were obtained. Closed circle: thin boards were not obtained. Open triangle: thin board-like plates were obtained although their mechanical strength was too weak to keep themselves. Total amount of lignin and cellulose was 30 mg. The condition of compression molding was 180 °C, 25 MPa for 10 min. Refer to Table 1 for the number subscripted to the open circle in a figure.

Table 4-1 Mixture ratio and surface roughness of woody thin boards used in this study.

| Board | C/L/W ^a [mg/mg/mg] | Surface roughness ^b | | |
|-------|----------------------------------|--------------------------------|----------------|----------------|
| | | R_a [nm] | R_{jis} [nm] | R_{rsm} [nm] |
| 1 | 18/12/20 | 9.02 | 21.1 | 200.6 |
| 2 | 21/9/20 | 16.1 | 48.8 | 573.1 |
| 3 | 24/6/20 | 14.4 | 45.2 | 401.5 |
| 4 | 18/12/30 | 13.3 | 44.9 | 405.8 |
| 5 | 21/9/30 | 3.80 | 13.3 | 631.8 |
| 6 | 24/6/30 | 16.6 | 31.2 | 188.0 |

a. C: cellulose, L: lignin, W: water. b. Definition of surface roughness. R_a : the arithmetic average, R_{rsm} the root mean square average, R_{jis} : the Japanese industrial standard-characterized roughness.

4.3.2 Surface properties of woody thin boards

4.3.2.1 Macroscopic surface properties of woody thin boards

The contact angle is a macroscopic index for the interaction between the surface of boards and liquid droplet. In the case of water droplet, the contact angle is considered as the index of water repellency. Figure 4-2(a) shows the contact angle for each board. Boards-2~4 had large contact angles (55~60 °C) relative to board-1, -5 and -6 (45~48 °C). Comparing the contact angle with the composition, it was unlikely that the contact angle for woody thin boards depended on their composition ratio of lignin/cellulose/water (Fig. 4-1 and Table 4-1).

In general, the water repellency is determined by the interaction between the surface of boards and water droplets. The interaction of interface with polar liquid such as water depends on the polarity of interface. The measurement principle of the impedance analyzer gives the permittivity at the surface of samples. Therefore, we determined the polarity (hydrophilicity) of boards by measuring the relative permittivity. Figure 4-2(b) shows the relative permittivity of each board. Overall, the relative permittivity of boards-1~6 was in the range of 5 to 10, which was consistent with the results reported by Paz *et al.* [24]. In our experiments, the boards-2~4 had lower relative permittivity than other boards. Meanwhile, it was unlikely that the relative permittivity, as well as contact angle, depended on their composition ratio of woody thin boards shown in Fig. 4-1 or Table 4-1.

From a comparison of Fig. 4-2(a) with Fig. 4-2(b), it seems to show a certain correlation between the contact angle of boards and their permittivity (Fig. 4-2(c), $r = 0.920$), suggesting that woody thin boards with lower permittivity have the stronger water repellency. This apparent correlation implies the possibility that the interaction of water droplets with surface of woody thin boards originates from their low relative permittivity. As stated before, the permittivity (polarity) was not always determined by the composition ratio of lignin/cellulose/water of the whole woody thin board. The investigation of chemical composition at the surface would be therefore required to discuss the polarity at the surface of woody and thin boards.

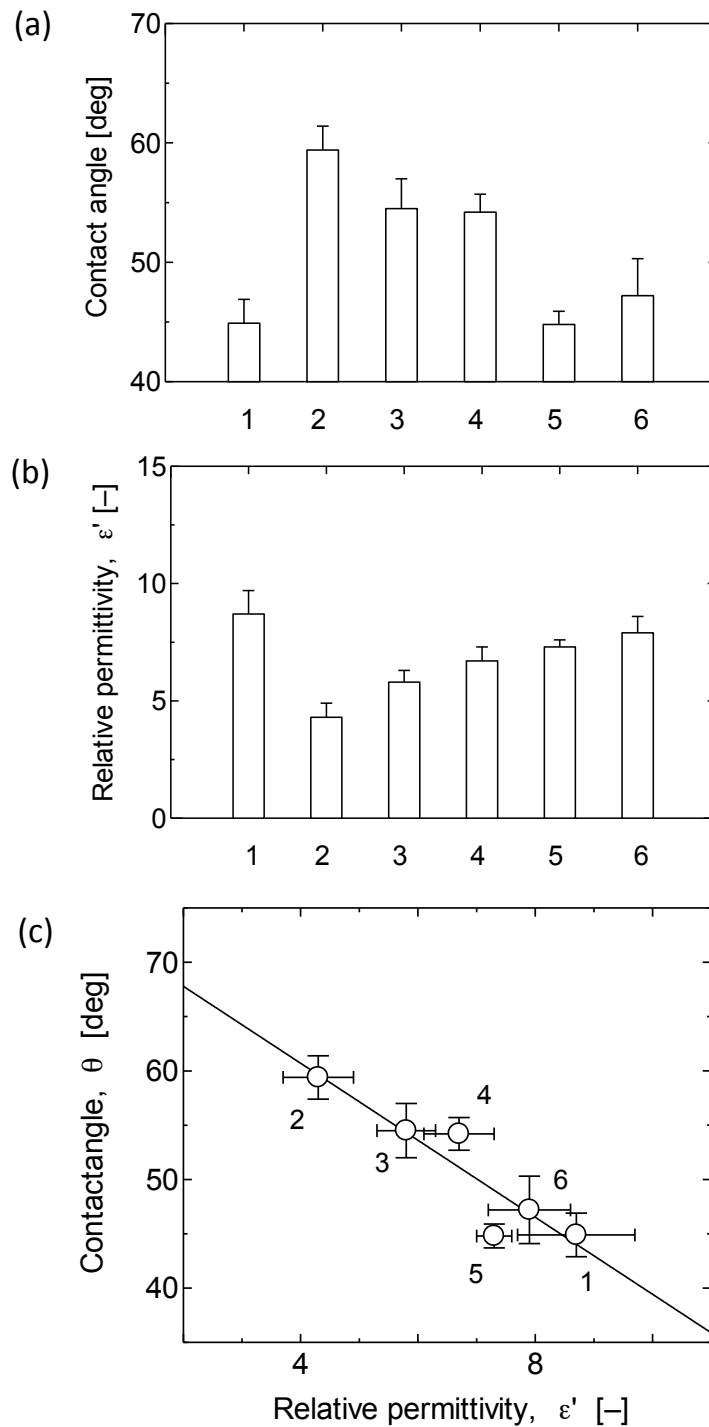


Figure 4-2 (a) Contact angle for woody thin boards and (b) their relative permittivity. (c) Comparison of the contact angles of woody thin boards with their relative permittivity. Solid line is the regressed line ($r = 0.920$). All the experiments were performed at least three times.

4.3.2.2 Chemical composition of the surface of woody thin boards as microscopic property

Fourier transferred infrared (IR) spectroscopy equipped with an attenuated total reflectometry (ATR) unit, which is called as ATR-FTIR, is one of the most powerful techniques to detect the chemical composition of 100 nm in depth of surface.

Figure 4-3(a) shows the spectra for six boards. Overall characteristics observed in spectra were first discussed. The major peaks that show up in the spectra are the broad band at 3320 cm^{-1} , as attributed to hydroxyl groups in phenolic and aliphatic structures and the bands centered at 2925 and 2858 cm^{-1} predominantly arising from C-H stretching in aliphatic C-H and aromatic methoxyl groups. The band at 1625 cm^{-1} is attributed to conjugate carbonyl stretching in lignin according to the previous report [25, 26]. Likewise, the bands for aromatic skelton vibration in lignin are assigned at 1600 , 1511 , 1422 cm^{-1} . Besides, the bands at 1127 and 1035 cm^{-1} arise from the aromatic C-H in-plane deformation for syringyl and guaiacyl type, respectively. In contrast, aromatic C-H out of plane bending appears at 844 cm^{-1} .

In the following, we compared the absorbance of lignin-derived peak (hydroxyl group, carbonyl group, and aromatic skelton vibration) if these bands depended on the composition ratio of lignin and cellulose. Overall, the board-1 had the smallest strength in the functional groups, as shown in Fig. 4-3(b)-(d). Boards-2 and -3 had significantly large strength of absorption and the board-2 had the highest peak with respect to those three adsorptions. In this measurement using ATR-FTIR as well as the measurements of both the contact angle and the relative permittivity, it was unlikely that the strength of absorption for boards depended on their composition ratio of lignin/cellulose/water.

To discuss the influence of surface composition of woody thin boards against the relative permittivity, the absorbance of each peak was again plotted against the corresponding relative permittivity (Fig. 4-4(a)). The relative permittivity of boards (Fig. 4-4(a) right: $r = 0.920$) was apparently correlated with the aromatic skelton vibration better than the hydroxyl group (Fig. 4-4(a) left: $r = 0.810$) and the carbonyl group (Fig. 4-4(a) middle: $r = 0.820$). The hydroxyl groups are involved not only in lignin but also in cellulose. In contrast, other two groups derive from only lignin. In general, the increase in the number of hydroxyl group must become hydrophilic, which is not consistent with the correlation as shown in the left-sided figure of Fig. 4-4(a). It is, therefore, implied that the correlation for the hydroxyl group corresponds to the presence of lignin rather than cellulose.

From results obtained by ATR-FTIR, lignin was likely to be present at the surface layer of board-2 and -3 whereas lignin was unlikely to be present at the surface layer of boards-1, -5 and -6.

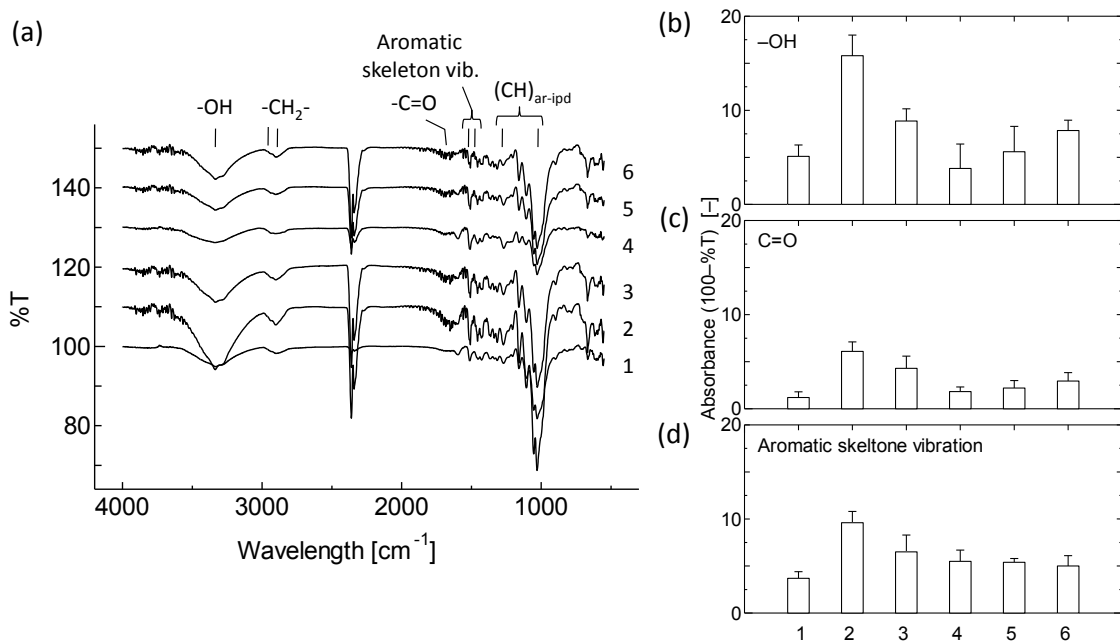


Figure 4-3 (a) ATR-FTIR spectra for various woody thin boards. Peak absorbance for (b) hydroxyl group, (c) carbonyl group, and (d) aromatic skeleton vibration. All the experiments were performed at least three times.

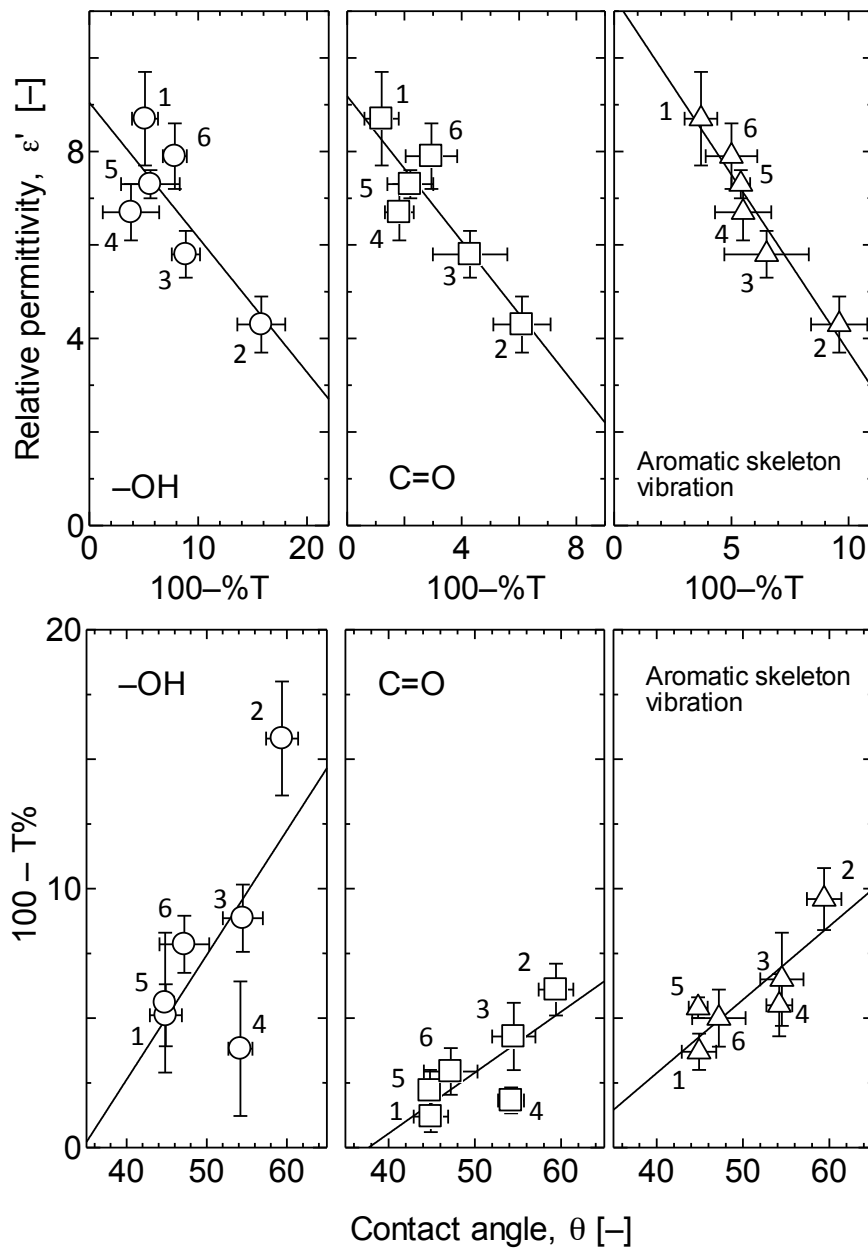


Figure 4-4 (a) Comparison of the intensity of various adsorptions of various woody thin boards with their relative permittivity. Regression coefficients of three (from left to right) were $r = 0.810, 0.820, \text{ and } 0.920$, (b) Comparison of the contact angle with the intensity of various adsorption of various woody thin boards. Regression coefficients of three (from left to right) were respectively. $r = 0.675, 0.783, 0.856$, respectively.

4.3.2.3 X-ray diffraction (XRD) study of woody thin boards

In contrast to the last section addressing the orientation of lignin in the boards, the present section addressed cellulose by using an XRD measurement. Previously, an XRD could give the plausible interpretation about the structure of microcrystalline cellulose at the surface of materials [27, 28]. We examined the XRD measurement and Fig. 4-5(a) shows the XRD spectra for boards-1~6. The peaks observed at $2\theta = 17.4^\circ$ and 22.5° resulted from a crystalline I structure of cellulose, according to the previous reports [27, 28]. In Fig. 4-5(a), peaks at $2\theta = 18.5^\circ$ and 22.5° are assigned to the amorphous and crystalline I states (Miller's index: (200)), respectively [29]. The CI calculated from intensities I_{am} at $2\theta = 18.5^\circ$ and $I_{(200)}$ at 22.5° was shown in Fig. 4-5(b). Overall, the CI values were at around 90 % and also independent of the composition of cellulose/lignin/water system, except for the board-6 (CI = 78%). Judging from the spectra of boards, it was unlikely that crystalline cellulose I altered to crystalline cellulose II, III, or IV (that have the main peak at $2\theta = 19\sim 21^\circ$) and the (100-CI) value here is corresponding to the content of amorphous cellulose. Therefore, it was considered that microcrystalline cellulose remained in the board over the compression molding at 180 °C and 25 MPa for 10 min although a part of cellulose altered to the amorphous type of cellulose, which was not depending on the composition of cellulose, water and lignin.

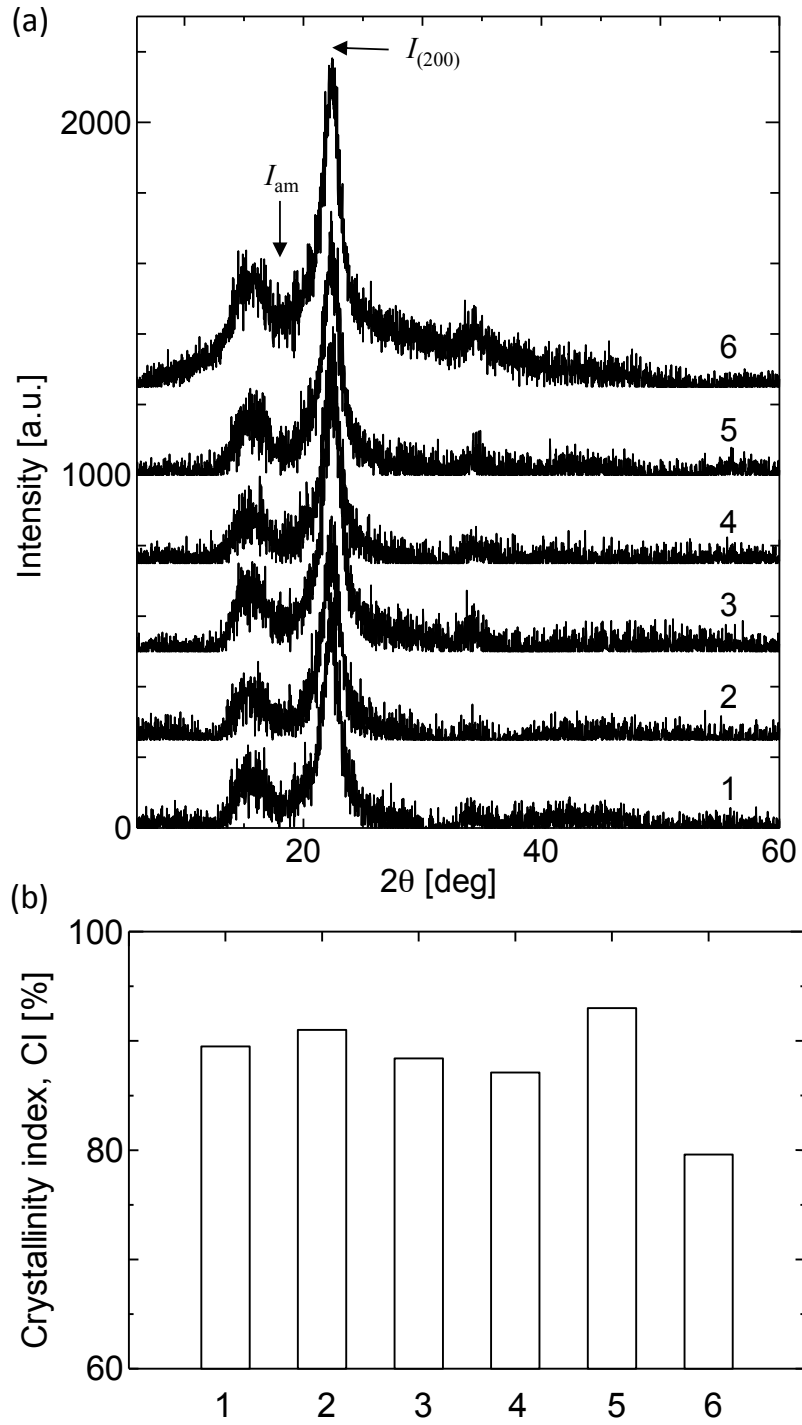


Figure 4-5 (a) XRD spectra for various woody thin boards. (b) The crystallinity index (CI) for woody thin boards. The definition of CI is $CI (\%) = 100 \times (I_{(200)} - I_{am}) / I_{(200)}$.

4.3.2.4 Surface state of woody thin boards

Roughness of surface also gives the qualitative information about the presence of lignin on the surface of woody thin boards. For examples, Moniruzzaman and Ono [27] have reported that the presence of lignin on cellulose in woody material appears to give the rough surface. Thereby, we observed the surface of woody thin boards to confirm the presence of lignin on cellulose.

A scanning electron microscopic (SEM) is a powerful tool for the visualization of macroscopic surface structure of samples. SEM images of boards are shown in Fig. 4-6 (left). Boards-5 and -6 had the smooth surface (Fig. 4-6, left). In contrast, it was found that boards-2, -3, and -4 had the rough surface. Roughness at the surface of these boards was also microscopically observed by using an atomic force microscopy (AFM). The typical AFM images were shown in Fig. 4-6 (middle). There was a bulge and valley in the surface of board-2 whereas a relatively smooth surface was there in board-5. Such geometries reflect the microfibrillar structure of cellulose [21]. It seems that cellulose microfibrils lies one upon others to form the surface of woody thin boards. We discussed the orientation of lignin on cellulose by using the phase image of AFM (Fig. 4-6 (right)). The elastic modulus for microcrystalline cellulose I, amorphous state of cellulose I, and lignin were 14~150 GPa [30], 2~10 GPa [31], and 2.1~6.7 GPa [32], respectively. In general, the elastic modulus of materials correlates with their phase image obtained by an AFM observation. We addressed the boards-5 and -6 that were not significantly including lignin. The phase images had the high phase region, suggesting the presence of microcrystalline cellulose on the surface. Addressing boards-2 and -3, the regions with different phases could be observed (arrows A) other than the phase region (arrows B) similar to that observed in boards-5 and -6. The region arrowed by B was assigned to cellulose. Meanwhile, the region arrowed by A could not be identified as lignin or amorphous cellulose from only the AFM observation.

The direct observation using SEM and AFM suggests that there exists microfibrillar structure of cellulose I on the surface of woody thin boards.

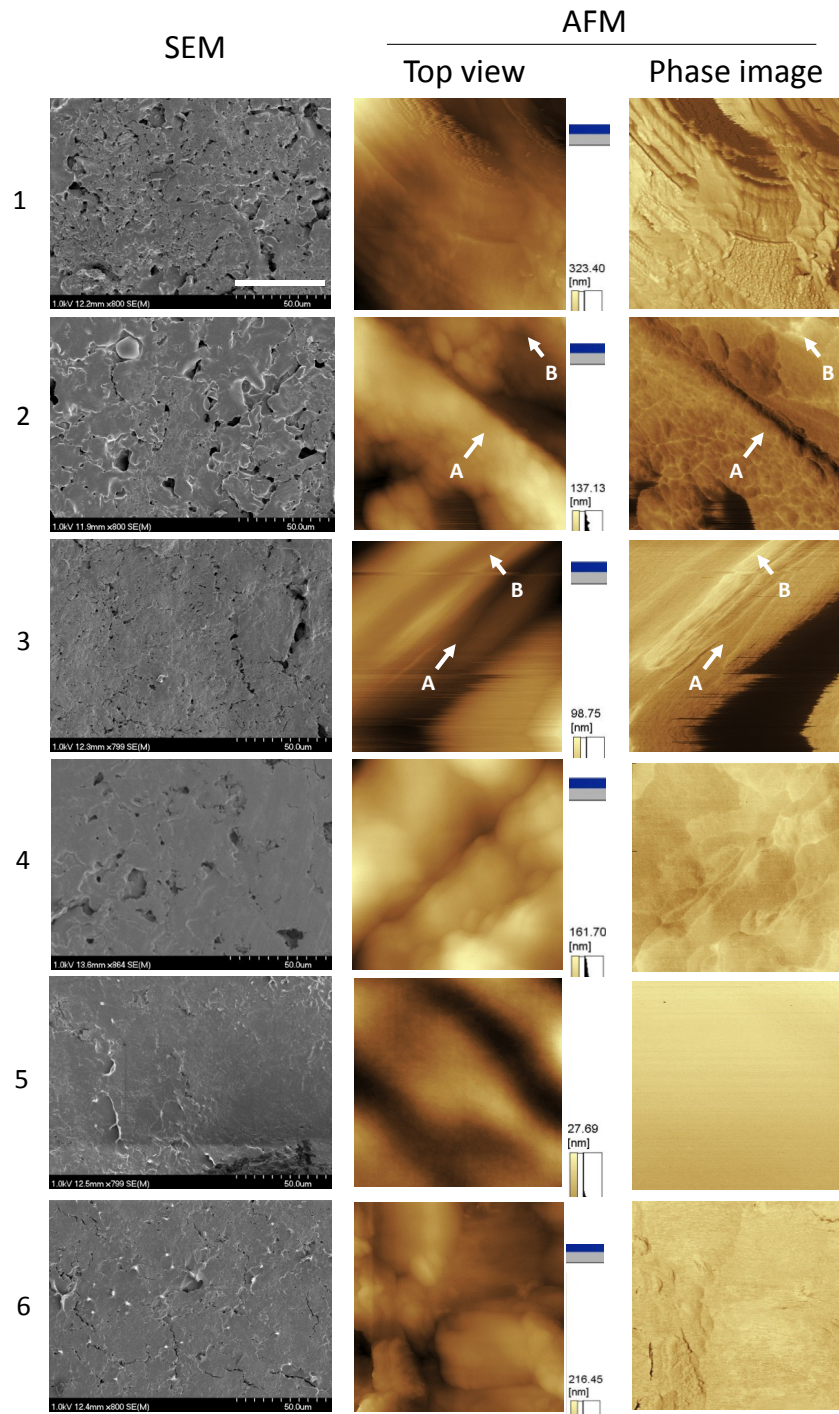


Figure 4-6 SEM (left) images of woody thin boards. Topographic (middle) and phase (right) images obtained by AFM observations. Scan size of SEM and AFM is 150 mm×110 mm and 1mm×1mm, respectively. White bar in SEM image represents 50 mm. The white arrows in phase images for boards-2 and -3 indicate the lignin (A) and the cellulose surface (B).

4.3.3 Microscopic surface structure of woody thin boards

The surface roughness is an alternative factor for the water repellency. For examples, the *Lotus effect* has been well known as the water repellency that originates from the surface with the extreme roughness [17,18]. In this section, we investigated how the orientation of lignin into the surface of woody thin boards affected the surface geometry.

We first discussed the surface roughness along with the line in AFM images of boards-2 and -5, by using Figs. 4-7(a) and (b), respectively. Assemblies of cellulose fibrils were observed in both cases. The surface profiles along with the line A-B was shown in Figs. 4-7(c) and (d), indicating that the surface of board-2 relative to board-5 was obviously rough. By using the profile, we estimated the arithmetic average (R_a), the root mean square average (R_{rms}), and the Japanese industrial standard-characterized R_{jis} . The calculated indexes are summarized in Table 1. Overall, three indexes showed the similar trend, although some exceptions were involved (board-6 in R_a and board-5 in R_{rms}). The R_{jis} value as a typical example was shown in Fig. 4-7(e). Boards-2, -3, and -4 have the relatively definite rough surface in contrast to boards-1, -5, and -6. This result quantitatively supported the qualitative discussion with SEM and AFM observations.

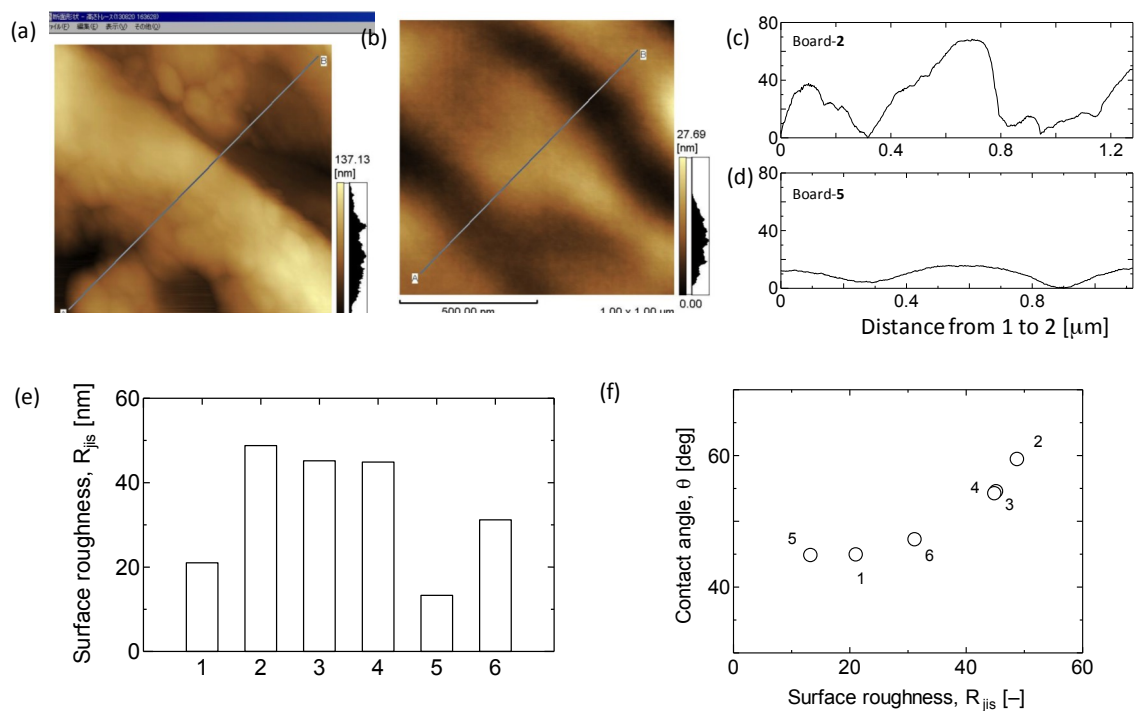


Figure 4-7 AFM images of (a) board-2 and (b) board-5. Profiles of z-axis for (c) board-2 and (d) board-5. (e) Roughness R_{jis} of woody thin boards. (f) Comparison of contact angle of woody thin boards with their surface roughness R_{jis} .

4.3.4 Possible interpretation of water repellency, hydrophobicity and surface roughness for woody thin boards

From a comparison of a roughness R_{jis} with contact angle, a certain correlation was observed as shown in Fig. 4-7(f). The same was coarsely true for comparisons of R_a and R_{rms} with contact angle although some deviations were observed (data not shown). Meanwhile, both had no causation, because there is a common reason, the orientation of hydrophobic lignin into the surface of woody thin boards. Again, considering the correlation seen in Fig. 4-2(c), the orientation of lignin at the surface resulted in an increased hydrophobicity of surface to improve the water repellency. Alternatively, a creation of roughness originated from lignin remained at the surface of woody thin boards (See board-2 in Fig. 4-6). Therefore, the apparent correlation between the contact angle and the surface roughness had no causation in the present conditions. Supplementary, the contact angle should be, ideally, negatively correlated with the surface roughness [33,17].

Based on the above discussion, it was revealed that the water repellency depended on the hydrophobicity of surface rather than the surface roughness. Meanwhile, it seems that the orientation of lignin at the surface had nothing to do with the structure of microcrystalline cellulose in woody thin boards. The present finding would give the better insight on the surface modification by the hydrophobic polymer to improve the water repellency of woody thin boards and control their surface geometry.

4.4 Conclusions

In this study, we made attempts to construct woody thin boards using the commercially available lignin and cellulose. The compression molding without water made it impossible to form woody thin boards. The same was true for small amounts of water (less than 35 %) or too much water (greater than 55 %). Both an adequate moisture and composition ratio of lignin / cellulose was required for the compression molding of woody thin boards. It was revealed that remaining lignin at surface of woody thin boards resulted in an increased hydrophobicity of surface and a creation of surface roughness. In the present case, an increased hydrophobicity of surface rather than a creation of surface roughness was likely to contribute to the improved water repellency.

References

[1] Leu, S.Y.; Yang, T. H.; Lo, S. F.; Yang, T. H., Optimized material composition to improve the physical and chemical properties of extruded wood-plastic compositions (WPCs). *Constr. Build. Mater.* 2012, 29,120-127.

- [2] Bouafif, H.; Koubaa, A.; Perre, P.; Cloutier, A., Effect of fiber characteristics on the physical and mechanical properties of wood plastic compositions. *Compos. Part A-Appl. S.* 2009, *40*, 1975-1981.
- [3] Ayrilmis, N.; Kaymakci, A., Fast growing biomass as reinforcing filler in thermoplastic composites: *Paulownia elongate* wood. *Ind. Crop. Prod.* 2013, *43*, 457-464.
- [4] Stark, N. M.; Matuana, L. M.; Clemons, C. M., Effect of processing method on surface and weathering characteristics of wood-flour/HDPE compositions. *J. Appl. Polym. Sci.* 2004, *93*, 1021-1030.
- [5] Binhussain, M. A.; El-Tonsy, M. M., Palm leave and plastic waste wood composite for out-door structures. *Constr. Build. Mater.* 2013, *47*, 1431-1435.
- [6] Stark, N. M.; Matuana, L. M., Characterization of weathered wood-plastic composite surfaces using FTIR spectroscopy, contact angle, and XPS. *Polym. Degrad. Stabil.* 2007, *92*, 1883-1890.
- [7] Kuo, P. Y.; Wang, S. Y.; Chen, J. H.; Hsueh, H. C.; Tsai, M. J., Effects of material compositions on the mechanical properties of wood-plastic composites manufacture by injection molding. *Mater. Design* 2009, *30*, 3489-3496.
- [8] Sombatsompop, N.; Chaochanchaikul, K., Effect of moisture content on mechanical properties, thermal and structural stability and extrude texture of poly(vinyl chloride)/wood sawdust composites. *Polym. Int.* 2004, *53*, 1210-1218.
- [9] Sombatsompop, N.; Prapruit, W.; Chaochanchaikul, K.; Pulngern, T.; Rosarpitak, V., Effect of cross section design and testing conditions on the flexural properties of wood/PVC composite beams. *J. Vinyl Addit. Techn.* 2010, *16*, 33-41.
- [10] Lin, Z.; Renneckar, S., Nanocomposite-based lignocellulosic fibers 2: layer-by-layer modification of wood fibers for reinforcement in thermoplastic composites. *Compos. Part A-Appl. S.* 2011, *42*, 84-91.
- [11] Alamri, H.; Low, L. M., Effect of water absorption on the mechanical properties of nanoclay filled recycled cellulose fibre reinforced epoxy hybrid nanocomposites. *Compos. Part A-Appl. S.* 2013, *44*, 23-31.
- [12] Islam, M. N.; Haque, M. M.; Huque, M. M., Mechanical and morphological properties of chemically treated coir-filled polypropylene composites. *Ind. Eng. Chem. Res.* 2009, *48*, 10491-10497.
- [13] Guo, J.; Tang, Y.; Xu, Z., Wood plastic composite produced by nonmetals from pulverized waste printed circuit boards. *Environ. Sci. Techn.* 2010, *44*, 463-468.
- [14] Hosseinaei, O.; Wang, S.; Enayati, A. A.; Rials, T. G., Effect of hemicellulose extraction on properties of wood flour and wood-plastic composite. *Compos. Part A-Appl. S.* 2012, *43*,

686-694.

- [15] Deka, B. K.; Maki, T. K., Effect of silica nanopowder on the properties of wood flour/polymer composite. *Polym. Eng. Sci.* 2012, 52, 1516-1523.
- [16] Fu, Y. C.; Li, G.; Yu, H. P.; Liu, Y. X., Hydrophobic modification of wood via surface-initiated ATRP of MMA. *Appl. Surf. Sci.* 2012, 258, 2529-2533.
- [17] Ma, M.; Hill, R. M., Superhydrophobic surfaces. *Curr. Opin. Coll. Int'f. Sci.* 2006, 11, 193-202.
- [18] Hsieh, C. T.; Chang, B. S.; Lin, J. Y., Improvement of water and oil repellency on wood substrates by using fluorinated silica nanocoating. *Appl. Surf. Sci.* 2011, 257, 7997-8002.
- [19] Yan, W.; Acharjee, T. C.; Coronella, C. J.; Vasquez, V. R., Thermal pretreatment of lignocellulosic biomass. *Environ. Prog. Sustian.* 2009, 28, 435-440.
- [20] Buckley, F.; Maryott, A. A., Tables of dielectric dispersion data for pure liquids and dilute solutions, Nat. Bur. Stand. Circular. Washington, D. C. 1958, p. 589.
- [21] Baker, A. A.; Helbert, W.; Sugiyama, J.; Miles, M. J., High-resolution atomic force microscopy of native Valonia cellulose I microcrystals. *J. Struct. Biol.* 1997, 119, 129-138.
- [22] International standard. Geometrical product specifications (GPS)-surface texture: profile method-terms, definitions, and surface texture parameters, International Organization for Standardization: ISO 4287; 1987; Geneva.
- [23] Japanese industrial standard. Geometrical product specifications (GPS)-surface texture: profile method-terms, definitions, and surface texture parameters. JIS B 0601; 2001; Japan.
- [24] Paz, A.; Thorin, E.; Topp, G. C., Dielectric mixing models for water content determination in woody biomass. *Wood Sci. Technol.* 2010, 45, 249-259.
- [25] She, D.; Xu, F.; Geng, Z. C.; Sun, R. C.; Jones, G. L.; Bird, M. S., Physicochemical characterization of extracted lignin from sweet sorghum stem. *Ind. Crops Prod.* 2010, 32, 21-28.
- [26] Montoneri, E., An IR study to investigate the structural relationship of lignin-like matter and lignosulphonates obtained from animal-vegetable wastes. *Waste Manag.* 2005, 25, 161-169.
- [27] Moniruzzaman, M.; Ono, T., Ionic liquid assisted enzymatic delignification of wood biomass: A new 'green' and efficient approach for isolating of cellulose fibers. *Biochem. Eng. J.* 2012, 60, 256-260.
- [28] Kadokawa, J.; Murakami, M.; Kaneko, Y., A facile method for preparation of composites composed on cellulose and a polystyrene-type polymeric ionic liquid using a polymerizable ionic liquid. *Compos. Sci. Technol.* 2008, 68, 493-498.
- [29] Park, S.; Baker, J. O.; Himmel, M. E.; Parilla, P. A.; Johnson, D. K., Cellulose

crystallinity index: measurement techniques and their impact on the interpreting cellulose performance. *Biotechnol. Biofuels* 2010, 3, 1-10.

[30] Iwamoto, S.; Kai, W.; Isogai, A.; Iwata, T., Elastic modulus of single cellulose microfibrils from Tunicate measured by atomic force microscopy. *Biomacromolecules* 2009, 10, 2571-2576.

[31] Ishikawa, A.; Okano, T.; Sugiyama, J., Fine structure and tensile properties of ramie fibres in the crystalline form of cellulose I, II, III_I and IV_I. *Polymer* 1997, 38, 463-468.

[32] Cousins, W. J., Elastic modulus of lignin as related to moisture content. *Wood Sci. Technol.* 1976, 10, 9-17.

[33] Ayrlmis, N., Effect of fire retardants on surface roughness and wettability of wood plastic composites panels. *Bioresources* 2011, 6, 3178-3187.

Chapter 5

Characterization the fuel properties of solid chars obtained from subcritical water treatment of various biomasses

5.1 Introduction

The solid char could be used to prepare biodegradable materials as described in Chapter 3 and 4. The solid char prepared in the present study was rich in cellulose and lignin. The higher heating value (HHV) of lignin was 21.13 MJ/kg that was much higher than that of biomass (15~19.7 MJ/kg). We thus speculated that the solid char might have the potential to be applied as a bio-fuel.

Humulus lupulus (common hop plant), *Plumeria alba* (an evergreen shrub) and *Calophyllum inophyllum* L. (an evergreen tree) are very abundant in the United States. The 2009 production of *H. lupulus* in the U.S. was 3.1×10^4 tons, and the production is expected to keep growing [1]. The mature female inflorescence or cone of *H. lupulus* is used in the brewing and pharmaceutical industries, and the leaves and stem materials have been burned or landfilled as a means of disposal [2]. *P. alba* is a 6–7-m-tall tree that is widely planted in the Hawaiian Islands. The milky sap of the stem and leaves is used in treatments for skin disease, and the extracted stem and leaves showed potential for use as an energy source although they have been disposed of as waste [3, 4]. *Calophyllum inophyllum* L. (also known as Alexandrian laurel) is an evergreen tree with the average height of 8–20 m; it is widely planted in the Hawaiian Islands. *Calophyllum inophyllum* L. provides prized timber that can be used for carving, cabinetmaking and boat building [5], and its processing at timber mills produces a high amount wood flour. The remains of *Calophyllum inophyllum* L. as well as those of *H. lupulus* and *P. alba* might have potential for energy production, but it is necessary to find new ways of using their remaining biomasses. Additionally, these three biomasses have different component ratios (Table 5-1), and they could thus act as model materials for other biomasses with similar component ratios.

For these reasons, we used *H. lupulus* (HL), *P. alba* (PA) and *Calophyllum inophyllum* L. (CIL) as raw materials for subcritical water treatment in the present study. Further, we characterized the fuel properties of prepared solid char.

5.2 Materials and Methods

5.2.1 Materials

The three types of biomass, HL, PA and CIL were produced in Guam. Their components are shown on Table 5-1. CIL contained the highest lignin content. HL and PA contained similar lignin content, and HL had the highest hemicellulose content. These biomasses were used without any pretreatment except milling before all of the experiments. All reagents used were purchased from Wako Pure Chemical Industries (Osaka, Japan).

5.2.2 Subcritical water treatment

The subcritical water treatment of biomass was carried out in the same as described in Chapter 2. 200 mg of biomass and 8 mL of water was used. The reactor was treated at the temperature range from 180 to 260 °C with the treatment time of 10 min. After treatment the mixture in the reactor was filtered and the obtained solid char was dried at 105 °C for 24 h. The solid chars obtained at various temperatures were abbreviated as HL-xxx or PA-xxx or CIL-xxx, where HL, PA and CIL are the names of biomasses and xxx showed the subcritical water treatment temperature.

5.2.3 Characterization of solid char

The lignin, cellulose and hemicellulose contents in the biomass and solid char were measured by the same methods as described in Chapter 3.

The element contents (C, H and N) were measured by an elemental analyzer (2400II, PerkinElmer, Kanagawa, Japan). The HHVs of the biomasses and solid chars were determined from their element contents and calculated by the following equation [6]:

$$\text{HHV} = 5.22C^2 - 319C - 1647H + 38.6CH + 133N + 21028 \quad (5-1)$$

where C , H and N represent the carbon, hydrogen and nitrogen contents of the biomass or solid char, respectively, expressed in mass percentage on a dry basis. The energy yield was calculated from the HHV as well as the solid char mass yield by the following equation:

$$\text{Energy yield (\%)} = \text{HHV}_{\text{solid char}} / \text{HHV}_{\text{raw biomass}} \times \text{solid char mass yield} \quad (5-2)$$

The hydrophobicity of the biomasses and solid chars were evaluated by the following method: Approx. 100 mg of biomass or solid char was placed in a plastic dish and then the dish was placed in a large plastic bottle containing saturated sodium chloride solution with the relative humidity of 75%, at the experimental temperature of 30 °C. It took 15 to 20 days for the biomasses and solid chars to reach equilibrium. The final moisture content was calculated by the weight difference between before and after treatment, and this value was used to

estimate the hydrophobicity of each sample.

For scanning electron microscopy (SEM) measurements, the biomasses and solid chars were sputter-coated with Pt and examined with a scanning electron microscope (S-4700, Hitachi, Tokyo, Japan).

5.3 Results and Discussion

5.3.1 The solid char yield

The solid char yield reflects the thermal stability of a biomass during subcritical water treatment. The yields of all solid chars obtained from the HL, PA and CIL biomasses were examined, and the results are shown in Figure 5-1. The yield decreased with the increase in the subcritical water treatment temperature, indicating that temperature was an important factor that affected the solid char yield. Among the three types of biomass, the solid char yield prepared at the same temperature was in the order of CIL-xxx > PA-xxx > HL-xxx. At 260 °C, CIL produced a solid char yield of 50.9%, which was much higher than those of PA (31.5%) and HL (26.5%). This was due to the higher content of lignin in CIL (Table 5-1), because lignin has a higher decomposition temperature than cellulose and hemicellulose, and the lignin made the greatest contribution to the production of char [7]. The CIL biomass thus showed more thermal stability than the PA and HL biomasses, and higher solid char yield could be obtained from the biomass containing higher lignin content during the subcritical water treatment.

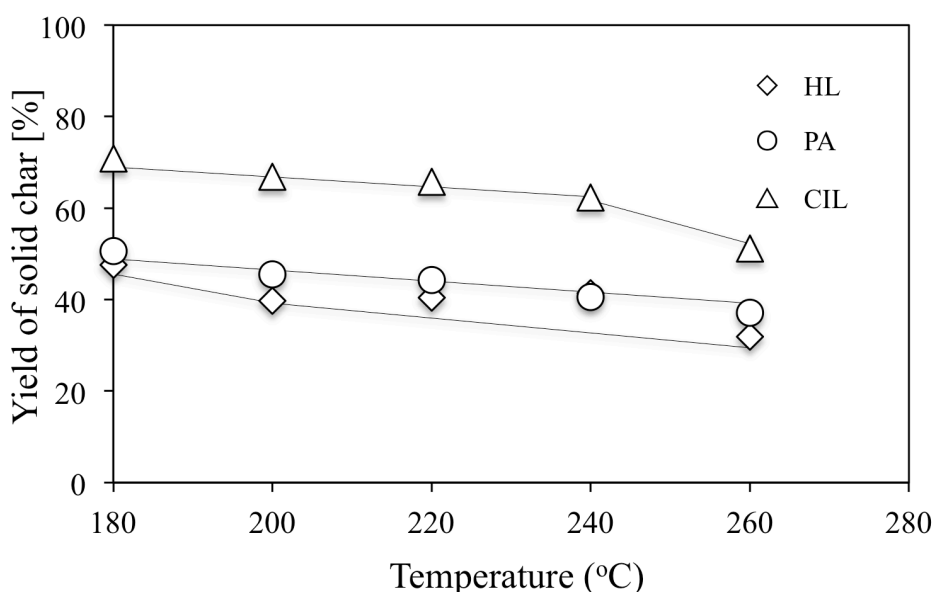


Figure 5-1. Mass yield of solid chars derived from subcritical water treatment of HL, PA and CIL at various temperatures for 10 min (N=3).

5.3.2 The components of biomasses and solid chars

As noted earlier, cellulose, hemicellulose and lignin are the main components of biomass. Knowing the component content in a solid char will help elucidate the degradation mechanism of the biomass and determine the optimum conditions for subcritical water treatment. Table 5-2 shows the weights of the remaining cellulose, hemicellulose and lignin in the solid chars. The cellulose and hemicellulose in the three solid chars were significantly decomposed with the increase in the subcritical water treatment temperature, whereas lignin was slightly decomposed at higher temperatures. Regarding the decomposition of cellulose and hemicellulose in the solid chars, the weights of cellulose and hemicellulose in HL were reduced from 38.4 to 13.8 mg (64.1% decrease) and from 72.9 to 7.4 mg (89.8% decrease), respectively, with the increase of the subcritical water treatment temperature. In this case, much more hemicellulose was decomposed, which was consistent with the report by Yan *et al.* that hemicellulose was more reactive than cellulose and could be easily hydrolyzed even at 200 °C [8]. However, our result was different from the conclusions that hemicellulose started decomposing at 200 °C and became fully devolatilized at 250 °C [9]; in another study, cellulose presented a slow decomposition rate below 250 °C and the rate became rapid above 300 °C [10].

In contrast, we obtained the opposite result: more cellulose than hemicellulose was decomposed when we subcritical water treatment of PA and CIL. For example, 39.7 mg of cellulose in CIL with the reduction rate of 78.9% was decomposed when the subcritical water treatment temperature reached 260 °C, whereas only 45.4% (14.7 mg) of the hemicellulose was decomposed at 260 °C. It was thus confirmed that the reduction of the solid yield was not due mainly to the decomposition of hemicellulose but rather was due to the decomposition of both cellulose and hemicellulose (Fig. 5-1). We suspect that the reactivity of both cellulose and hemicellulose in the biomasses was affected by the biomass species and its component weight ratio.

Table 5-1. Component weights of HL, PA and CIL as well as solid chars obtained at various temperatures for 10 min.

| Biomass/solid char | Cellulose (mg) | Hemicellulose (mg) | Lignin (mg) |
|---|----------------|--------------------|-------------|
| HL | 38.4±4.9 | 72.9±4.9 | 49.3±2.6 |
| HL-180 | 35.0±4.7 | 17.8±4.7 | 38.7±1.9 |
| HL-200 | 29.6±0.9 | 15.3±0.9 | 32.0±1.0 |
| HL-220 | 24.5±1.0 | 19.5±1.0 | 33.8±0.6 |
| HL-240 | 26.5±0.5 | 11.5±0.5 | 44.3±2.0 |
| HL-260 | 13.8±1.1 | 7.4±1.2 | 40.8±1.7 |
| PA | 73.6±8.0 | 45.4±8.0 | 50.4±1.8 |
| PA-180 | 25.9±0.4 | 20.0±0.4 | 49.0±1.3 |
| PA-200 | 24.8±0.5 | 17.0±0.5 | 44.5±0.2 |
| PA-220 | 23.3±4.7 | 15.9±4.7 | 44.6±1.1 |
| PA-240 | 16.1±2.5 | 17.3±2.5 | 43.2±0.4 |
| PA-260 | 14.8±0.9 | 12.5±0.9 | 42.7±0.4 |
| CIL | 50.3±3.2 | 32.4±3.2 | 72.6±9.4 |
| CIL-180 | 35.1±3.8 | 25.0±3.8 | 68.3±5.1 |
| CIL-200 | 40.7±0.7 | 12.6±0.7 | 74.4±5.1 |
| CIL-220 | 38.1±1.7 | 13.4±1.7 | 78.0±5.5 |
| CIL-240 | 19.8±2.1 | 20.7±2.1 | 77.0±1.0 |
| CIL-260 | 10.6±3.5 | 17.7±3.5 | 64.1±0.9 |
| The values after ± show the standard deviations | | | N=3 |

5.3.3 Elemental analysis of biomasses and solid chars

The element content is an important factor in the evaluation of the fuel properties of solid chars. Higher carbon content and lower oxygen content can efficiently elevate the combustion properties of solid char [11]. We thus analyzed the element content of the HL, PA and CIL biomasses and the prepared solid chars. Table 5-3 shows that the carbon contents of the three types of solid chars increased with the increase in the subcritical water treatment temperature, whereas the oxygen contents were decreased at higher subcritical water treatment temperatures. This phenomenon was due to the reduction of hydroxyl groups in the form of water during subcritical water treatment, and the results also indicated that subcritical water treatment could largely improve the fuel properties of these biomasses.

The hydrogen and nitrogen contents of the solid chars showed no significant change compared to their raw biomasses. The element contents of HL-260, PA-260 and CIL-260 reached the same level as those of lignite with 61.6% carbon, 5.7% hydrogen, and 30.1% oxygen content [12]. The three solid chars obtained in the present study also had similar element contents, although their parent biomasses contained different component weight ratios and their yields at 260 °C were different. We thus speculate that the final element content of the solid chars may have no relationship to the raw biomass component weight ratio but that this content was related to the original element content of the biomass during subcritical water treatment, because the three types of biomass examined herein had similar element contents.

Variations in the atomic H/C and O/C ratios of solid char can be used to efficiently evaluate the fuel grade of solid chars. We therefore calculated the atomic H/C and O/C ratios from the molecular weight of the raw biomasses and solid chars (as well as lignin and lignite) and plotted the values obtained in a van Krevelen diagram (Fig. 5-2). Both the H/C and O/C ratios of all three solid chars decreased with the increase in the subcritical water treatment temperature, and these ratios were much lower than those of their parent biomasses even at 180 °C. The H/C and O/C ratios of HL-260, PA-260 and CIL-260 were close to that of lignite, and the ratios of CIL-260 were also similar to those of lignin. The above results revealed that HL-260, PA-260 and CIL-260 could combust with lignite without a significant change in the combustion properties of lignite. It was reported that a fuel with low H/C and O/C ratios could efficiently reduce energy loss, smoke, and water vapor generation during the combustion process [12]. Therefore, subcritical water treatment could largely elevate the combustion properties of a biomass.

The HHV and energy yield of solid char are important factors to evaluate the subcritical water treatment and determine the optimum conditions. We examined the HHV calculated

from the solid char element content and energy yield. The results are shown in Figures 5-3 and 4. The HHVs of all three types of solid char increased with the increase in the subcritical water treatment temperature (Fig. 5-3), and the energy yield values decreased at the same time (Fig. 5-4). The increase in HHV was due to the reduction of low-energy chemical bonds such as H–C and O–C and the increase in a high-energy chemical bond (C–C) during subcritical water treatment [12].

In the present experiment, the HHVs of HL, PA and CIL were 17.5, 17.7 and 18.4 MJ/kg and they increased to 25.3, 25.7 and 23.6 MJ/kg, respectively, as the temperature increased to 260 °C (Fig. 5-3a, 3b and 3c). The obtained solid chars that had HHVs between 23.5 and 25.7 MJ/kg are comparable to those of some commercial coals such as Northumberland No. 81/2 Sem. Anth. Coal (24.7 MJ/kg), Jhanjra Bonbahal Seam Coal–R–VII (24.1 MJ/kg) and German Braunkohle lignite (25.1 MJ/kg) [13]. Although lignin plays an important role in contributing to the HHV of solid char [14], in our study, CIL-260, which has a higher lignin content than those of HL-260 and PA-260 had the lowest HHV. Among these three biomasses, PA-260 had the largest HHV elevation (45.2%) compared to those of HL-260 (44.5%) and CIL-260 (28.3%), although their parent biomasses had similar HHVs. This result was probably due to the differences in biomass components (especially the cellulose and hemicellulose contents) because both of cellulose and hemicellulose were significantly decomposed at higher subcritical water treatment temperatures (Table 5-2). We found that CIL-260 had the lowest HHV and energy content elevation, but it showed a higher energy yield (65.2%) than HL-260 (38.5%) and PA-260 (45.7%) (Fig. 5-4). This was due to the higher lignin content of CIL, which led to the higher mass yield of solid char because the lignin was hardly decomposed at the temperature range from 180 to 260 °C (Table 5-2). Therefore, the subcritical water treatment was able to markedly elevate the HHV of the biomass.

Based on the aforementioned results, we concluded that the solid chars obtained at a higher subcritical water treatment temperature could be co-combusted with German Braunkohle lignite without a significant change in the fuel properties of the German Braunkohle lignite, because of their similar HHVs and H/C and O/C atomic ratios (Fig. 5-2).

Table 5-2. Element contents of biomasses and solid chars obtained at various temperatures for 10 min.

| Biomass/Solid char | C (%) | H (%) | N (%) | Oa (%) |
|----------------------------|-------|-------|-------|--------|
| HL | 43.3 | 6.2 | 2.5 | 48.0 |
| HL-180 | 45.1 | 5.9 | 1.3 | 47.7 |
| HL-200 | 49.7 | 6.4 | 1.9 | 42.0 |
| HL-220 | 52.8 | 6.4 | 1.9 | 38.9 |
| HL-240 | 55.9 | 6.0 | 2.2 | 35.9 |
| HL-260 | 60.5 | 6.0 | 2.7 | 30.8 |
| PA | 44.5 | 6.1 | 0.6 | 48.8 |
| PA-180 | 51.8 | 6.5 | 0.8 | 40.9 |
| PA-200 | 56.0 | 7.0 | 0.8 | 36.2 |
| PA-220 | 57.6 | 7.0 | 0.7 | 34.7 |
| PA-240 | 59.0 | 6.9 | 0.6 | 33.5 |
| PA-260 | 60.7 | 6.8 | 0.6 | 31.9 |
| CIL | 46.7 | 5.6 | 0.1 | 47.6 |
| CIL-180 | 51.0 | 5.3 | 0.4 | 43.3 |
| CIL-200 | 53.1 | 5.2 | 0.4 | 41.3 |
| CIL-220 | 54.7 | 5 | 0.4 | 39.9 |
| CIL-240 | 57.0 | 5.1 | 0.4 | 37.5 |
| CIL-260 | 59.1 | 4.9 | 0.3 | 35.7 |
| a Calculated by difference | | | | |

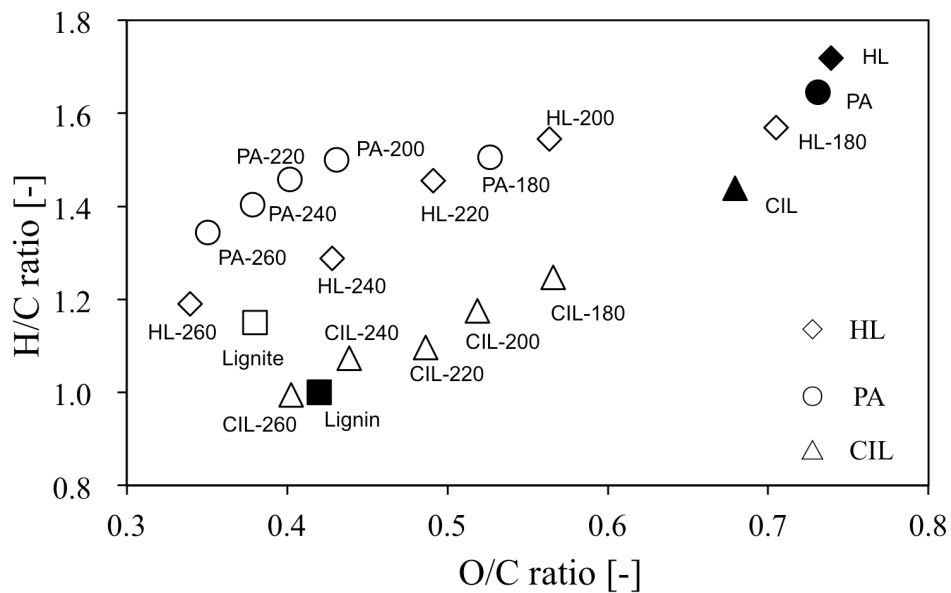


Figure 5-2. Van Krevelen diagram of biomasses, solid chars, lignite as well as lignin.

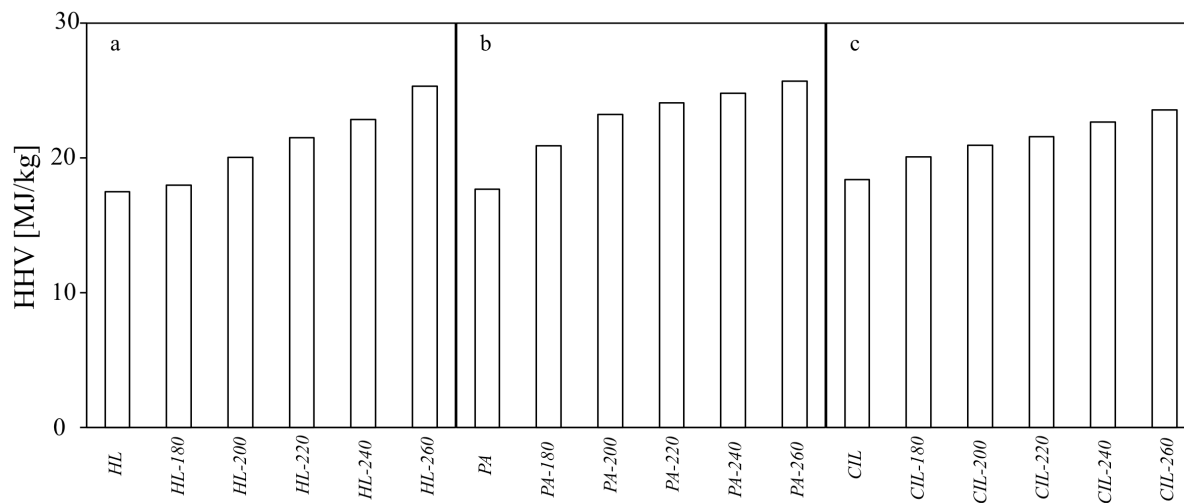


Figure 5-3. The HHVs of biomasses and their delivered solid chars:

(a) HL, (b) PA and (c) CIL.

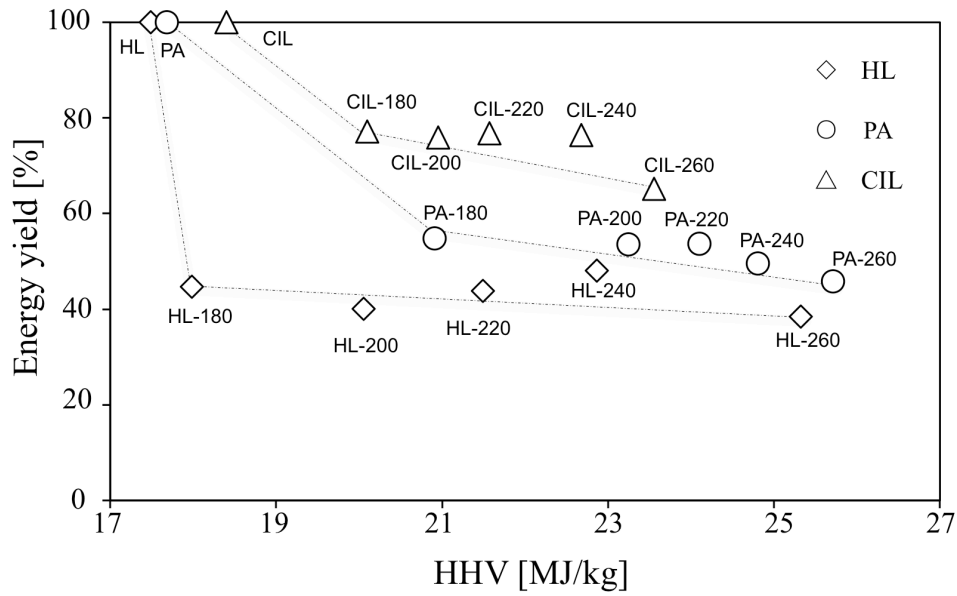


Figure 5-4. Energy yield against HHV for all biomasses and their delivered solid chars.

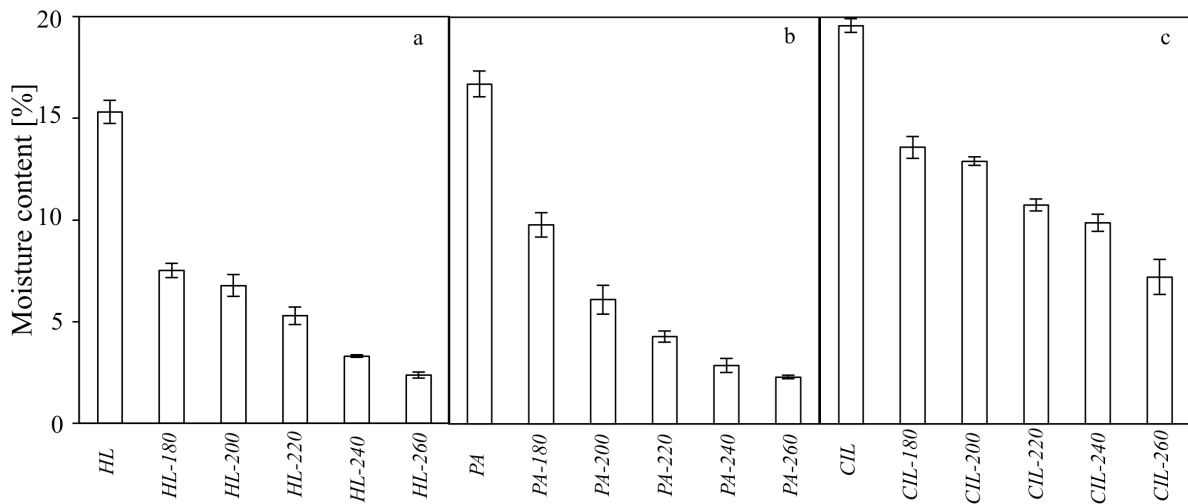


Figure 5-5. Moisture content of biomasses and their delivered solid chars: (a) HL, (b) PA and (c) CIL. (N=3).

5.3.4 The hydrophobicity of biomasses and solid chars

The hydrophobicity of solid char obtained from a biomass is an important factor that is related to the storage and energy density of the solid char. A solid char with higher hydrophobicity is much more stable and unlikely to deteriorate biologically. We therefore characterized the hydrophobicity of the three types of biomass and solid chars in this study, evaluated by their final moisture contents after the samples were incubated at 75% relative humidity at 30 °C. As shown in Figure 5-5, all of the solid chars became more hydrophobic with the increase in the subcritical water treatment temperature, which was consistent with the result reported by Acharjee *et al.* [15]. Among these three solid chars, the solid chars that from HL and PA were more hydrophobic than that from CIL in the same conditions. For example, HL-260 and PA-260 had the moisture content values of 2.4% and 2.3%, respectively (Fig. 5-5a and 5b), which is much lower than that the 7.2% value of CIL-260 (Fig. 5-5c). Among the three main components of biomass, hemicellulose has a greater water sorption capacity compared to lignin [16] and the process used to obtain the solid char affected its hydrophobicity. The differences in hydrophobicity among HL-260, PA-260 and CIL-260 were thus due to the differences in components, because CIL-260 contained a higher content of hemicellulose (19.1%) compared to those of HL-260 (11.9%) and PA-260 (17.9%). The results described above demonstrate that solid char with high hydrophobicity could be obtained through subcritical water treatment.

5.3.5 The SEM topography of the biomasses and solid chars

Scanning electron microscopy (SEM) is a technique that can detect the surface topography of a sample. We obtained SEM images of the three biomasses and solid chars to further determine the impact of the subcritical water treatment on the biomasses (Fig. 5-6). The SEM demonstrated that the subcritical water treatment had a pronounced impact on all of the solid chars. We observed that the solid chars had pore structures and cracks compared to their parent biomasses, and the pore structures and cracks became stronger with the increase in the subcritical water treatment temperature (Fig. 5-6d-i).

The pore structures of CIL-220 and CIL-260 were less pronounced than those of the other two solid chars obtained under the same conditions, which was probably due to the higher lignin contents of these fuels. This result indicated that the biomass surface was damaged after subcritical water treatment, and that this damage was due to the evolution of volatile materials during subcritical water treatment, because biochar with higher porosity and various pore structures would be produced by the volatilization of higher volatile materials [17]. As mentioned above, solid char contains a high carbon content (Table 5-3) and it also

contains internal pores and cracks. Therefore, the solid chars obtained in the present study have the potential to be used as carbon feedstock for producing carbon materials such as activated carbon in addition to being used for burning as a bio-fuel.

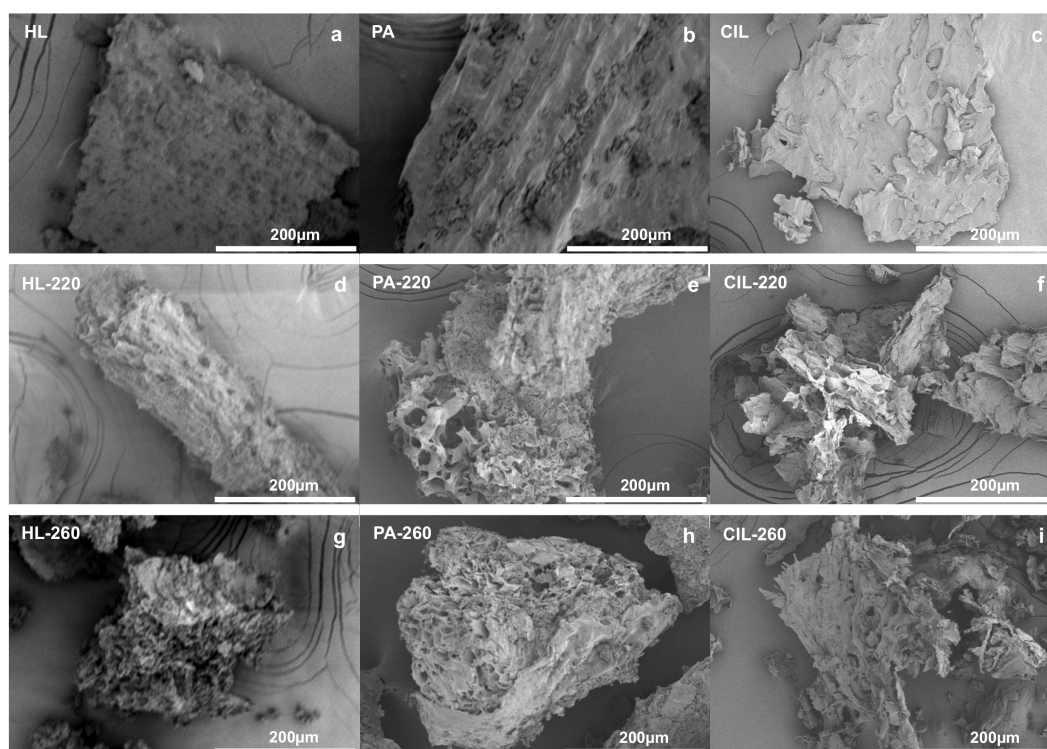


Figure 6. SEM images of (a) CL, (b) PA, (c) CIL, (d) CL-220, (e) PA-220, (f) CIL-220, (g) CL-260, (h) PA-260 and (i) CIL-260.

5.4 Conclusions

We conducted the subcritical water treatment of HL, PA and CIL at various temperatures for 10 min, and we found that the solid char from CIL showed the highest yield. The mass loss of biomass after subcritical water treatment was due to the significant decomposition of cellulose and hemicellulose. The biomass species and its component weight ratio affected the reactivity of cellulose and hemicellulose. The carbon content of each biomass was largely increased after subcritical water treatment. The HHV as well as atomic H/C and O/C ratios were also significantly elevated. The HHVs, H/C and O/C values of HL-260, PA-260 and CIL-260 were similar to those of German Braunkohle lignite, indicating that these solid chars could be co-combusted with German Braunkohle lignite. CIL-260 had the lowest HHV among the three solid chars obtained under the same conditions, but it had the highest energy yield. The hydrophobicity of the solid char was reduced with the increase in the subcritical water treatment temperature. CIL-260 was much more hydrophobic than HL-260 and PA-260 because of its higher hemicellulose content. Pores and cracks were observed on the solid

surface and they became stronger at higher temperature. This result indicated that subcritical water treatment could completely destroy the biomass surface. We proposed that the obtained solid char has the potential to be used as a source of carbon materials such as activated carbon in addition to use as a bio-fuel.

Reference

- [1] Nass.usda.gov [Internet]. National hop report updated 2013 Dec 23; cited 2014 Nov 27. Available from:
http://www.nass.usda.gov/Statistics_by_State/Regional_Office/Northwest/includes/Publications/Hops/HP12_1.pdf.
- [2] Gardea-Torresdey, J.; Hejazi, M.; Tiemann, K.; Parsons, J. G.; Duarte-Gardea, M.; Henning, J., Use of hop (*Humulus lupulus*) agricultural by-products for the reduction of aqueous lead (II) environmental health hazards. *J. Hazard. Mater.* 2002, *91*(1-3), 95-112.
- [3] Raju, R. A., Wild plants of Indian sub-continent and their economic use. 1st ed. Delhi: CBS publishers and distributors; 2000.
- [4] Kalita, D.; Saikia, C. N., Chemical constituents and energy content of some latex bearing plants. *Bioresource Technol.* 2004, *92*, 219-227.
- [5] Friday, J. B.; Okano, D., *Calophyllum inophyllum* L (kamani), ver. 2.1. In: Elevitch CR, editor. Species profiles for pacific island agroforestry. Permanent Agriculture Resources (PAR), Holualoa, Hawaii, 2006. <http://www.traditionaltree.org>.
- [6] Friedl, A.; Padouvas, E.; Rotter, H.; Varmuza, K., Prediction of heating values of biomass fuel from elemental composition. *Anal. Chem. Acta* 2005, *554*, 191-198.
- [7] Yang, H.; Yan, R.; Chen, H.; Zheng, C.; Lee, D. H.; Liang, D. T., In-depth investigation of biomass pyrolysis based on three major components: Hemicellulose, cellulose and lignin. *Energy Fuels* 2006, *20*, 388-393.
- [8] Yan, W.; Hastings, J. T.; Acharjee, T. C.; Coronella, C. J.; Vasquez, V. R., Mass and energy balances of wet torrefaction of lignocellulosic biomass. *Energy Fuels* 2010, *24*, 4738-4742.
- [9] Gaur S, Reed TB. Thermal data for natural and synthetic fuels. NewYork: Marcel Dekker;1998.
- [10] Golova OP. Chemical reactions of cellulose under the action of heat. *Usp. Khim*, 1975;44:1454.
- [11] Khan, A. A.; Jong, W.; Jansens, P. J.; Spliethoff, H., Biomass combustion in fluidized bed boilers: potential problems and remedies. *Fuel Process Technol.* 2009, *90*, 21-50.
- [12] Liu, Z. G.; Quek, A.; Hoekman, S. K.; Balasubramanian, R., Production of solid biochar

- fuel from waste biomass by hydrothermal carbonization. *Fuel* 2013, *103*, 943-949.
- [13] Channiwala, S. A.; Parikh, P. P., A unified correlation for estimating HHV of solid, liquid and gaseous fuels. *Fuel* 2002, *81*, 1051-1063.
- [14] Chen, W. H.; Ye, S. C.; Sheen, H. K., Hydrothermal carbonization of sugarcane bagasse via wet torrefaction in association with microwave heating. *Bioresource Technol.* 2012, *118*, 195-203.
- [15] Acharjee, T. C.; Coronella, T. C.; Vasquez, V. R., Effect of thermal pretreatment on equilibrium moisture content of lignocellulosic biomass. *Bioresource Technol.* 2011, *102*, 4849-4854.
- [16] Bjork, H.; Rasmuson, A., Moisture equilibrium of wood and bark chips in superheated steam. *Fuel* 1995, *74*(2), 1887-1890.
- [17] Haykırı-Açma, H.; Ersoy-Meriçboyu, A.; Küçükbayrak, S., Effect of mineral matter on the reactivity of lignite chars. *Energy Convers. Manag.* 2001, *42*, 11-20.

Chapter 6

Conclusions

In conclusion, the degradation mechanism of cellulose as a model of biomass and applications of solid char remained after subcritical water treatment of biomass were considered in the present study. The relationships between degradation mechanism and structure change of microcrystalline cellulose were investigated, and the solid char was employed to prepare biodegradable materials that had the potential to use as alternate plastic products.

The degradation kinetic parameters and structure changes of microcrystalline cellulose (MCC), which served as fundamental researches for degradation of biomass in subcritical water, were investigated at the temperature range from 100 °C to 300 °C. The yield of MCC residue began to decrease at 205 °C and reached to the lowest value at 275 °C. However, it showed an increase at the temperature higher than 275 °C. The degradation area of MCC (205 °C~275 °C) was separated into zone 1 and zone 2 with 245 °C as a boundary. The activation energy (E), pre-exponential factor (A) and reaction order (n) of MCC in each zone were 226.5 kJ mol⁻¹, 2.3×10^{23} s⁻¹ and 0.6 (zone 1) and 423.1 kJ mol⁻¹, 9.0×10^{40} s⁻¹ and 0.5 (zone 2), respectively. There showed a breaking point of 245 °C for the Arrhenius plot in the reaction area. The surface morphology of MCC residue had no significant change below 260 °C, as indicated by SEM images. However, it was completely destroyed at the temperature above 275 °C and MCC residues with strong pore structures were obtained at higher temperature. The structures of crystalline region of MCC residue below 275 °C had no significant change although 89.2% of MCC was degraded at 275 °C. However, they nearly disappeared at higher temperature with the steeply reducing of crystallinity index of MCC at the same time. As for the degradation mechanism of MCC, it was proposed that only the surface of MCC was degraded at 205 °C ~245 °C and the hydrogen and glycosidic bonds on the interior of MCC fibrils destroyed at the temperature range from 245 °C to 275 °C; finally, the remained MCC as well as generated oligomer and monomer were further degraded at higher temperature.

The solid char, obtaining at subcritical water treatment of walnut shell at 200 °C for 15 min was used to prepare biodegradable foam by compounding with corn starch using a

technique similar to compression molding. It was found that replacing 20% of the corn starch by the residue had no deleterious effects on the density and morphology, as indicated by scanning electron microscopy. The prepared foams had a dense outer skin and a less dense interior with large, mostly open cells. The flexural strains were similar to that of foamed polystyrene and the flexural modulus and flexural stresses were larger. The prepared biodegradable foam was a promising material to take place of plastic products in the further.

Woody thin boards could be prepared from lignin, cellulose, and water, by a compression molding at 180 °C and 25 MPa for 10 min. The boards with higher contact angles gave lower values of relative permittivity on their surface. The attenuated-total reflection Fourier transfer infrared spectroscopy suggested that more lignin existed on the surface of boards with the high contact angle, which was also supported by a scanning electron microscopy and an atomic force microscopy. It was therefore revealed that the orientation of lignin at the surface resulted in an increased hydrophobicity of surface and contributed to the improvement of water repellency.

The fuel properties of obtained solid chars were characterized. It was found that the lignin made the main contribution to the solid char yield. The reactivity of cellulose and hemicellulose in biomass was related to the biomass species and the component weight ratio of biomass. Subcritical water treatment could efficiently elevate the fuel properties such as carbon content, atomic H/C and O/C ratios, higher heating value (HHV) and hydrophobicity of three kinds of biomasses. The HHVs of solid chars prepared at 260 °C could be comparable with those of commercial coals like Northumberland No.81/2 Sem. Anth. Coal, Jhanjra Bonbahal Seam Coal-R-VII and German Braunkohle lignite. Meanwhile, they could be co-combustion with German Braunkohle lignite without significant change of combustion properties of German Braunkohle lignite because of their similar atomic H/C and O/C ratios as well as HHVs. subcritical water treatment could completely destroy the biomass surface and make the numerous pores and cracks on the solid chars surface. This indicated that the solid chars had the potential to use as carbon materials like activated carbon while not only used as a bio-fuel.

The results obtained in the present work should provide a theoretic support to determine the optimum conditions for subcritical water liquefaction of biomass to gain liquid products or solid char, and stimulate the novel applications of solid char as well as effective utilization of all the products obtained from subcritical water liquefaction of biomass.

Acknowledgments

The work presented here could be successfully carried out owing to the direct and indirect contributions from many people. First and foremost, I would like to appreciate my supervisors: Professor Yukitaka Kimura, Associate Professor Toshinori Shimanouchi and Professor Tsutomu Ono. Their expertise and advises inspired my interest on my research and helped me to finish my research.

I would like to thank Associate Professor Shenji Wu in College of Material and Environment Engineering, Hangzhou dianzi University for giving me a chance to continue my study in Okayama University.

I appreciate Professor Michihiro Miyake, Professor Yoshiei Kato and Associate Professor Azhar Uddin in Graduate School of Environmental and Life Science, Okayama University for their technical assistances.

I also appreciate the JASSO Honors Scholarship, Wesco International Student Scholarship and Rotary Yoneyama Memorial Foundation for their financial supports to my livelihood in Japan.

I am grateful to the members in the Rotary Club of Okayama Northwest. Especial my counselor Dr. Kazuo Okamoto and his friends: Mr. Kumao Kawanishi, Mr. Mineo Takahashi as well as Mr. Hideo Okamura. I thank them for giving me good advises about living in Japan as well as teaching me some of the Japanese cultures that lead me know more about Japan and Japanese culture.

I would like to offer my thanks to Mr. Tomoya Kanba, Miss. Miki Iwamura, Mr. Yuki Takahashi, Mr. Ryota Mano, Mr. Kohei Takashima, Mr. Tatsuya Tanifuji, Mr. Mikio Tanaka, Mr. Takayuki Kaneko, Mr. Kenta Yamamoto, Mr. Yuki Shirahike, Miss. Kaede Iwamoto, Miss. Maho Shimizu and Miss. Saki Fukuma for their contributions to my research.

I give my deeply grateful to my family and my best friends whose supports greatly encouraged me to complete my research.

List of publications

The following papers have been published during the course of this thesis.

1. Shimanouchi, T.; Ueno, S.; Yang, W.; Kimura, Y., Extraction of reducing sugars with anti-oxidative compounds from peels of *Carya cathayensis* sarg: Use of subcritical water. *Environ. Eng. Res.* 2014, *19* (1), 41-45.
2. Yang, W.; Shimanouchi, T.; Kimura, Y., Characterization of hydrochar prepared from hydrothermal carbonization of peels of *Carya cathayensis* sarg. *Desalin. Water Treat.* 2014 in press.
3. Yang, W.; Shimizu, I.; Ono, T.; Kimura, Y., Preparation of biodegradable foam from walnut shells treated by subcritical water. *J. Chem. Technol. Biot.* 2015, *90*, 44-49.
4. Yang, W.; Shimanouchi, T.; Wu, S. J.; Kimura, Y., Investigation of the degradation kinetic parameters and structure changes of microcrystalline cellulose in subcritical water. *Energy Fuels* 2014, *28*, 6974-6980.
5. Yang, W.; Shimanouchi, T.; Iwamura, M.; Takahashi, Y.; Mano, R.; Takashima, K.; Tanifuji, T.; Kimura, Y. Elevating the fuel properties of *Humulus lupulus*, *Plumeria alba* and *Calophyllum inophyllum* L through wet torrefaction. *Fuel* 2015, *146*, 88-94.
6. Yang, W.; Shimanouchi, T.; Kimura, Y., Characterization of the residue and liquid products produced from husks of nuts from *Carya cathayensis* sarg by hydrothermal carbonization. *ACS Sustain. Chem. Eng.* 2015 in press.
7. 島内寿徳; 神庭朋也; Yang Wei; 木村幸敬, 木質バイオマスの亜臨界水抽出と撥水性界面形成の応用。 *ケミカルエンジニアリング* 2014, *59* (7), 66-71.

APPENDIX-1

Extraction of reducing sugar with anti-oxidative scavenger from peels of *Carya cathayensis* Sarg: Use of subcritical water

1.1 Introduction

Biomass is the largest and promising renewable energy source and has the advantages on both low sulphur content and carbon dioxide capture capability. In particular, wood biomass has therefore been utilized for its conversion to biofuel [1]. It has been reported that biofuels could be extracted from peels, juice, fruit and seed, together with a variety of natural compounds with radical scavenging activity [2]. The extraction of biofuel from wood biomass would therefore be a promising method, because the biofuels from peels might show the anti-oxidation of materials.

In China, *Carya cathayensis* Sarg is used as food. Meanwhile, an annual 7000 ton of peels of *Carya cathayensis* Sarg (PCCS) is generated without any treatment. To treat PCCS as wood biomass has been expected to obtain biofuels.

Subcritical water is one of the possible media to treat the biomass in a green and environmentally friendly manner [3]. Subcritical water is water that maintains its liquid state under pressurized conditions in the temperature range of 100 to 374 °C. Subcritical water has unique characteristics, such as a low relative dielectric constant [4-6] and a high ion product [7], which is advantageous for the extraction of compounds that are a resource of biofuels. Actually, it has been demonstrated that the treatment of biomass by subcritical water could yield reducing sugar that can be converted to a biofuel [8]. In addition, the treatment of wood biomass by subcritical water favors the yield of natural compounds with anti-oxidant activity; i.e., phenol derivatives, furfural, and 5-hydroxymethylfurfural [3, 9]. Therefore, it is considered that treatment of PCCS by subcritical water is a possible method to obtain a biofuel that is resistant to oxidation.

In this study, we treated PCCS by subcritical water. We investigated the optimal condition to acquire the reducing sugar involving the compounds with radical scavenging activity.

1.2 Materials and Methods

1.2.1 Materials

The PCCS were produced in Lin'an, China. D-glucose, phenol, Folin-Ciocalteu phenol reagent, bovine serum albumin (BSA, molecular weight 66000), and 1,1-diphenyl-2-picrylhydrazyl (DPPH) were purchased from Wako Pure Chemical Industries, Ltd., Osaka Japan. The other chemicals were of analytical grade.

1.2.2 Preparation of powdered PCCS

PCCS was used as raw material in all the experiments. We analyzed the content of PCCS and the contents of cellulose, hemicelluloses, lignin, and others (such as proteins and decomposed compounds) included in PCCS were 13%, 22%, 56%, and 9%, respectively. PCCS were milled and screened with a diameter under 0.3 mm using a milling machine (WB-1; Osaka Chemical Corporation, Osaka, Japan) and the powder was dried at 105 °C for 24 h before the experiment.

1.2.3 Subcritical water treatment of PCCS

The 10 mL in volume of the powdered PCCS and distilled water were loaded into the batch reactor cell. This batch reactor cell was placed in an oil bath, to elevate the temperature to 130 to 280 °C. The pressure in the reactor cell was approximately 8 MPa. The treatment time was 0 to 240 min. After the treatment, the extract obtained from PCCS was separated from the residues by filtration. These procedures are shown in Fig. 1.

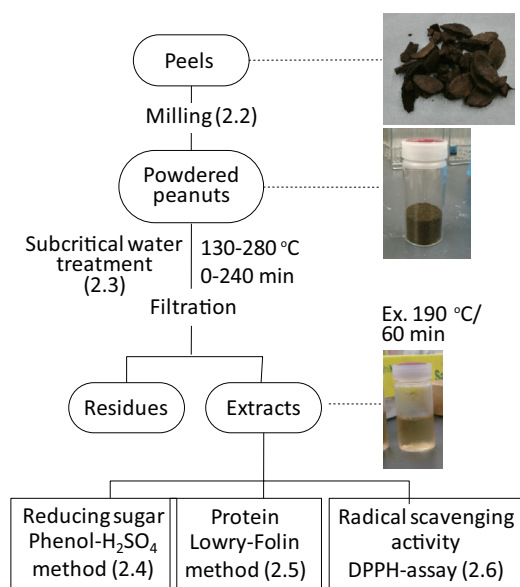


Figure 1. Flowchart of extracts from peels of *Carya cathayensis* Sarg.

1.2.4 Measurement of reduced sugar

The reducing sugar obtained was measured by using a phenol-H₂SO₄ method [10]. In short, 1 mL of a diluted sample was mixed with 25 L of 80% phenol solution. Thereafter, this mixture was vigorously mixed with 2.5 mL of H₂SO₄ solution and incubated for 30 min. The absorbance of the mixture was measured at 485 nm by using a UV-Vis spectrophotometer (Hitachi U-2000; Hitachi, Tokyo, Japan). Instead of a sample, the absorbance of D-glucose solution was measured in the same manner to acquire the calibration line of concentration of D-glucose, and its absorbance at 485 nm. By using the calibration line, the obtained absorbance of samples was converted to the concentration of reducing sugar.

1.2.5 Measurement of protein

The concentration of protein included in extracts obtained from PCCS was estimated by the Lowry-Folin method. First, 0.1 mol/L of NaOH (0.4 g) was added to 100 mL of 2 w/v% Na₂CO₃ solution (solution I). Citric acid (0.1 g) was added to 10 mL of 0.5 w/v% CuSO₄ 5H₂O solution (solution II). The 100 mL of solution I was thereafter mixed with 2 mL of solution II (solution III). Solution IV was prepared by mixing 10 mL distilled water with 10 mL Folin-phenol reagent. Next, 0.6 mL of samples or BSA solution was mixed with 3.0 mL of solution III to incubate for 10 min. The 0.3 mL of solution IV was thereafter mixed with them to incubate for 30 min and its absorbance was measured at 750 nm by using a UV-Vis spectrophotometer (Hitachi U-2000). The protein concentration of the sample was estimated, by converting its absorbance at 750 nm based on the calibration line obtained from BSA.

1.2.6 Measurement of scavenger activity

The radical scavenging activity was determined by using DPPH, according to the method in [11]. In short, 80 L of extract was added with 320 L distilled water and 2 mL of 0.12 mM DPPH in methanol. The mixtures were then mixed vigorously and allowed to stand at room temperature in the dark for 30 minutes. The absorbance of the sample mixture was then measured at 517 nm, using the UV-Vis spectrophotometer (Hitachi U-2000). The control sample was prepared in the same manner as the preparation of sample mixtures, except that deionized water was used instead of the samples. The blank sample was handled in the same manner, but deionized water was used instead of DPPH solution. The percentage of DPPH radical scavenging activity was defined as:

$$1 - 100 A_{\text{blank}} / A_{\text{sample}} (\%)$$

where A_{blank} and A_{sample} stands for the absorbance of blank and samples, respectively.

1.3 Results and Discussion

1.3.1 Absorption characteristic of extract

In the first series of experiments, we spectrophotometrically investigated the extract. The absorption spectrum for extracts was measured to investigate which compounds were involved. The absorption was observed in the wavelength range between 200 and 240 (Fig. 2), which resulted from the $\pi \rightarrow \pi^*$ transition of benzene derivatives in the extract [12]. The broad absorption observed in the range between 300 and 400 nm was considered to result from the presence of carbonyl or aldehyde derivative [13]. Those results suggested that the extract included the compounds with benzene ring, carbonyl or aldehyde.

It is therefore considered that PCCS might include reducing sugars, proteins, and compounds with scavenging activity, together with cellulose/hemicelluloses/lignin. In the following section, we quantified the amounts of those compounds extracted during the treatment of subcritical water.

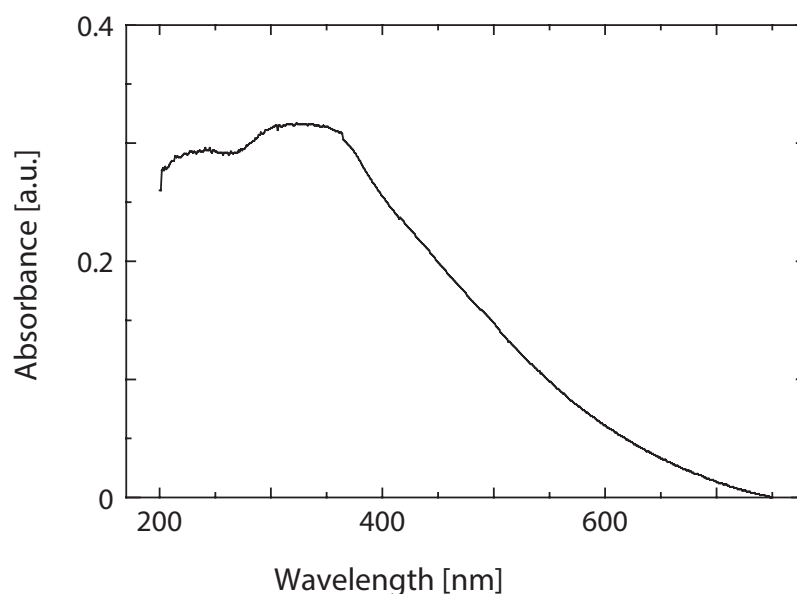


Figure 2. Absorption spectrum for extracts from peels of *Carya cathayensis* Sarg by subcritical water.

1.3.2 Extraction of reducing sugar, protein and compounds with scavenging activity from PCCS

Of sugars obtained from biomass, glucose is one of the major monosaccharides to be converted to bioethanol. Glucose that is an aldose shows reducing activity. The reducing sugar from PCCS was then measured by using a phenol- H_2SO_4 method advantageous for the detection of reducing sugar under a variety of temperature conditions.

As shown in Fig. 3(a), no extraction of reducing sugar was observed at 25 °C. Overall, more than 0.1 g/g-sample of reducing sugar could be obtained in temperature conditions other than 25 °C. Previously, a small amount of carbohydrates (0.02 g/g-sample [14]) was obtained by hot water for 30 min. It was considered that the treatment by subcritical water was more efficient in extracting the reducing sugar than the ordinary hot water. In the temperature range between 130 °C and 170 °C, the extraction of reducing sugar was observed in the manner of first order kinetic. Meanwhile, maximal value of extracted reducing 0.4 sugar was observed at the temperature condition of more than 190 °C in Fig. 3(a) and (b). In our series of studies, polysaccharides were favored to be decomposed to monosaccharides under the subcritical water [15], and further decomposition of monosaccharides, such as aldose and ketose, yields furfural or 5-hydroxymethylfurfural [1], which would result in the intermediate-like production behavior of reducing sugar in the temperature range of more than 190 °C.

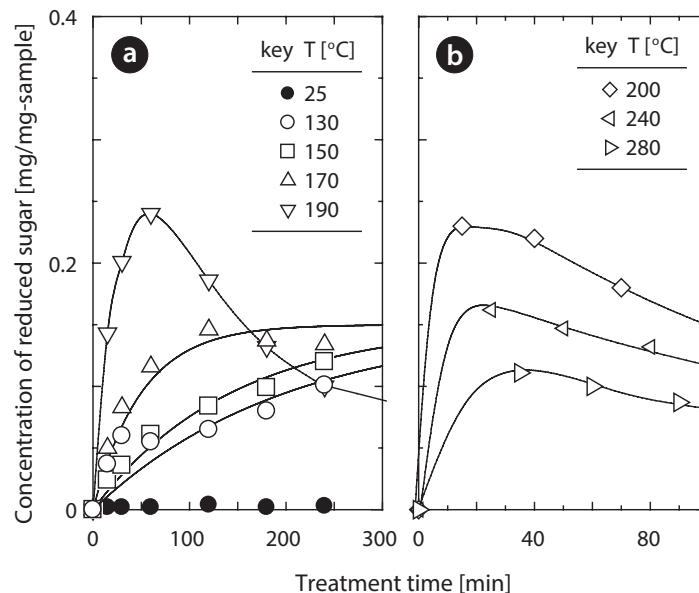


Figure 3. Extraction of reduced sugar from peels of *Carya cathayensis* Sarg by subcritical water.

Alternatively, the extraction of protein from PCCS was monitored under various temperature conditions. Overall, the time- course of extracted protein was similar to the reducing sugar, as shown in Fig. 4(a) and (b). Meanwhile, the extracted amounts of proteins increased with elevated temperature. A small amount of protein was extracted from PCCS at 25 °C. Such extraction behavior was often observed in other fruit and leaves [14]. This is because part of the proteins might be dispersed on the powdered peels.

To estimate the scavenging activity involved in the extraction from PCCS, the DPPH-assay was examined. The time-course of radical scavenging activity in Fig. 5(a) and (b) was similar to those of proteins in Fig. 4(a) and (b). In the high temperature range 12 (more than 200°C), the radical scavenging activity was increased. Such rough correspondence between protein and DPPH-assay is consistent with the previous finding that the proteins showed anti-oxidative activity [10].

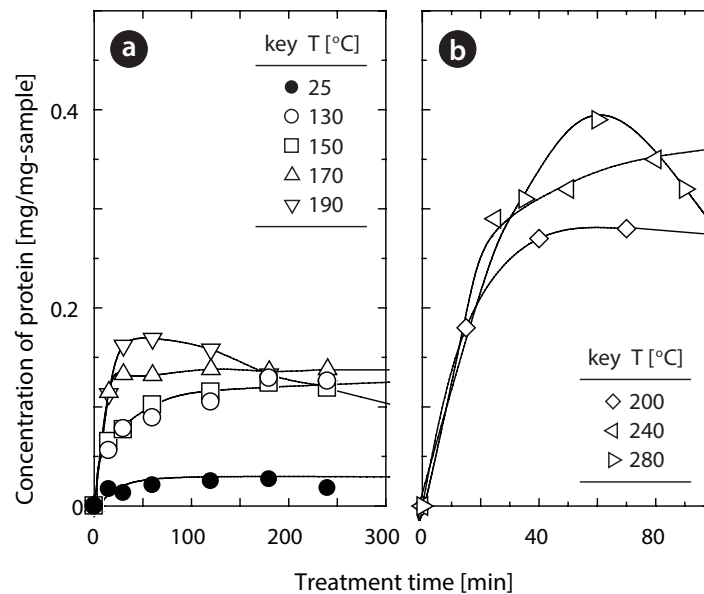


Figure 4. Extraction of protein from peels of *Carya cathayensis* Sarg by subcritical water.

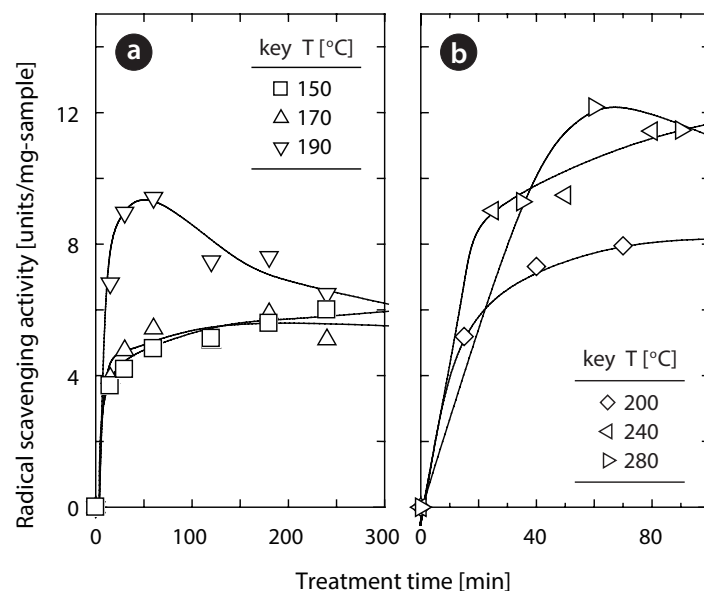


Figure 5. Extraction of compounds with radical scavenging activity from peels of *Carya cathayensis* Sarg by subcritical water.

1.3.3 Optimization of reducing sugar extracts with radical scavenging activity

To determine the optimal condition for extraction of reducing sugar including compounds with radical scavenging activity, the concentration of reducing sugar was plotted against the corresponding radical scavenging activity. A bell-typed curve was observed, as shown in Fig. 6. At the lower temperature range, both reducing sugar and scavenging activity were small. At 190°C, the maximum value of reducing sugar (0.24 mg/mg-sample) was observed at 9.7 units/mg-sample of radical scavenging activity.

With elevated temperature up to 280°C, the concentration of reducing sugar was reduced, whereas the corresponding radical scavenging activity increased. This indicated the instability of reducing sugar under high temperatures, relative to the compound with radical scavenging activity.

We estimated the potential conversion of obtained extracts to bioethanol. In general, 2 mol of bioethanol can be obtained from 1 mol of glucose. The production of 1 L in volume for 15% bioethanol requires 1.29 mol (232.4 g) of glucose. It is therefore considered that 100 g of samples including 0.24 g/g-sample of reducing sugar would yield 1 L of bioethanol. This estimation implies that the present method might be considerably effective for acquiring the bioethanol.

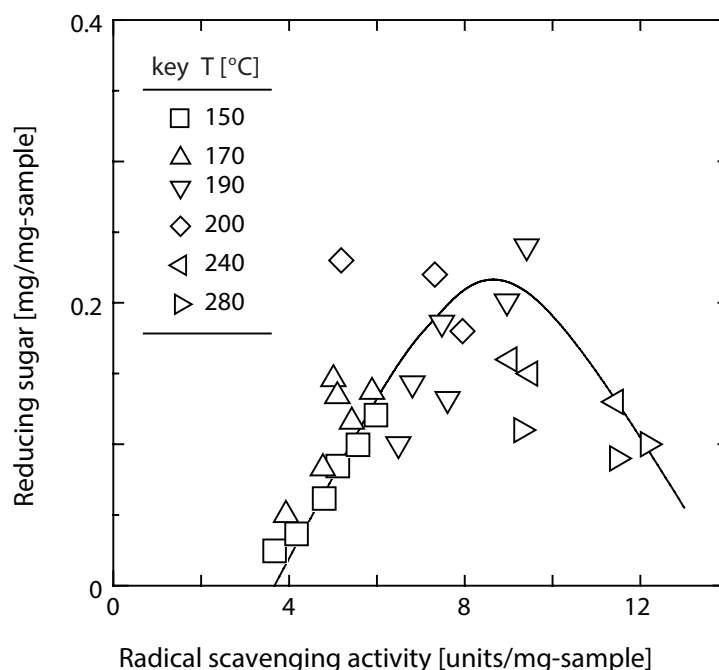


Figure 6. Relationship between the concentration of reducing sugar and the corresponding scavenger activity.

1.3.4 Implications of compounds with scavenging activity

To clarify the radical scavenging activity of extracts, we contrasted them with the corresponding protein concentration. It was found from Fig. 7 that the radical scavenging activity discontinuously increased with increase in the protein concentration. This discontinuously increasing trend was observed between two temperature ranges: 130 to 190 °C and 200 to 280 °C.

In temperature range (130 °C~190 °C), the possible correlated line could be extrapolated into zero protein concentration suggesting that the radical scavenging activity might result from extracted proteins themselves. In contrast to the range (130 °C~190 °C), it was considered that the correlation in the high temperature range (200 °C~280 °C) related to aromatic amino acids rather than proteins, because proteins are decomposed into amino acids under high temperatures [10]. According to the principle of the Lowry method (that quantifies the aromatic amino acids), the decomposition of proteins should increase the apparent protein concentration, which might be a possible reason for the discontinuous increase observed in Fig. 7. Besides, the extracted carbohydrates, such as glucose and fructose, yield the phenol derivatives, furfural, or 5-hydroxymethylfurfural [3, 9, 16]. These compounds have been reported to show anti-oxidative activity [3, 9]. The decomposition of carbohydrates might contribute to the increase in scavenging activity in the high temperature range (200 °C~280 °C). Thus, the discontinuous correlation against the temperature might result from the contribution of compounds other than proteins.

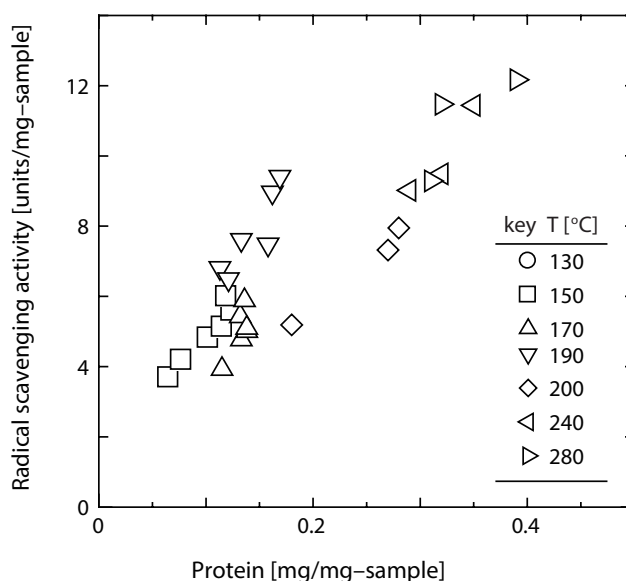


Figure 7. Relationship between the scavenger activity of extracts and the corresponding protein concentration

1.4 Conclusions

The reducing sugar and protein were extracted above 130 °C, whereas they were not extracted at 25 °C. The optimal condition for the treatment of PCCS (190 °C for 60 min) could yield 0.24 g/g-sample of reducing sugar and 9.7 units/mg-sample of radical scavenging activity. It was roughly estimated that 100 g of extracts obtained under optimal condition could be converted to 1 L of 15% bioethanol.

References

- [1] Hu, L.; Zhao, G.; Hao, W.; Tang, X.; Sun, Y.; Lin, L.; Liu, S. J., Catalytic conversion of biomass-derived carbohydrates into fuels and chemicals via furanic aldehydes. *RSC Adv.* 2012, 2, 11184-11206.
- [2] Marx, S.; Brandling, J.; van der Gryp P., Ethanol production from tropical sugar beet juice. *Afr. J. Biotechnol.* 2012, 11, 11709-11720.
- [3] Pourali, O.; Asghari, F. S.; Yoshida, H., Production of phenolic compounds from rice bran biomass under subcritical water conditions. *Chem. Eng. J.* 2010, 160, 259-266.
- [4] Yang, Y.; Belghazi, M.; Lagadec, A.; Miller, D. J.; Hawthorne, S. B., Elution of organic solutes from different polarity sorbents using subcritical water. *J. Chromatogr. A* 1998, 810, 149-159.
- [5] Eckert, C. A.; Bush, D.; Brown, J. S.; Liotta, C. L., Tuning solvents for sustainable technology. *Ind. Eng. Chem. Res.* 2000, 39, 4615-4621.
- [6] Wagman, D. D.; Evans, W. H.; Parker, V. B.; Schumm, R. H.; Halow, I.; Bailey, S. M.; Churney, K. L.; Nuttall, R. L., The NBS tables of chemical thermodynamic properties: selected values for inorganic and C1 and C2 organic substances in SI units. *J. Phys. Chem. Ref. Data* 1982, 11(Suppl 2), 1-407.
- [7] Uematsu, M.; Frank, E. U., Static dielectric constant of water and steam. *J. Phys. Chem., Ref. Data* 1980, 9, 1291-1306.
- [8] Orak, H. H.; Yagar, H.; Isbilir, S. S., Comparison of antioxidant activities of juice, peel, seed of pomegranate (*Punica granatum* L.) and inter-relationships with total phenolic, tannin, anthocyanin, and flavonoid contents. *Food Sci. Biotechnol.* 2012, 21, 373-387.
- [9] Dutta, S.; De, S.; Saha, B., Advances in biomass transformation to 5-hydroxymethylfurfural and mechanistic aspects. *Biomass Bioenerg.* 2013, 55, 355-369.
- [10] Wiboonsirikul, J.; Kimura, Y.; Kanaya, Y.; Tsuno, T.; Adachi, S., Production and characterization of functional substances from a by-product of rice bran oil and protein

production by a compressed hot water treatment. *Biosci. Biotechnol. Biochem.* 2008, 72, 384-392.

[11] Lertittikul, W.; Benjakul, S.; Tanaka, M., Characteristics and anti-oxidative activity of Maillard reaction products from a porcine plasma protein-glucose model system as influenced by pH. *Food Chem.* 2007, 100, 669-677.

[12] Hammond, V. J.; Price, W. C.; Teegan, J. P.; Walsh, A. D., The absorption spectra of some substituted benzenes and naphthalenes in the vacuum ultra-violet. *Discuss. Faraday Soc.* 1950, 9, 53-60.

[13] Scott, A. I., Interpretation of the ultraviolet spectra of natural products. New York: Pergamon; 1964.

[14] Thenmozhi, A.; Rao, U. S., Comparative free radical scavenging potentials of different parts of *Salanum torvum*. *Free Rad. Antioxid.* 2012, 2, 24-29.

[15] Oomori, T.; Khajavi, S. H.; Kimura, Y.; Adachi, S.; Matsuno, R., Hydrolysis of disaccharides containing glucose residue in subcritical water. *Biochem. Eng. J.* 2004, 18, 143-147.

[16] Shimanouchi, T.; Kataoka, Y.; Yasukawa, M.; Ono, T.; Kimura, Y., Simplified model for extraction of 5-hydroxymethylfurfural from fructose: use of water/oil biphasic system under high temperature and pressure conditions. *Solvent Extr. Res. Dev. Jpn.* 2013, 20, 205-212.

APPENDIX-2

Characterization of hydrochar prepared from hydrothermal carbonization of peels of *Carya cathayensis* sarg

2.1 Introduction

Biomass is an important and abundant resource in the world; the annual production was 8 times to the total annual world fossil energy consumption [1]. The advantages of low sulfur content, carbon dioxide capture capability and regenerable ability make biomass become a promising biofuel for taking place of fossil fuel in the future. However, most of biomass was directly combusted as a fuel in the past decades. The high moisture content, hygroscopic feather, low energy value, high volatile content and high oxygen content make biomass define as a low-grade fuel. Therefore, it is necessary to improve the fuel value of biomass. There are many methods to improve fuel value of biomass, one of them is convert biomass to biochar because biochar presents many advantages compare with biomass feedstock such as high carbon content, high energy density, recalcitrant nature and its ability to lower emission of greenhouse gases [2-4].

In recent years, conversion of biomass to biochar (hydrochar) by hydrothermal carbonization method using subcritical water has become a popular topic, because hydrothermal carbonization method gives some advantages comparing with other biochar preparation method: 1) hydrothermal carbonization employs relatively lower temperatures (150~350 °C), 2) the biomass does not need a pre-dried process which cost more, 3) the gases generated during hydrothermal carbonization process could dissolve in water and it makes no further pollution to the air, 4) water in a reactor could dilute the acidic property of bio-oil generated during hydrochar produce process and thus decrease the corrosion to the equipment [2, 5]. Most researchers have focused on preparing hydrochar using pure subcritical water and there was no research about preparing hydrochar by organic solvent-modified subcritical water, where the relative dielectric constant could be changed by addition of organic solvent [2, 6, 7]. It was known that the liquefaction of lignocellulose biomass with methanol- or acetone-modified subcritical water could be significantly changed when compared with that of sole solvent [8]. Additionally, the critical value could be reduced when water was mixed

with acetone or ethanol whose critical value was lower than that of water and the organic solvent could be recycled.

Therefore, in this study, organic solvent (acetone and ethanol)-modified subcritical water was used to hydrothermal carbonation of peels of *Carya cathayensis* sarg (PCCS) in order to investigate the effect of dielectric constant on the properties of prepared hydrochar. The prepared hydrochar would be used as a solid fuel or composed with liquid fuels to make slurry fuels.

2.2 Materials and Methods

2.2.1 Materials

PCCS, which used as a raw material in all the experiment, were produced in Lin'an, China. The cellulose, hemicellulose, lignin and ash contents of PCCS were 13.1%, 22.3%, 56.2% and 5.1% respectively. PCCS were milled using a milling machine (WB-1 Osaka Chemical Corporation, Osaka, Japan) and then screened the powder with the diameter under 0.3 mm. The powder was dried at 105 °C for 24 h before experiment. Ethanol and acetone were purchased from Wako Pure Chemical Industries (Osaka, Japan).

2.2.2 Biochar preparation

Hydrothermal carbonization of PCCS was performed in a batch reactor (Taiatsu Technology Corporation, Osaka, Japan), which was made from SUS316 stainless steel with the volume of 10 mL. On each experiment, 200 mg of the powder was mixed with 8 mL of ultrapure water or water-organic solvent in the volume ratio from 0 to 100% at ambient temperature. Afterward, the mixture was transferred to the batch reactor and the reactor was tightly closed. The reactor was set in a ceramic furnace (ARF-40K, Asahi-Rika, Chiba, Japan) with a temperature controller (TXN-700, AS ONE, Osaka, Japan). Hydrothermal carbonization was carried out at 280 to 360 °C at various organic solvent volume ratios for 15 min and at 280 °C and 360 °C for 15 to 45 min. It took 14 to 21 min to make the temperature inside the reactor reach to the desired temperature. In order to stop the reaction rapidly, the reactor was immersed into an ice bath as soon as the reaction time elapsed. The mixture in the reactor was then filtered using a G-4 glass filter (Vidtec, Fukuoka, Japan). The hydrochar (remained solid) was dried at 110 °C until the weight reached to a constant value. Each experiment was conducted for three times.

2.2.3 Element analysis

The carbon, hydrogen and nitrogen contents of the hydrochar were measured using a PerkinElmer 2400II elemental analyzer (Kanagawa, Japan). The ash content was evaluated by burning the PCCS at 550 °C for 4 h. It was assumed that all of the ash was remained in hydrochar during the hydrothermal carbonization process. Therefore, the ash content could be calculated for each hydrochar from overall mass yield.

2.2.4 Calorific value determination

The higher heating value (HHV) of hydrochar was calculated by a partial least squares regression (PLS) method provided by Friedl *et al.* [9]. The equation was as follows:

$$\text{HHV (PLS)} = 5.22C^2 - 319C - 1647H + 38.6CH + 133N + 21028 \quad (1)$$

where C = carbon, H = hydrogen and N = nitrogen content expressed on a dry ash-free mass percentage.

2.2.5 Thermogravimetric analysis (TGA)

The thermogravimetric analysis was carried out by a thermogravimetry (TG-60A, Shimadzu, Kyoto, Japan). A platinum crucible loaded with 5 to 7 mg of hydrochar was first heated to 105 °C from the room temperature at the heating rate of 20 °C /min and held for 10 min in order to remove the moisture, then continuously heated to 600 °C. N₂ was used as carrier gas with the flow rate of 100 mL/min.

2.2.6 Functional groups on biochar

The functional groups on the hydrochar were analyzed by a Jasco 4100 Fourier transform infrared spectroscopy (FTIR, Jasco, Tokyo, Japan).

2.3 Results and Discussions

2.3.1 Effect of hydrothermal carbonization temperature on hydrochar yield

The effect of hydrothermal carbonization temperature and treatment time on hydrochar yield is shown in Fig. 1. The hydrochar yield was 44.9% at 280 °C for 15 min and it decreased to 27.9% when the temperature increased to 360 °C (Fig. 1a). The hydrothermal carbonization temperature had more effect on hydrochar yield than that of treatment time (Fig. 1b). The decrease of hydrochar yield at higher temperature was due to the continuously decomposition of cellulose and a portion of lignin, because hemicellulose was almost volatilized and carbonized below 250 °C and volatilization of cellulose became faster at the temperature

higher than 250 °C [10-12]. The reduction of hydrochar yield at longer treatment time was probably due to the decomposition of less reactive components of cellulose and a portion of lignin.

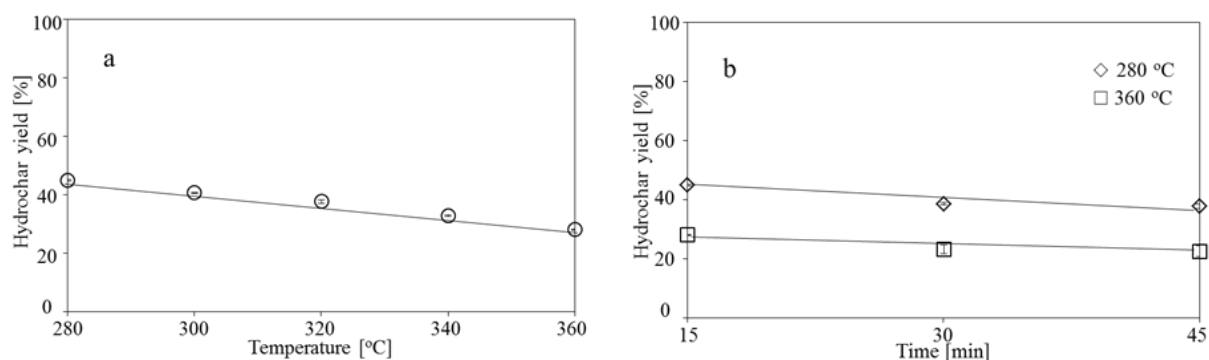


Figure 1. The yield of hydrochar from hydrothermal carbonization of PCCS prepared (a) at various treatment temperatures for 15 min and (b) at (◇) 280 °C and (□) 360 °C for various treatment times

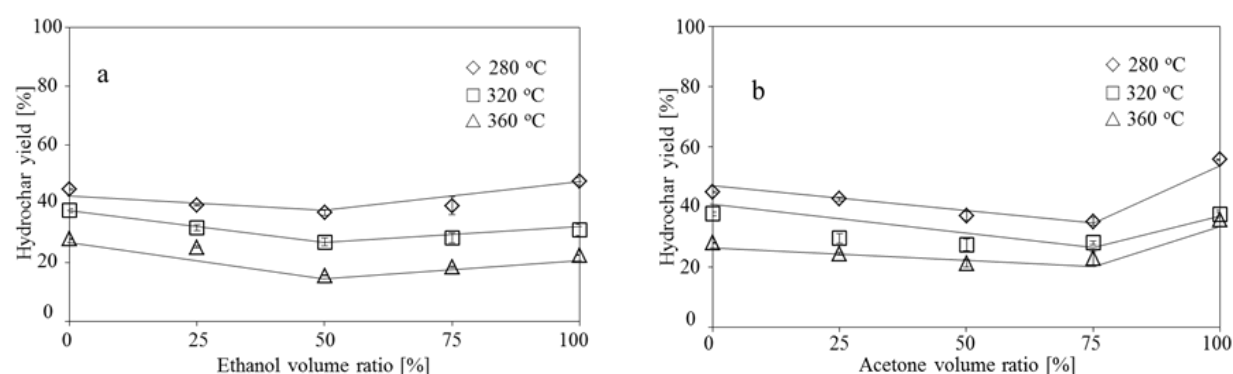


Fig. 2 Effect of (a) ethanol and (b) acetone volume concentration on hydrochar yield at (◇) 280 °C, (□) 320 °C and (△) 360 °C for the treatment of 15 min.

2.3.2 Effect of organic solvent volume ratio on hydrochar yield

The critical values of organic solvent-water mixture were obtained by linear fitting of the data obtained from Yuan *et al.* and Bicker *et al.* and the critical values are shown on Table 1 [13, 14].

Figure 2 shows the effect of ethanol and acetone volume ratios on hydrochar yield at 280, 320 and 360 °C. The hydrochar yield decreased with increasing of ethanol volume ratio from 0 to 50% and then increased at the volume ratio from 75 to 100% (Fig. 2a). The variation tendency of hydrochar yield was coincident with that of sub-and supercritical liquefaction of rice straw in the presence of ethanol- or 2-propanol-water mixture and the hydrogen-donor solvent (ethanol) probably responded for this phenomenon [13]. However, the hydrochars obtained at the ethanol volume ratio from 75 to 100% were lower than that at 0% and it was

different with that of rice straw. When the experiment was carried out with acetone, the hydrochar yield formation was slight decreased when the acetone volume ratio increased from 0 to 75% and then promoted (Fig. 2b).

Judging from all the results, a synergistic effect of water-acetone or water-ethanol for hydrothermal carbonization was observed: the liquefaction rate with acetone-water or ethanol-water mixture was larger than that of water or acetone or ethanol only. Therefore, it was considered that addition of organic solvent could promote both hydrolysis and pyrolysis reaction during the hydrothermal carbonation process. It was known that the liquid phase (bio-oil) after hydrothermal carbonization would be a good source for producing liquid fuel or hydrogen [15, 16]. Therefore, although lower hydrochar yield was obtained when using acetone-water or ethanol-water mixture, higher bio-oil yield could be obtained. Besides, it cost less energy during evaporation of organic solvent containing liquid phase to obtain bio-oil than that of containing water only, because acetone and ethanol have lower boiling point than water. Additionally, the evaporated acetone or ethanol could be reused and it made no further pollution. The research about producing of bio-oil by subcritical liquefaction of biomass will be investigated in the future.

Table 1 The critical value (T_c , T_p) of the used solvents

| Volume ratio (%) | Ethanol-water | | Acetone-water | |
|------------------|---------------|-------------|---------------|-------------|
| | T_c (°C) | T_p (MPa) | T_c (°C) | T_p (MPa) |
| 0 | 374.00 | 22.10 | 374.00 | 22.10 |
| 25 | 342.13 | 17.65 | 339.08 | 17.73 |
| 50 | 313.72 | 11.67 | 304.15 | 13.36 |
| 75 | 278.40 | 8.74 | 269.23 | 8.99 |
| 100 | 243.00 | 6.30 | 235.00 | 4.60 |

2.3.3 Elemental analysis of hydrochar

Figure 3 shows the influence of various hydrothermal carbonization conditions on the elemental contents of hydrochar at ash-free basis. The carbon, hydrogen, nitrogen and oxygen contents of original PCCS were 51.5%, 4.8%, 0.9% and 42.8%, respectively. The carbon content of hydrochar was concentrated from 51.5% to 84.8% with increasing of hydrothermal

carbonization temperature, along with significant decreasing of oxygen content. However, the hydrogen and nitrogen contents were nearly the same. Meanwhile, the ash content was increased when the hydrothermal carbonization temperature increased (Fig. 3a). These results were due to the dehydration, decarbonation and demethanation during the hydrothermal carbonization process. The spectra peak of FT-IR, which would be discussed later, also demonstrated that the aforementioned reactions occurred during hydrothermal carbonization process. Additionally, the dehydration was more drastic than decarbonation and demethanation during hydrothermal carbonization (Fig. 4).

The carbon content was also increased when PCCS were treated at longer time at 280 and 360 °C, respectively. The oxygen content was even decreased to as low as 1.31% at 360 °C for 45 min (Fig. 3b). The low oxygen content was due to the decomposition of hemicellulose and cellulose, which contained high oxygen content at that treatment temperature. This result was in accordance with the low hydrochar yield, which was due to the decomposition of hemicellulose and cellulose during subcritical water treatment at 360 °C (Fig. 1b).

The carbon, hydrogen, oxygen, or nitrogen content should be changed with hydrochar yield. However, the carbon, oxygen, nitrogen and ash contents of hydrochars were almost the same and only the hydrogen content was changed with hydrochar yield when PCCS treated with acetone- and ethanol-modified subcritical water (Fig. 3c, 3d). Therefore, we considered that polymerization reaction or other reactions had been occurred between acetone/ethanol and cellulose or lignin in the hydrochar and these reactions supplemented the qualities of carbon and oxygen lost during hydrothermal carbonization. The results described above suggested that acetone- and ethanol-modified subcritical water could effectively stabilize the carbon, oxygen and hydrogen contents in hydrochar.

The H/C and O/C values were one of the important properties for characterization of solid fuels. Therefore, the H/C and O/C values of hydrochars prepared at various conditions as well as coal band on the van Krevelen diagram are shown in Fig. 4. The O/C and H/C values significantly decreased after hydrothermal carbonization. It was due to the dehydration, decarbonation and demethanation reactions during hydrothermal carbonization process. The H/C and O/C values of all the hydrochars could be compatible with those of subbituminous and lignite coal except the ash content. The H/C and O/C values of hydrochars obtained at 360 °C for various treatment times could even be compatible with that of bituminous coal. These results suggested that hydrothermal carbonization process using subcritical water would be an effective method to lower H/C and O/C values of hydrochar, which intended to use as a fuel.

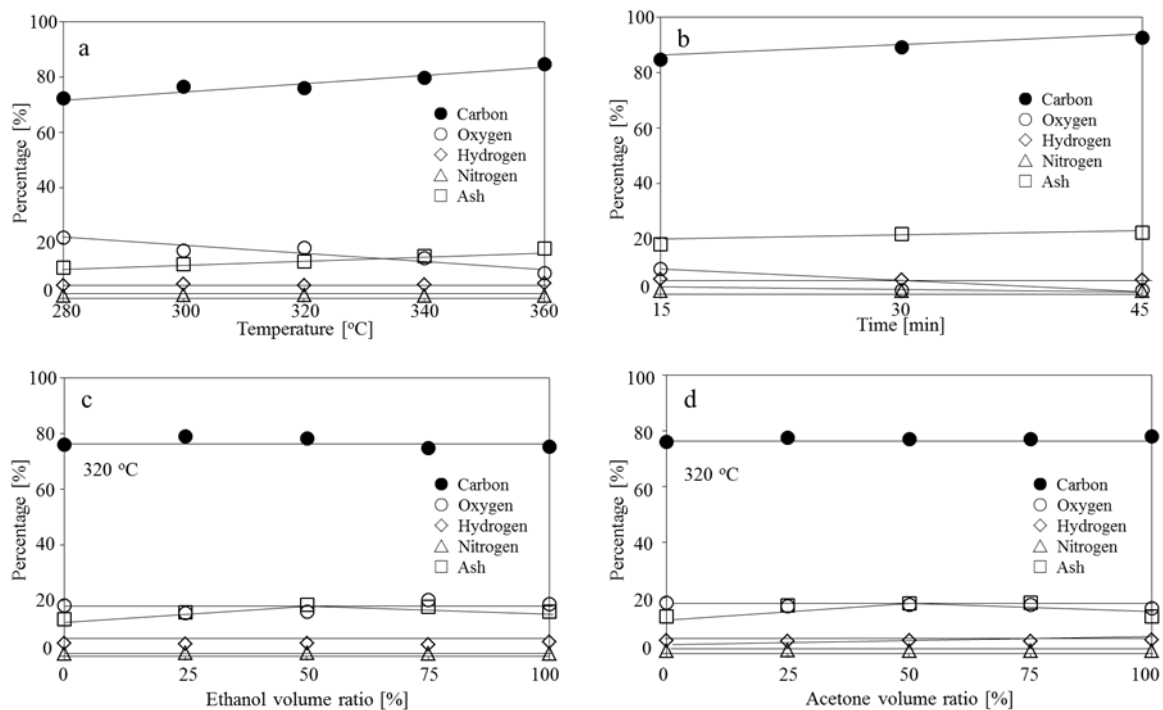


Figure 3. Effect of (a) various treatment temperatures (b) various treatment times at 360 °C (c) ethanol volume ratio at 320 °C and (d) acetone volume ratio at 320 °C on the (●) carbon, (○) oxygen, (◇) hydrogen, (△) nitrogen and (□) ash contents of hydrochar.

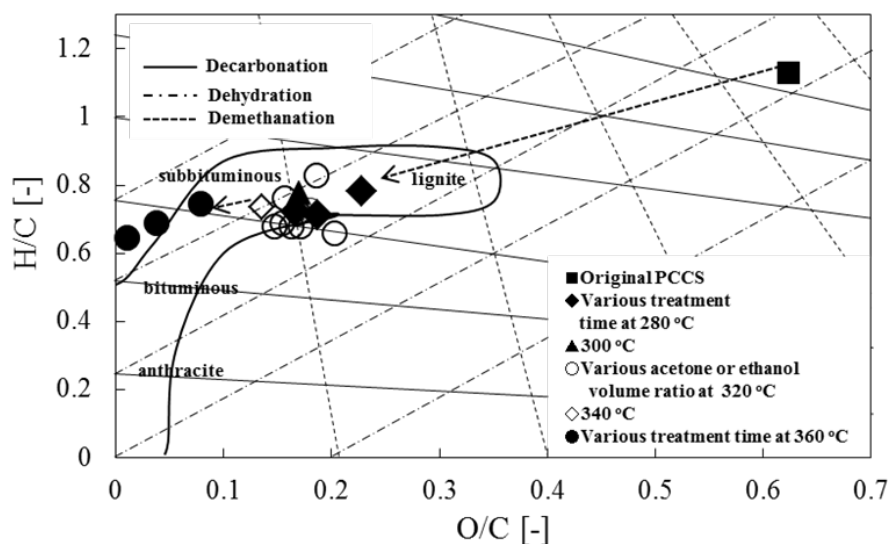


Figure 4. Van Krevelen diagram of (■) original PCCS, hydrochars prepared at (◆) 280 °C for various treatment times, (▲) 300 °C, (○) 320 °C for various acetone or ethanol volume ratios, (◇) 340 °C, (●) 360 °C for various treatment times as well as coal band.

2.3.4 Caloric value of biochar

HHV is another important property to evaluate solid fuels and the HHVs of hydrochars were calculated from the element contents of carbon, hydrogen and nitrogen on dry ash-free basis. The HHV of hydrochar increased from 30.8 to 40.2 MJ/kg with the temperature increasing from 280 to 360 °C. It was an increase of 52.4% to 127.6% compared to the original PCCS (20.2 MJ/kg) (Fig. 5a). The HHV was continuously elevated at the longer treatment time on 280 and 360 °C, respectively (Fig. 5b). The HHVs of hydrochars were much higher than those of methanol (22.7 MJ/kg) and pyrolytic oil (24.7 MJ/kg) and they could also be compatible with those of lignite char (31.3 MJ/kg) and charcoal (34.4 MJ/kg), additionally, the HHVs of hydrochars prepared at 360 °C could even be compatible with those of diesel oil (45.7 MJ/kg) and heavy fuel oil (42.9 MJ/kg) [17].

The HHVs of hydrochars obtained from acetone- and ethanol-modified subcritical water carbonization at 320 °C were almost the same although acetone- and ethanol-water mixture accelerated the liquefaction rate of PCCS (Fig. 5c).

The results aforementioned suggested that hydrothermal carbonization of biomass would be an effective method to get energy-dense hydrochars from biomass.

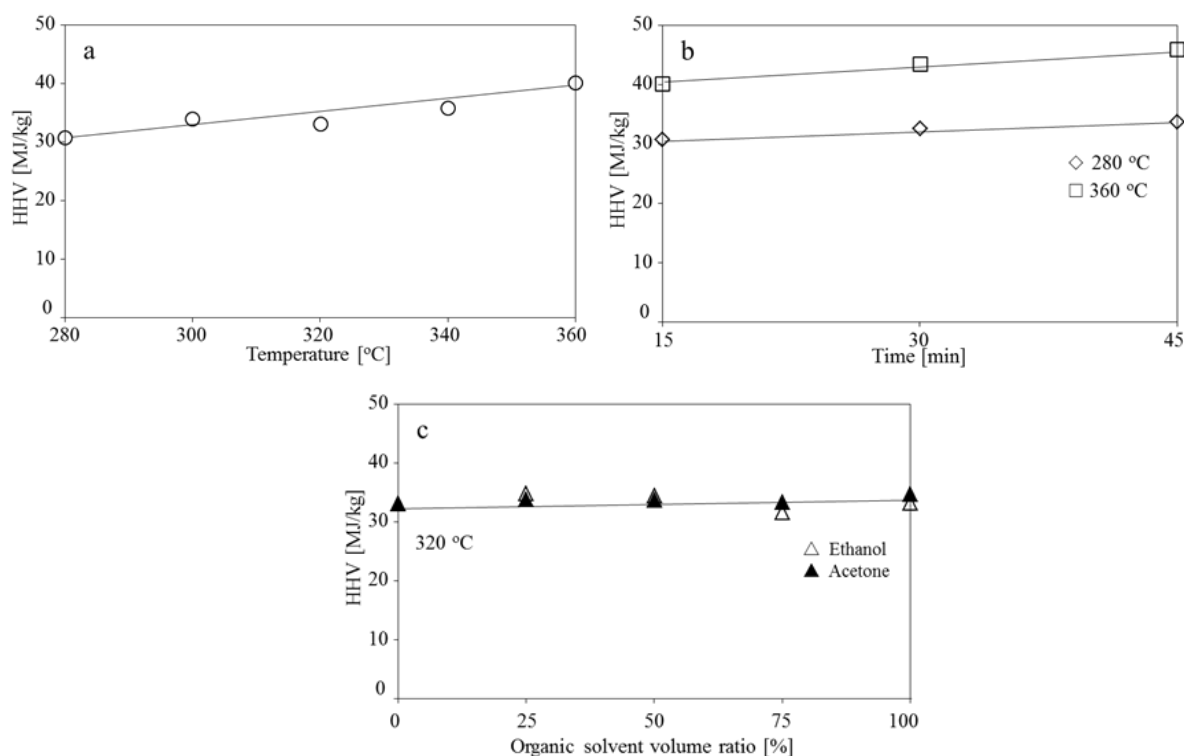


Figure 5. Effect of (a) treatment temperature (b) treatment time (□) 280 °C and (◇) 360 °C and (c) organic solvent volume ratio (▲) acetone and (△) ethanol at 320 °C on the HHV of hydrochar.

2.3.5 Thermogravimetric analysis

Thermogravimetric analysis of hydrochars prepared at various conditions is shown in Fig. 6. The weight loss mainly occurred at the temperatures between 200 °C and 500 °C. The thermal stability was promoted with the increasing of hydrothermal carbonization temperature (Fig. 6a). Higher ash and lower volatile matter content probably responded the thermal stability of hydrochars. The thermal stabilities of hydrochars obtained at the ethanol volume ratio from 0 to 75% were more stable than that prepared at 100% (Fig. 6b). However, the thermal stability of hydrochars prepared by acetone-modified subcritical water had no regulation. The thermal stability of hydrochars did not change a lot at the acetone concentration of 0%, 25% and 75%, but it was decrease at the concentration of 50% and 100% (Fig. 6c).

From all the results described above, it was found that hydrochar with high thermal stability could be obtained by hydrothermal carbonization method.

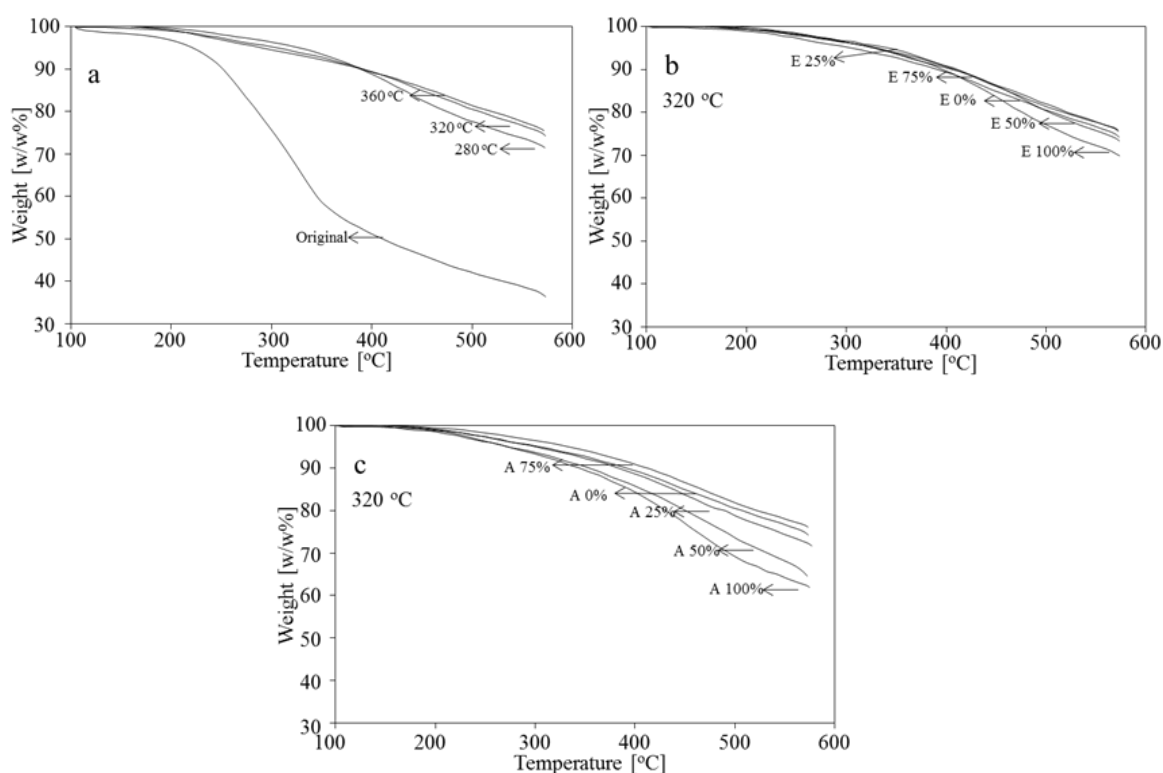


Figure 6. TGA curves of hydrochars prepared at (a) various hydrothermal carbonization temperatures and various (b) acetone and (c) ethanol volume ratios at 320 °C. A (E) 50% = Acetone (ethanol) volume ratio of 50%

2.3.5 Functional groups on biochar

The FT-IR spectra of hydrochar prepared at various conditions are shown in Fig. 7. Figure 7a shows the effect of temperature on the functional groups of hydrochar. The spectra

peak of C-O linkage at the wave range from 1120 to 1050 cm^{-1} disappeared compared to the original PCCS. It indicated that the ether bond in hemicellulose and cellulose and the methoxy group in lignin that are easy to break in hydrothermal process were fractured during subcritical water treatment [2]. The benzene peak, which were typically around 1600, 1510 and 1440 cm^{-1} had no significant change. This result supposed that the lignin derived aromatic structure was very stable even the temperature reached to 360 °C. The phenolic OH peak at 1330 cm^{-1} was decreased or disappeared during the subcritical water treatment and the β -anomers or β -linked glucose polymers peak absorbed at around 893 cm^{-1} disappeared with the increasing of treatment temperature.

The phenomenon was in accordance with those described above when PCCS were treated by acetone- or ethanol-modified subcritical water except the peak at 893 cm^{-1} (Fig. 7b). The β -anomers or β -linked glucose polymers peak at 893 cm^{-1} was shifted to around 873 cm^{-1} after treatment.

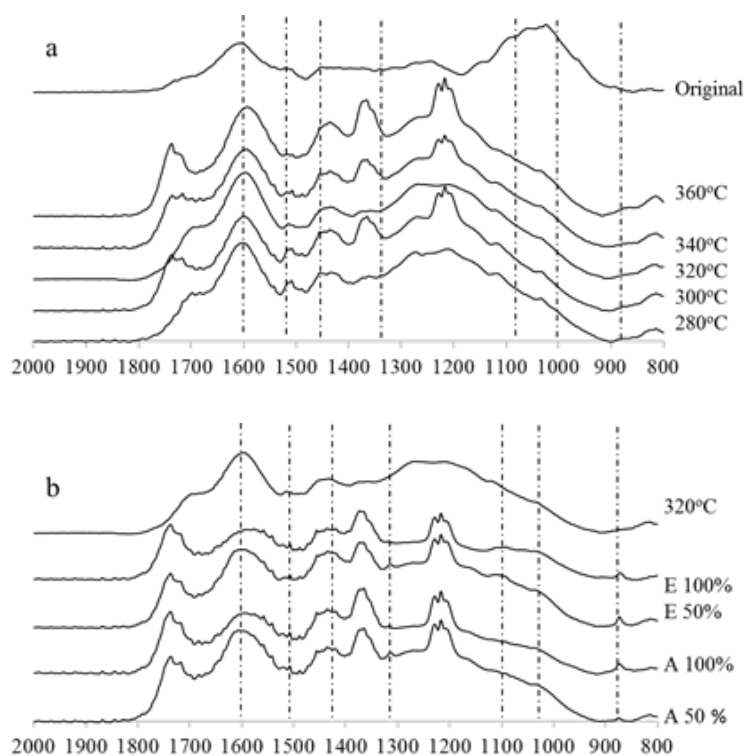


Figure 7. FT-IR spectra of hydrochar prepared on (a) different temperature and (b) various organic solvent volume ratios at 320 °C. A(E) 50% = Acetone (ethanol) volume ratio of 50%.

2.4 Conclusion

Hydrothermal carbonization of PCCS by subcritical water or acetone- or ethanol-modified subcritical water at various treatment temperatures and times were carried out in this study and coal-like hydrochars were obtained. The hydrochar yield decreased with

increasing of treatment temperature, but hydrochar with higher carbon content, higher HHV, lower volatile matter content, lower oxygen content and O-containing functional groups was obtained at the same time. The carbon content and HHV of hydrochar were among 72.3%-92.6% and 30-46MJ/kg, respectively. The HHVs of hydrochars were much higher than those of methanol and pyrolytic oil and they could be compatible with those of lignite char and charcoal. These results indicated that hydrothermal carbonization could be an effective process to produce higher carbon content and higher energy-density hydrochar. The O/C and H/C values of hydrochars could be compatible with those of lignite and subbituminous. Especially the O/C and H/C values of hydrochars prepared at 360 °C were similar to that of bituminous except the ash content. When treated with acetone- or ethanol-modified subcritical water, a synergistic effect of acetone-water or ethanol-water for hydrothermal carbonization was observed: the liquefaction rate with acetone-water or ethanol-water mixture was larger than that of water or acetone or ethanol only. Although lower hydrochar yield was obtained when using acetone-water or ethanol-water mixture, more bio-oil, which was good source for producing liquid fuel or hydrogen, could be obtained at the same time. Acetone- or ethanol-modified subcritical water could effectively stabilize the carbon and oxygen contents in hydrochar.

References

- [1] Xu, C. B.; Lad, N., Production of heavy oil with high caloric value by direct liquefaction of woody biomass in sub/near-critical water. *Energy Fuels* 2008, 22, 635-642.
- [2] Kang, S. M.; Li, X. G.; Juan, F.; Jie, C., Characterization of hydrochars produced by hydrothermal carbonization of lignin, cellulose, d-xylose, and wood meal. *Ind. Eng. Chem. Res.* 2012, 51, 9023-9031.
- [3] Vaccari, F. P.; Baronti, S.; Lugato, E.; Genesio, L.; Castaldi, S.; Fornasier, F.; Miglietta, F., Biochar as a strategy to sequester carbon and increase yield in durum wheat. *Eur. J. Agron.* 2011, 34, 231-238.
- [4] Lehmann, J.; Gaunt, J.; Rondon, M., Bio-char sequestration in terrestrial ecosystems: A review. *Mitig. Adapt. Strategies Glob. Change* 2006, 11, 403-427.
- [5] Xue, Y. W.; Gao, B.; Yao, Y.; Inyang, M.; Zhang, M.; Zimmerman, A. R., Hydrogen peroxide modification enhances the ability of biochar (hydrochar) produced from hydrothermal carbonization of peanut hull to remove aqueous heavy metals: Batch and column tests. *Chem. Eng. J.* 2012, 200, 673-680.
- [6] Sun, K.; Ro, K.; Guo, M. X.; Novak, J.; Mashayekhi, H.; Xing, B. S., Sorption of bisphenol A, 17 α -ethinyl estradiol and phenanthrene on thermally and hydrothermally

produced biochars. *Bioresource Technol.* 2011, *102*, 5757-5763.

[7] Liu, Z.; Zhang, F., Removal of lead from water using biochars prepared from hydrothermal liquefaction of biomass. *J. Hazard. Mater.* 2009, *167*, 933-939.

[8] Yao, Y. G.; Yoshioka, M.; Shiraishi, N., Soluble properties of liquefied biomass prepared in organic solvents I: The soluble behavior of liquefied biomass in various diluents. *Mokuzai Gakkaishi* 1994, *40*, 176-184.

[9] Friedl, A.; Padouvas, E.; Rotter, H.; Varmuza, K., Prediction of heating values of biomass fuel from elemental composition. *Anal. Chim. Acta* 2005, *544*, 191-198.

[10] Ranu, P.; Mizanur Rahman, A. N. M.; Bhattacharya, S. C., Upgrading of biomass by means of torrefaction. *Energy* 1990, *15*, 1175-1179.

[11] Anuphon, P.; Animesh, D.; Prabir, B., Torrefaction of agriculture residue to enhance combustible properties. *Energy Fuels* 2010, *24*, 4638-4645.

[12] Mark, J. P.; Krzysztof, J. P.; Frans, J. J. G. J., Torrefaction of wood Part 1: Weight loss kinetics. *J. Anal. Appl. Pyrolysis* 2006, *77*, 28-34.

[13] Yuan, X. Z.; Li, H.; Zeng, G. M.; Tong, J. Y.; Xie, W., Sub- and supercritical liquefaction of rice straw in the presence of ethanol-water and 2-propanol-water mixture. *Energy* 2007, *32*, 2081-2088.

[14] Bicker, M.; Hirth, J.; Vogel, H., Dehydration of fructose to 5-hydroxymethylfurfural in sub- and supercritical acetone. *Green Chem.* 2003, *52*, 80-284.

[15] Huber, G. W.; Cheda, J. N.; Barrett, C. J.; Dumesic, J. A., Production of liquid alkanes by aqueous processing of biomass derived carbohydrates. *Science* 2005, *308*, 1446-1450.

[16] Valenzuela, M. B.; Jones, C. W.; Agrawal, P. K., Batch aqueous reforming of woody biomass. *Energy Fuels* 2006, *20*, 1744-1752.

[17] Channiwala, S. A.; Parikh, P. P., A unified correlation for estimating HHV of solid, liquid and gaseous fuels. *Fuel* 2002, *81*, 1051-1063.

APPENDIX-3

Characterization of the residue and liquid products produced from husks of nuts from *Carya cathayensis* sarg by hydrothermal carbonization

3.1 Introduction

Biomass, as an important and abundant renewable resource in the world, is considered to be a promising energy alternative to fossil fuels in the future because it is more environment-friendly than fossil fuels in many aspects. Namely, it captures carbon dioxide through photosynthesis, which can offset the carbon dioxide emitted during combustion of biomass, and it also emits less sulfur than fossil fuels when it is combusted. However, biomass is regarded as a low-grade fuel because of its inherent properties such as high moisture content, high volatile content, low energy density and high oxygen content [1]. It is necessary to apply pretreatment processes to overcome these drawbacks.

There are several methods to pretreat biomass: fast and slow pyrolysis to obtain bio-oil and gasification to obtain bio-gases [2, 3]. However, all of these treatments are carried out at high temperatures and with a carrier gas throughout the process in order to isolate oxygen and/or carry bio-gases and volatile materials out of the reactor. In addition, all existing treatments require pre-drying of the biomass in order to improve the quality of the product.

Compared with the methods described above, hydrothermal carbonization using subcritical water has some advantages [4, 5]. Lower treatment temperatures (180-260 °C) and the elimination of both a pre-drying step and the need for a carrier gas should make hydrothermal carbonization a lower-cost treatment option. Additionally, this method can avoid the noxious air pollution caused by nitrogen and sulfur oxides and corrosion to the treatment equipment from the acidic properties of the generated products in the liquid phase. Taken together, hydrothermal carbonization is a promising method for biomass pretreatment. Up to now, much information could be obtained about hydrothermal carbonization of various biomasses by subcritical water [6-12]. For example, Yan *et al.* and Reza *et al.* pretreated loblolly pine with hot compressed water to upgrade the fuel properties of loblolly pine [4, 6, 7]. Chen *et al.* performed hydrothermal carbonization of sugarcane bagasse via wet torrefaction for biofuel production [5]. In all of the above researches, the fuel properties of

raw biomass were significantly elevated after hydrothermal carbonization and a solid char with high energy density and calorific value was obtained. However, to our knowledge, there has been no report about the influence of pH on the hydrothermal carbonization of biomass, a key issue since the ion product of subcritical water would be changed with the addition of acid or alkali. It is known that cellulose and hemicellulose are hydrolyzed/decomposed during subcritical water hydrothermal liquefaction [13, 14] and that the addition of acid could accelerate the hydrolysis/decomposition rates, but the effect of pH on hydrothermal carbonization of biomass is still unclear, given its more complex structure than pure cellulose and hemicellulose.

In this study, subcritical water was applied to hydrothermal carbonization of husks of nuts from *Carya cathayensis* Sarg (HCCS, in other words, HCCS is husks of hickory nuts) as a model waste biomass. Roughly 7000 tons of this biomass are generated annually in China, and an effective treatment method for this resource has been anticipated. The purpose of this research is to upgrade the value of HCCS as a fuel source including carbon content, energy value and water-resisting property. The effect of pH on hydrothermal carbonization of HCCS was also investigated in order to determine the optimal conditions for hydrothermal carbonization of HCCS. Further, the fuel properties of obtained liquid products were characterized to evaluate their potential for application as resource for bio-fuel production.

3.2 Materials and Methods

3.2.1 Materials

HCCS, as the raw material in all the experiments, came from Lin'an, China. The husks were milled and screened using a milling machine (WB-1, Osaka Chemical Corp., Osaka, Japan) to obtain powder with a diameter under 0.3 mm, and the powder was dried at 105 °C for 24 h before the experiments. The reagents used here were all purchased from Wako Pure Chemical Industries (Osaka, Japan).

3.2.2 Hydrothermal carbonization of husks of *Carya cathayensis* Sarg (HCCS)

Figure 1 shows the flow scheme of HCCS treatment during hydrothermal carbonization. Hydrothermal carbonization of HCCS was carried out in a batch reactor (Taiatsu Technology Corp., Osaka, Japan) made from SUS 316 with the volume of 10 mL. A mixture of 200 mg of HCCS and 8 mL of ultrapure water with a pH of 4.0, 5.9, 7.0, 10.0 or 13.0 (pH was adjusted by HCl or NaOH; the pH of ultrapure water was 5.9) was loaded into the batch reactor, and

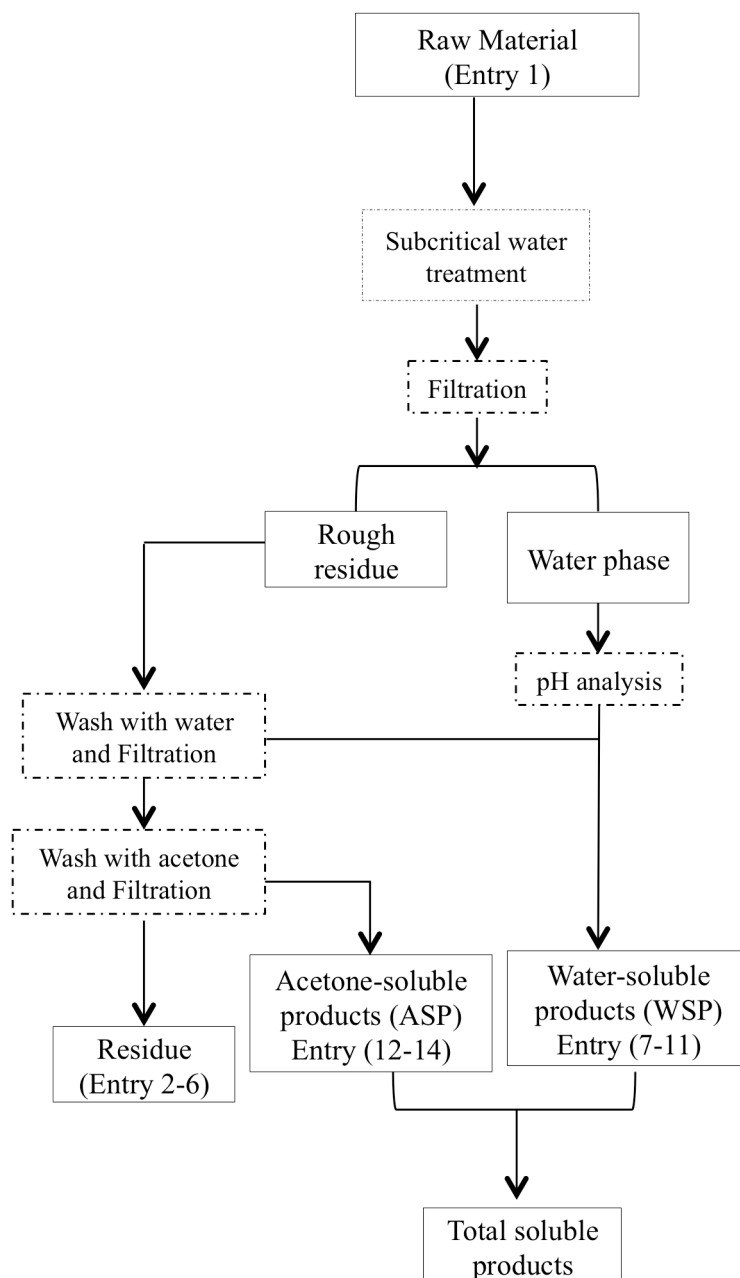


Figure 1. The flow scheme of HCCS treatment during hydrothermal carbonization.

the reactor was tightly sealed. The reactor was then set in a ceramic furnace (ARF-40K, Asahi-Rika, Chiba, Japan) with a digital temperature controller (TXN-700, AS ONE, Osaka, Japan). Hydrothermal carbonization was carried out from 180 to 260 °C with the treatment time of 10 min at various pHs. The reactor was immersed in an ice bath as soon as the reaction time elapsed. The mixture was filtered with a G-4 glass filter (Vidtec, Fukuoka, Japan). The pH of obtained filtrate was measured by a HM-25R pH meter (DKK-TOA Crop. Tokyo, Japan). The remaining solid (rough residue) was first washed with 20 mL ultrapure water and then with 20 mL acetone. After that, all of the obtained filtrates were dried at 60 °C

and the remaining liquid products were designated as water-soluble products (WSP) and acetone-soluble products (ASP), respectively. The residue was dried at 105 °C to reach a constant weight. It should be noted that the partition of the sodium ions (in the case of pH 13) between residue and WSP would be affected by the ion exchange of the sodium ions with the HCCS and neutralization of generated organic acid by NaOH during hydrothermal carbonization. Our X-ray fluorescence (XRF) measurement revealed that the residue contained low amount of sodium ion (less than 0.02 wt%), which was similar to that of raw HCCS. Therefore, to simplify the calculation, we assumed that these sodium ions were primarily present in the residue and all the sodium ions from NaOH were remained in the WSP. We did not consider about the hydroxide ion from NaOH because it might be contained in all of the hydrothermal carbonization products, including water and other volatile products that were difficult to calculate. We also assumed that no ash was dissolved in the subcritical water during hydrothermal carbonization. The yields of the residue, WSP, ASP and total soluble products were calculated by the following equations:

$$\text{Yield}_{(\text{residue})}(\%) = (\text{mass of dry and ash-free residue}) / (\text{mass of dry and ash-free HCCS}) \times 100\% \quad (1)$$

$$\text{Yield}_{(\text{WSP})}(\%) = (\text{mass of WSP}) / (\text{mass of dry and ash-free HCCS}) \times 100\% \quad (2)$$

$$\text{Yield}_{(\text{ASP})}(\%) = (\text{mass of ASP}) / (\text{mass of dry and ash-free HCCS}) \times 100\% \quad (3)$$

$$\text{Yield}_{(\text{Total soluble products})}(\%) = \text{Yield}_{(\text{WSP})} + \text{Yield}_{(\text{ASP})} \quad (4)$$

3.2.3 Analysis of the HCCS, residue, WSP and ASP

The lignin contents of the HCCS and residue were determined by a 72% sulfuric acid method, and the holocellulose and cellulose were measured by the method described by T. Yokoyama *et al.* [15, 16]. The hemicellulose content was calculated by the weight difference between holocellulose and cellulose. The weight of each component was calculated by the following equation:

$$\text{Component weight} = C \times \text{weight of the residue} \quad (5)$$

where C is the cellulose, hemicellulose or lignin content in the residue.

The FTIR spectra of WSP and ASP were analyzed by Fourier transform infrared spectroscopy (Jasco 4100, Jasco, Tokyo, Japan). The spectra were acquired in the range of 4000-1000 cm^{-1} .

The C, H and N contents of the residue, WSP and ASP were analyzed using a PerkinElmer 2400 II elemental analyzer (Kanagawa, Japan). The elemental content of the residue was further corrected for ash content to give the elemental content of the residue on an

ash-free basis, and the element content of WSP was corrected for the sodium ion content to express the element content on a sodium ion-free basis.

The HHVs of the residue, WSP and ASP were determined from their elemental contents and they were calculated by the equation as follows [17]:

$$\text{HHV (MJ/kg)} = 5.22C^2 - 319C - 1647H + 38.6CH + 133N + 21028 \quad (6)$$

where C = carbon, H = hydrogen and N = nitrogen content expressed on mass percentage.

The method to evaluate equilibrium moisture content (EMC) of the HCCS and residue was as follows: About 100 mg of HCCS or the residue was placed in a plastic dish and then into a big plastic bottle containing a saturated salt solution at the experimental temperature of 30 °C. Each experiment was performed in triplicate. Potassium acetate, magnesium nitrate and sodium chloride with relative humidities (RH) of 23%, 53% and 75%, respectively, were used to control the relative humidity in the plastic bottle. It took 20-30 days for the HCCS and residue to reach equilibrium. The EMC was calculated by the weight difference before and after treatment.

3.3 Results and Discussion

3.3.1 Effect of treatment temperature and pH on the yields of residue, WSP and ASP

Figure 2a and 2b show the effect of hydrothermal carbonization temperature and pH on the yields of residue, WSP and ASP for the treatment time of 10 min, respectively. The yield of the residue was drastically reduced with increasing of hydrothermal carbonization temperatures, and it reached about 48.1% of the initial HCCS when the temperature was 260 °C (Fig. 2a), probably due to the hydrolysis/decomposition of cellulose, hemicellulose and apportion of lignin. The yield of WSP showed a slight decrease with the increase in the hydrothermal carbonization temperature and the yield of ASP increased as the hydrothermal carbonization temperature increased to 260 °C. However, the yield of total soluble products hardly changed as the temperature increased from 180 to 260 °C, which revealed that the HCCS hydrolysis/decomposition rate and total soluble products hydrolysis/decomposition rate reached an equilibrium state in the 180-260 °C temperature range. Therefore, the optimal temperature for liquefaction of HCCS to obtain total soluble products in the conditions of our study (e.g., milled input, 10-min treatment time) was 180 °C.

The yields of the residue, WSP and ASP were nearly the same when the pH was increased from 4.0 to 10.0 at each hydrothermal carbonization temperature. However, the yields of WSP and ASP, especially the yield of WSP increased when the pH was 13.0,

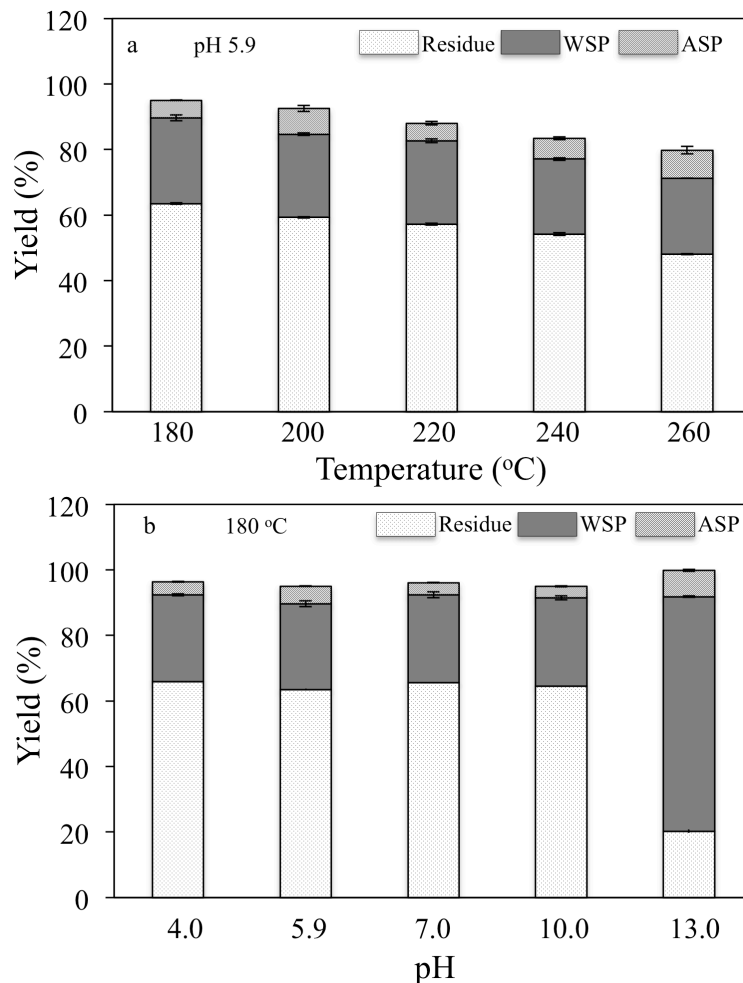


Figure 2. Effect of (a) temperature and (b) pH on yields of residue, WSP and ASP. (n=3). Treatment time: 10 min.

resulting the yield of total soluble products reached to over 80% even at 180 °C. Meanwhile, the residue yield fell steeply to 20% (Fig. 2b). The similar results were obtained when evaluation of the effect of pH on the yields of residue, WSP and ASP at the temperatures of 220 and 260 °C (data not shown). These results suggested that higher pH could effectively liquefy the HCCS during the hydrothermal carbonization process. As reported by Lynam *et al.*, more cellulose could be reacted with large amounts of acetic acid (concentration: 1.79 M and 2.31 M), and acetic acid at those concentrations appeared to perform a catalytic role in hydrothermal carbonization [18]. Likewise, in this study, the weights of cellulose, hemicellulose and lignin showed no significant changes in the pH range from 4.0 to 10.0 but were steeply decreased when the pH was 13.0. These phenomena (Table 1), discussed below, indicate that HCl or NaOH at concentrations of 10^{-4} M (pH 4.0-10.0) are not high enough to accelerate the hydrolysis/decomposition of cellulose whereas NaOH at 0.1 M (pH 13.0) did

effectively promote the hydrolysis/decomposition of cellulose in the hydrothermal carbonization process.

The mass yield after hydrothermal carbonization was reduced from 95.1% to 79.8% as the temperature increased from 180 to 260 °C. This phenomenon meant that 4.9% to 20.2% of volatile products (i.e. formic acid, acetic acid, furfural and water) [13, 14] and bio-gases such as CO₂ and NO_x were generated during hydrothermal carbonization [19]. The pH ranging from 4.0 to 10.0 had no effect on the mass yield. However, there was an increase in mass yield when the pH reached 13.0 (Fig. 2b) and the same results were obtained at 220 and 260 °C (data not shown). This fact means that a higher NaOH concentration inhibited the generation rates of volatile products and bio-gases.

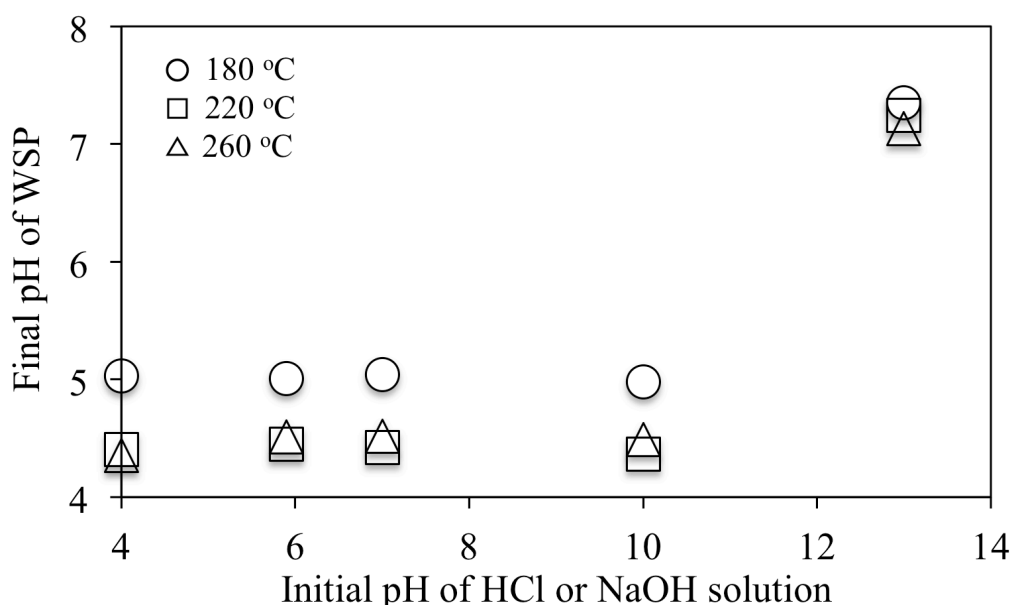


Figure 3. Effect of initial pH on the final pH of WSP obtained at various temperatures.

3.3.2 The final pH of WSP

Organic acids were generated during hydrothermal carbonization of biomass and they would change the final pH of water phase. We thus measured the pH of WSP obtained after hydrothermal carbonization of HCCS, and the results are shown in Fig. 3. The final pH of WSP decreased with the increase in the hydrothermal carbonization temperature and it reduced to 4.4 at 260 °C and initial pH 5.9. Changing the pH from 4.0 to 10.0 had no dramatic effect on the final pH of WSP obtained at the temperature of 180 °C and the final pH of WSP was around 5.0. However, the final pH was 7.4, which was still maintained at the weak alkali value when the initial pH was 13.0. The similar results were also obtained during evaluating the final pHs of WSP in other temperatures. The decrease of final pH during hydrothermal carbonization was mainly caused by the formation of carboxylic acids, including acetic acid,

lactic acid and formic acid [13], whereas the remaining of final pH in a weak alkali value revealed that the generated carboxylic acids were all neutralized by NaOH during hydrothermal carbonization.

3.3.3 Determination of compositions of HCCS and the residue

Cellulose, hemicellulose and lignin are the primary components of biomass. In this study, the main components of the residue prepared at various conditions were analyzed to help elucidate the reaction mechanism in hydrothermal carbonization. As shown in Table 1, the weights of cellulose, hemicellulose and lignin in 200 mg of HCCS before hydrothermal carbonization were 24.7, 41.8 and 106.4 mg, respectively (entry 1). Hemicellulose was dramatically decreased to 10.3 mg with hydrolysis/decomposition of 75% even at 200 °C (entry 3), and showed further slight reductions at higher temperatures. It seemed more difficult to hydrolyze/decompose cellulose than hemicellulose and the weight of cellulose was reduced from 19.3 to 10.2 mg with the decrease of 11.9% to 58.3% as the temperature increased from 180 to 260 °C (entries 2-6) at the pH of 5.9. The weight of lignin decreased from 83.7 to 77.6 mg with the decline of 21.4% to 27.1% in the temperature range of 180-260 °C (entries 2-6) at pH 5.9. Therefore, cellulose and hemicellulose were more reactive than lignin during hydrothermal carbonization of HCCS, and it was confirmed that this reduction of residue yield was primarily due to the hydrolysis/decomposition of hemicellulose and cellulose in HCCS.

The variation of pH within the range of 4.0-10.0 had no significant effect on the weights of cellulose, hemicellulose and lignin in the residue, resulting the constant values of residue yield. However, all of the solid components, especially the lignin, were dramatically decreased at pH 13.0 (entries 2-5) and almost all of them were hydrolyzed/decomposed at 260 °C (entry 6). It was previously reported that, the addition of H₂SO₄ to a final concentration of 0.1 M could remove a large amount of hemicellulose at 180 °C in 5-min hydrothermal carbonization of bagasse [5]. In contrast, all of the compositions were effectively liquefied when NaOH was employed at a concentration of 0.1 M (pH 13.0). Therefore, NaOH may be more effective for liquefying biomass than H₂SO₄ at 180 °C.

3.3.4 FTIR results of WSP and ASP

The mass corresponding to the reduction of HCCS over the hydrothermal carbonization process should be included in the water and acetone solutions, as shown in Figure 1. The fractions recovered by water and acetone were called water-soluble products (WSP) and acetone-soluble products (ASP), respectively. We used FTIR to characterize these fractions

Table 1. Effect of temperature or pH on the compositions, elemental content and HHVs of HCCS and residues.

| Entry | Temperature (°C) | PH | Main components ^a (mg) | | | Element content (%) | | | | Heating value |
|-------|---------------------|------|-----------------------------------|---------------|-----------|---------------------|-----|-----|----------------|------------------|
| | | | Cellulose | Hemicellulose | Lignin | C | H | N | O ^b | HHV (MJ/kg) |
| 1 | 25 | HCCS | 24.7±0.2 | 41.8±0.3 | 106.4±0.6 | 51.5 | 4.8 | 0.9 | 42.8 | 20.2 |
| | | 4.0 | 19.3±0.3 | 16.3±0.6 | 83.7±0.7 | 56.1 | 5.1 | 1.1 | 37.7 | 22.3 |
| | | 5.9 | 18.2±0.6 | 16.1±2.0 | 84.7±2.4 | 55.2 | 5.3 | 1.0 | 38.5 | 22.0 |
| 2 | 180 | 7.0 | 19.6±1.2 | 15.0±0.2 | 83.9±0.2 | 56.3 | 5.0 | 1.1 | 37.6 | 22.4 |
| | | 10.0 | 21.9±0.5 | 12.9±0.8 | 82.1±1.0 | 56.8 | 5.1 | 1.1 | 37.0 | 22.7 |
| | | 13.0 | 9.4±1.4 | 7.5±1.7 | 23.7±0.7 | 42.5 | 4.7 | 0.4 | 52.3 | 16.9 |
| 3 | 200 | 5.9 | 20.7±0.7 | 10.3±0.8 | 84.8±0.9 | 58.6 | 5.0 | 1.1 | 35.4 | 23.4 |
| | | 4.0 | 23.6±1.3 | 6.1±0.9 | 83.8±1.0 | 61.3 | 4.5 | 0.9 | 33.3 | 24.5 |
| | | 5.9 | 19.3±0.4 | 7.6±0.2 | 88.6±0.2 | 61.8 | 4.9 | 1.0 | 32.3 | 25.0 |
| 4 | 220 | 7.0 | 19.9±0.8 | 7.1±0.3 | 87.9±0.3 | 61.3 | 4.8 | 0.8 | 33.2 | 24.6 |
| | | 10.0 | 18.7±0.5 | 8.5±1.2 | 82.4±3.5 | 61.0 | 4.5 | 0.8 | 33.7 | 24.3 |
| | | 13.0 | 10.0±0.7 | 0.6±0.1 | 10.6±0.7 | 40.8 | 3.5 | 0.0 | 55.6 | 16.5 |
| 5 | 240 | 5.9 | 15.1±0.1 | 7.9±1.2 | 80.1±1.3 | 63.1 | 4.8 | 0.9 | 31.2 | 25.6 |
| | | 4.0 | 10.1±2.6 | 7.3±0.1 | 78.9±0.1 | 67.2 | 4.4 | 0.7 | 27.8 | 27.4 |
| | | 5.9 | 10.2±0.7 | 7.5±1.3 | 77.6±1.2 | 67.2 | 4.7 | 0.9 | 27.2 | 27.7 |
| 6 | 260 | 7.0 | 8.5±0.8 | 5.9±1.7 | 76.5±1.5 | 68.2 | 4.6 | 0.7 | 26.5 | 28.2 |
| | | 10.0 | 8.1±0.4 | 6.2±1.1 | 80.2±1.0 | 67.7 | 4.6 | 0.7 | 27.0 | 27.9 |
| | | 13.0 | 3.5±0.3 | 0.1±0 | 5.4±0.1 | 38.5 | 9.3 | 0.8 | 51.4 | 15.1 |

a: all the experiments were carry out in triplicate
b: calculated by difference

according to the temperature and pH of the hydrothermal carbonization (Fig. 4). The spectra showed that temperature and pH had no effect on the adsorption bands of WSP and ASP. The main adsorption bands from WSP were quite similar to those of ASP, indicating that WSP and ASP contained similar functional groups. The O–H stretching vibration around 3300 cm^{-1} indicated the presence of phenols and alcohols in WSP and ASP. The O–H stretching vibration of WSP was stronger than that of ASP because phenols, which have lower O–H content than alcohols, were more prevalent in ASP [20]. This peak in ASP became stronger at pH 13.0, probably due to the hydrolysis/decomposition of phenols. The absorption bands between 2840 and 2960 cm^{-1} corresponding to the C–H stretching indicated that hydrocarbon alkyls were one of the products during hydrothermal carbonization. The C=O stretching band at 1740 cm^{-1} indicated the presence of esters, carboxylic acids, ketone, aldehydes and/or phenol compounds in the WSP and ASP. The absorption bands around 1600 and 1510 cm^{-1} related to the mono- and polycyclic and substituted aromatic groups due mainly to the decomposition of lignin. The disappearance of the 1510 cm^{-1} peak in ASP at pH 13.0 suggested that some of the aromatic compounds decomposed at this pH. The absorbance at 1376 cm^{-1} corresponding to the $-\text{CH}_3$ bond and the aromatic C–H in-plane plus C–O in the primary stretching band at around 1050 cm^{-1} indicated the appearance of arone chemicals [21]. We attempted to use GC-MS as another analytic method to identify the compounds present in the WSP and ASP, but neither the WSP nor the ASP could dissolve in the organic solvents. Therefore, the compounds in WSP and ASP could not be identified in this study (data not shown).

3.3.5 Elemental contents and HHVs of residue, WSP and ASP

The elemental content of the residue shown in Table 1 helps to illustrate the decomposition progression of HCCS during hydrothermal carbonization. At pH 5.9 the carbon content of the residue increased from 55.2% to 67.2% with the increase of temperature from 180 to 260 °C, and its oxygen content decreased at the same time (entries 2-6 on Table 1). There was no great change in hydrogen or nitrogen contents. The pH range from 4.0 to 10.0 seemed to have no effect on the carbon and oxygen contents. However, lower carbon content and higher oxygen content were obtained in the residue at pH 13.0. The decrease of residual carbon content at pH 13.0 was due to the lignin content of the HCCS because lignin, having the highest carbon content among the main components of the biomass, hydrolyzed/decomposed at pH 13.0.

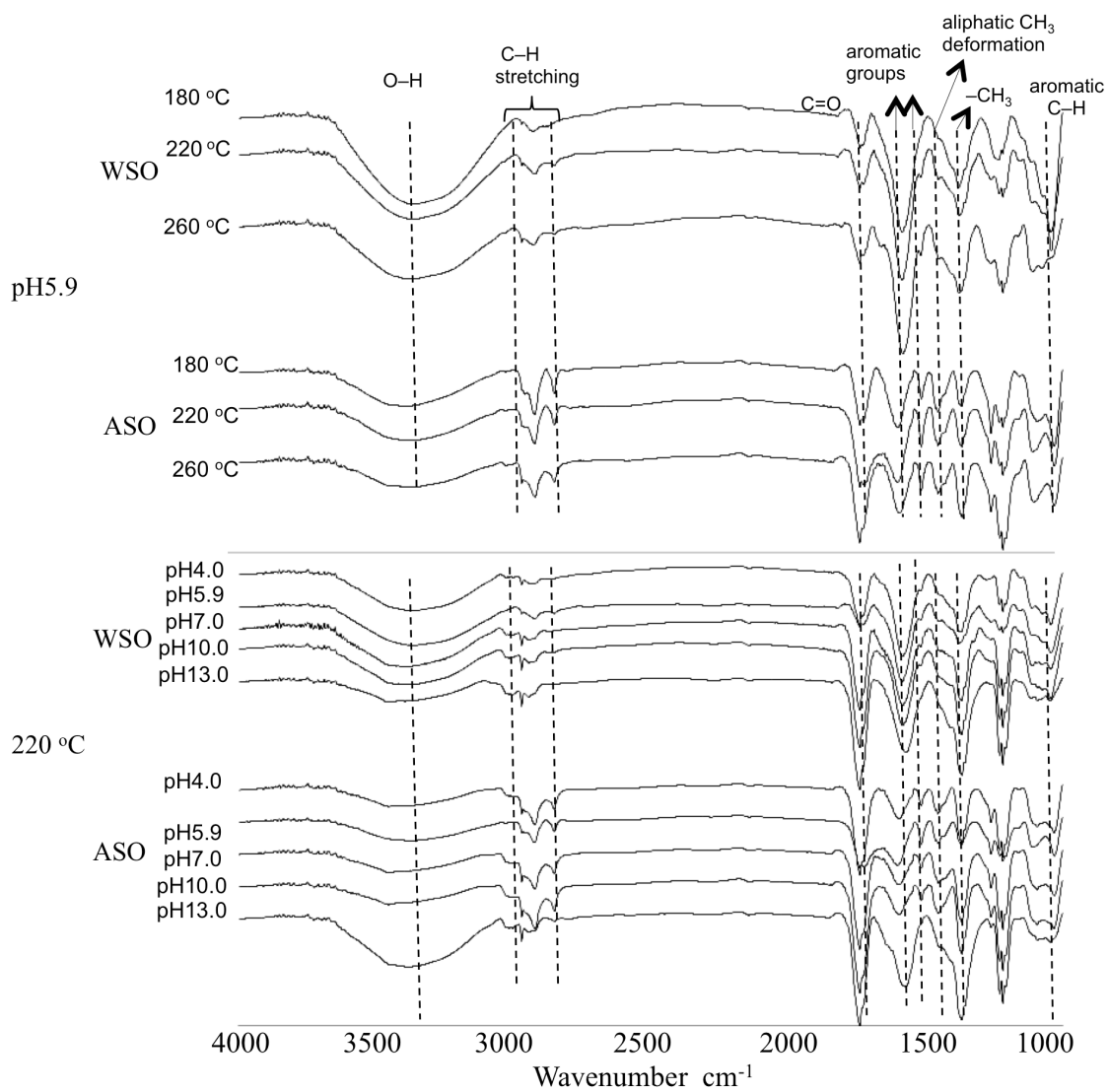


Figure 4. FTIR spectra of WSP and ASP prepared at various temperatures (above) and pHs (below) at 220 °C.

Table 2. Effect of temperature or pH on the elemental contents of WSP and ASP, and HHVs of WSP, ASP.

| Entry | Temperature (°C) | pH | WSP | | | | | Entry | ASP | | | | |
|-------|---------------------|------|----------|----------|----------|-----------------------|----------------|-------|----------|----------|----------|-----------------------|----------------|
| | | | C (%) | H (%) | N (%) | O ^a (%) | HHV (MJ/kg) | | C (%) | H (%) | N (%) | O ^a (%) | HHV (MJ/kg) |
| 7 | 180 | 4.0 | 35.2 | 4.7 | 0.6 | 59.4 | 15.0 | 12 | 53.5 | 6.3 | 0.7 | 39.6 | 21.6 |
| | | 5.9 | 39.5 | 4.3 | 0.6 | 55.7 | 16.1 | | 62.9 | 4.9 | 0.9 | 31.3 | 25.6 |
| | | 7.0 | 33.4 | 5.1 | 0.6 | 60.9 | 14.5 | | 48.0 | 6.3 | 0.6 | 45.2 | 19.1 |
| | | 10.0 | 34.7 | 4.5 | 0.6 | 60.2 | 14.9 | | 51.8 | 5.6 | 0.7 | 42.0 | 20.6 |
| | | 13.0 | 25.6 | 2.7 | 0.6 | 71.1 | 14.6 | | 23.0 | 4.5 | 0.4 | 72.1 | 13.1 |
| 8 | 200 | 5.9 | 34.7 | 4.2 | 1.0 | 60.1 | 15.1 | 13 | 63.7 | 6.0 | 1.0 | 29.4 | 26.9 |
| | | 4.0 | 34.1 | 4.9 | 1.2 | 59.8 | 14.8 | | 59.4 | 6.1 | 1.0 | 33.6 | 24.5 |
| | | 5.9 | 33.7 | 4.2 | 1.2 | 60.9 | 14.9 | | 61.9 | 5.1 | 1.2 | 31.9 | 25.2 |
| | | 7.0 | 32.1 | 5.2 | 1.1 | 61.6 | 14.2 | | 56.6 | 5.8 | 1.0 | 36.6 | 23.0 |
| | | 10.0 | 32.1 | 5.0 | 1.1 | 61.8 | 14.3 | | 60.7 | 6.3 | 1.0 | 31.9 | 25.5 |
| 9 | 220 | 13.0 | 31.4 | 3.1 | 0.5 | 65.1 | 14.9 | 14 | 23.1 | 5.4 | 0.4 | 71.1 | 12.4 |
| | | 5.9 | 32.4 | 4.0 | 1.5 | 62.2 | 15.1 | | 63.0 | 5.3 | 1.2 | 30.5 | 26.0 |
| | | 4.0 | 32.1 | 5.4 | 1.5 | 61.1 | 14.2 | | 64.4 | 6.0 | 1.1 | 28.5 | 27.3 |
| | | 5.9 | 34.2 | 4.3 | 1.6 | 59.9 | 15.0 | | 63.5 | 5.2 | 1.2 | 30.1 | 26.2 |
| | | 7.0 | 32.5 | 5.0 | 1.5 | 61.0 | 14.4 | | 63.5 | 5.7 | 1.1 | 29.7 | 26.6 |
| 11 | 260 | 10.0 | 36.3 | 5.4 | 1.6 | 56.7 | 15.2 | 16 | 64.0 | 5.9 | 1.3 | 28.9 | 27.0 |
| | | 13.0 | 26.2 | 3.6 | 0.4 | 69.8 | 14.0 | | 24.6 | 6.2 | 0.4 | 68.8 | 12.1 |

a: calculated by difference

The elemental contents of WSP and ASP are shown in Table 2. The temperature and pH seemed to have no significant effect on the elemental content of WSP. The elemental content of ASP showed no dramatic change at the pH range of 4.0-10.0 at various temperatures, and lower carbon content was obtained at pH 13.0. The carbon content of ASP was higher than that of WSP in the same conditions except at pH 13.0. This was consistent with the results obtained by direct liquefaction of woody biomass at 340 °C for 30 min [20]. The main components of the ASP in that study were phenolic compounds and derivatives, long-chain carboxylic acids/esters and hydrocarbons, and these compositions had higher carbon content than the carbohydrates, acetic acids, pyran derivatives and aldehydes in the WSP.

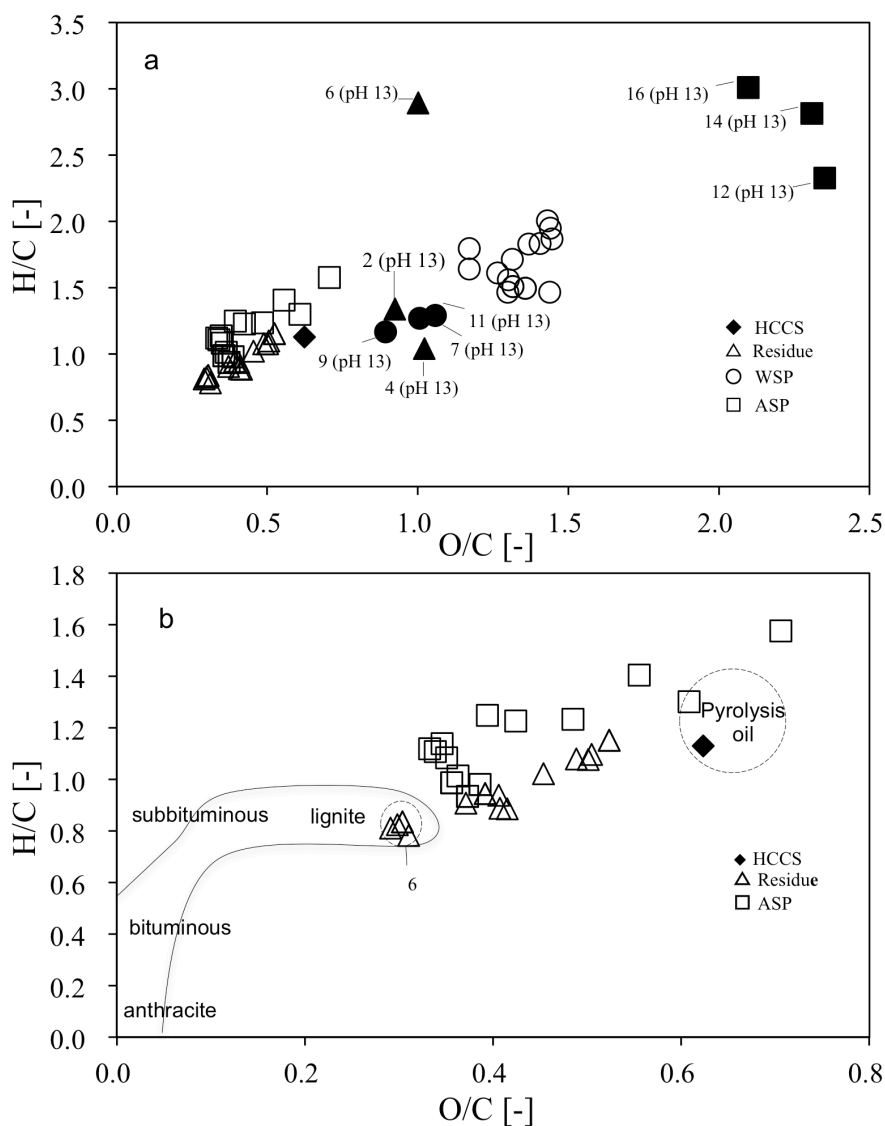


Figure 5. Van Krevelen diagram of (a) HCCS, residue, WSP and ASP prepared at 180-260 °C, pH 4.0-13.0 and (b) HCCS, residue and ASP prepared at 180-260 °C, pH 4.0-10.0 as well as areas of pyrolysis oils (dry basis) and coal band. The area of pyrolysis oils was referred from references 22 and 23.

Next, in order to examine the fuel properties of the residue, WSP and ASP, the H/C vs. O/C values of residue, WSP, ASP and flash pyrolysis oil (dry basis) [22, 23] were plotted on a van Krevelen diagram as shown in Fig. 5. From Fig. 5a, it is clearly seen that the residue and ASP had lower O/C and H/C values than those of WSP prepared under the same conditions except for the case of pH 13.0 (black keys in Fig. 5a), where the residue and ASP had higher O/C values than those prepared at other conditions. This result indicated that the residue and APS prepared at pH 13.0 had lower fuel properties than those prepared at other conditions, because a fuel with higher H/C and O/C ratios would lead to more energy loss, and more smoke and water vapor generation during the combustion process [8]. Therefore, it was not appropriate for hydrothermal carbonization of HCCS at high pH for bio-fuel production.

Figure 5b shows the H/C vs. O/C values of residue and ASP at 180 to 260 °C for the pH range of 4.0-10.0. Compared with HCCS, residues with lower H/C and O/C values were obtained through hydrothermal carbonization. The H/C and O/C values of residue moved towards to those of commercial coals with the increase in the hydrothermal carbonization temperature, and the H/C and O/C values of residues prepared at 260 °C (entry 6) could be comparable with those of lignite. The O/C and H/C values of ASP could also be comparable with those of pyrolysis oil.

Table 3. Comparison of HHVs of the present residues with those of some commercial coals and torrefied biomass.

| Biomass/commercial coal | HHV (MJ/kg) | Reference |
|--|-------------|------------|
| Residue (entries 2~6, pH 5.9) | 22.0–27.7 | This study |
| Northumberland No.81/2 Sem. Anth. Coal | 24.7 | 24 |
| Ggerman Braunkohole lignite | 25.1 | 24 |
| Jnanjra Bonbahal Seam Coal — R – VII | 24.1 | 24 |
| Green Ind. NO. 3–hvBb coal | 27.4 | 24 |
| Dry torrefied loblolly pine (300 °C, 80 min) | 23.5 | 19 |
| Dry torrefied loblolly pine (300 °C, 30 min) | 23.1 | 26 |
| Dry torrefied loblolly pine (250 °C, 8 h) | 24.8 | 26 |

The HHVs of residue, WSP and ASP are an important index to evaluate the performance of hydrothermal carbonization, we thus calculated the HHVs of residue, WSP and ASP from their element contents in this study. As shown on Table 1, the HHV of HCCS was 20.2 MJ/kg and the HHV of residue prepared at pH 5.9 increased with the increase in the hydrothermal

carbonization temperature. The increase in HHV was due to the decrease of low-energy chemical bonds (i.e. H–C and O–C) and the increase in a high-energy chemical bond (C–C) during hydrothermal carbonization [8]. The HHVs of these residues could be comparable with those of some commercial coals shown on Table 3, such as Northumberland No.81/2 Sem. Anth. Coal (24.7 MJ/kg), Jhanjra Bonbahal Seam Coal–R–VII (24.1 MJ/kg) and German Braunkohle lignite (25.1 MJ/kg). The HHV of residue prepared at 260 °C and pH 5.9 (27.7 MJ/kg) that exhibited an elevation rate of 37% compared to that of the original HCCS could even be comparable with that of Green Ind. NO. 3–hvBb coal (27.4 MJ/kg) [24]. This elevation rate of HHV was much higher than those for 15-min treatments of willow (17%) and beech (20%) at the mild pyrolysis temperatures of 270 and 280 °C, respectively [25]. It was also much higher than those of dry torrefied loblolly pine processed for 8 h at 250 °C, and 30 and 80 min at 300 °C, respectively, which had similar elemental content and HHV to that of HCCS (Table 3) [19, 26]. Therefore, it was considered that hydrothermal carbonization is better at elevating HHV than dry torrefaction. The pH range from 4.0 to 10.0 seemed to have no effect on the HHV of the residue because the composition and elemental content of the residue was nearly the same at this range; lower HHV was obtained at pH 13.0, which was due to the hydrolysis/decomposition of lignin as described above.

Changing the temperature and pH seemed to have no dramatic effect on the HHV of WSP. The HHVs of WSP were between 14.0 and 16.1 MJ/kg, lower than those obtained from the liquefaction of woody biomass at 340 °C for 30 min [20]. The temperature also had no effect on the HHV of ASP and it seemed that changing the pH from 4.0 to 10.0 above 200 °C led to no great change in the HHV of ASP. It was interesting that a lower HHV of ASP was obtained at pH 13.0, under which conditions lignin was greatly hydrolyzed/decomposed. This could be due to the change of carbon content of ASP because the carbon content dominated the HHV as shown in equation (6). The HHVs of WSP and ASP were much lower than those of heavy fuel oil, aviation gasoline and diesel oil [24]. Therefore, the HHVs of WSP and ASP should be improved before application by the means of lowering oxygen content.

From all of the results described above, we considered that hydrothermal carbonization could effectively upgrade the fuel properties of biomass, and the optimal conditions for 10-min hydrothermal carbonization of HCCS are 260 °C, pH 5.9. A pretreatment was needed before application of WPS and APS as biofuels. The residue, WSP and ASP prepared at pH 13.0 were not appropriate for application as bio-fuels.

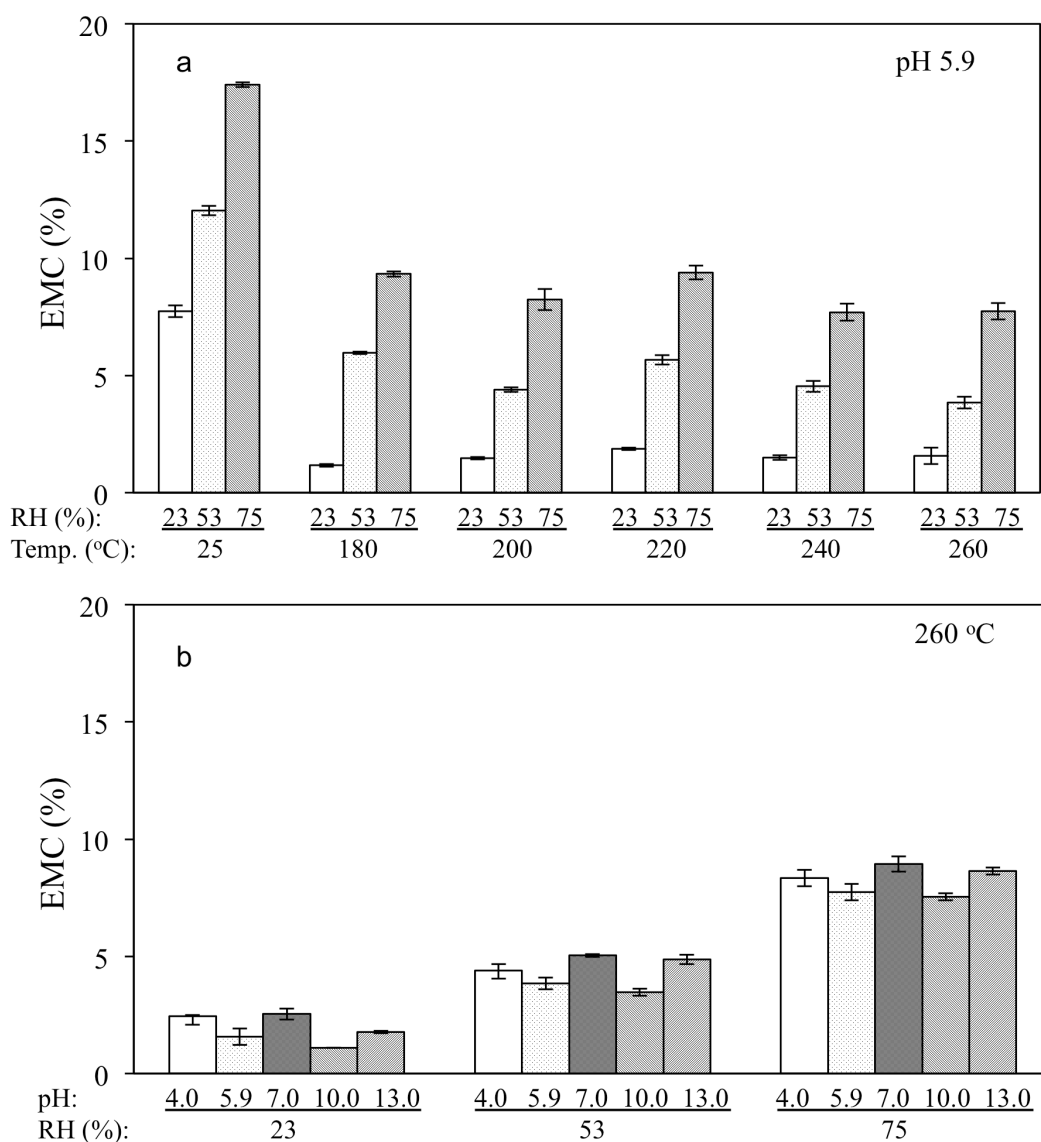


Figure 6. Equilibrium moisture content (EMC) of residue prepared at (a) various temperatures at pH 5.9 and (b) various pHs at 260 °C (n=3).

3.3.6 Equilibrium moisture contents of HCCS and residue

The moisture content strongly affected the biodegradation of biomass. The relative humidity of the surrounding air was one of the parameters that affected the EMC [27].

Figure 6a shows the effect of hydrothermal carbonization temperature on the EMC of the residue. The higher hydrothermal carbonization temperature made the residue more hydrophobic and the EMC was elevated at higher RH content. As shown in Table 1, the weights of cellulose, hemicellulose and lignin in the residue were reduced after hydrothermal carbonization. However, more cellulose and hemicellulose were hydrolyzed/decomposed than lignin, and hence the lignin content in the residue increased with the increase of hydrothermal carbonization temperature. Therefore, the EMC reduction at higher hydrothermal

carbonization temperatures was due to the increase of lignin content in the residue as lignin is more hydrophobic than cellulose or hemicellulose.

Figure 6b shows the relationship between EMC and the residue prepared at various pHs. There was no significant change of the EMC at the same RH. The constant EMC of the residue (pH 4.0-10.0) was due to its fairly constant composition since the composition of biomass affects the EMC of the biomass [27]. Although the composition of the residue changed at pH 13.0, the EMC of the residue was similar to those obtained at pH 4.0 to 10.0, probably due to the high ash content in the residue.

Therefore, hydrothermal carbonization was shown to be an effective process to improve the hydrophobicity of biomass; also, high ash content in the residue could affect the hydrophobicity of the residue.

3.4 Conclusion

The residue, WSP and ASP produced from hydrothermal carbonization of HCCS at various temperatures and pHs were characterized in this study. The residue yield was decreased when the treatment temperature increased from 180 to 260 °C while the total soluble products yield was almost the same. Changes in pH within the range from 4.0 to 10.0 had no significant effect on residue and total soluble products yields. However, a lower residue yield and higher total soluble products yield were obtained at pH 13.0. At 260 °C and pH 5.9, more hemicellulose (82.1%) was hydrolyzed/decomposed than cellulose (58.3%) or lignin (27.1%), and it was confirmed that the reactivity order of the components of HCCS was hemicellulose > cellulose > lignin. The final pH value of WSP was lower than initial pH value and it decreased with increase in the hydrothermal carbonization temperature. Changing the initial pH from 4.0 to 10.0 had no dramatic effect on the final pH value of WSP. However, the final pH value increased to around 7.3 when the initial pH elevated to 13.0, which meant that the generated carboxylic acids were all neutralized by NaOH. The HHV ranges of residue were from 22.0 to 28.2 MJ/kg for 10-min treatment in the temperature range of 180-260 °C and pH range of 4.0 to 10.0, and the HHV of residue decreased at pH 13.0. The HHVs of these residues were comparable with those of several commercial coals. The WSP and APS had lower HHVs than those of heavy fuel oil and diesel oil and they needed a pretreatment to increase their HHVs before application. The residue became more hydrophobic at higher treatment temperatures, indicating that hydrothermal carbonization could efficiently elevate the hydrophobicity of the biomass.

References

- [1] Kang, S. M.; Li, X. L.; Fan, J.; Chang, J., Characterization of hydrochars produced by hydrothermal carbonization of lignin, cellulose, d-xylose, and wood meal. *Ind. Eng. Chem. Res.* 2012, *51*, 9023-9031.
- [2] Krushna, P. S.; Kaustubha, M., Thermal and catalytic pyrolysis of Karanja seed to produce liquid fuel. *Fuel* 2014, *115*, 434-442.
- [3] Hanaoka, T.; Hiasa, S.; Edashige, Y., Syngas production by CO₂/O₂ gasification of aquatic biomass. *Fuel Proc. Technol.* 2013, *116*, 9-15.
- [4] Kang, S. M.; Li, X. L.; Fan, J.; Chang, J., Hydrothermal conversion of lignin: A reviewer. *Renew. Sust. Energ. Rev.* 2013, *27*, 546-558.
- [5] Chen, W. H.; Ye, S. C.; Sheen, H. K., Hydrothermal carbonization of sugarcane bagasse via wet torrefaction in association with microwave heating. *Bioresour. Technol.* 2012, *118*, 195-203.
- [6] Yan, W.; Hoekman, K. S.; Broch, A.; Coronella, C. J., Effect of hydrothermal carbonization reaction parameters on the properties of hydrochar and pellets. *Environ. Prog. Sustain. Energy* 2014, *33*, 676-680.
- [7] Reza, M. T.; Uddin, M. H.; Lynam, J. G.; Hoekman, S. K.; Coronella, C. J., Hydrothermal carbonization of loblolly pine: reaction chemistry and water balance. *Biomass Conv. Bioref.* 2014, *4*, 311-321.
- [8] Liu, Z.; Quek, A.; Hoekman, S. K.; Balasubramanian, R., Production of solid biochar fuel from waste biomass by hydrothermal carbonization. *Fuel* 2013, *103*, 943-949.
- [9] Libra, J. A.; Ro, K. S.; Kammann, C.; Funke, A.; Berge, N. D.; Neubauer, Y.; Titirici, M. M.; Fhüner, C.; Bens, O.; Kern, J.; Emmerich, K. H., Hydrothermal carbonization of biomass residuals: a comparative review of the chemistry, process and applications of wet and dry pyrolysis. *Biofuels* 2011, *2*, 89-24.
- [10] Funke, A.; Ziegler, F., Hydrothermal carbonization of biomass: a summary and discussion of chemical mechanisms for process engineering. *Biofuels Bioprod. Bioref.* 2010, 160-177.
- [11] Yu, Y.; Lou, X.; Wu, H. W., Some recent advances in hydrolysis of biomass in hot-compressed water and its comparisons with other hydrolysis methods. *Energy Fuels* 2007, *20*, 46-60.
- [12] Peterson A. A.; Vogel, F.; Lachance, R. P.; Fröling, M.; Antal, Jr. A. J.; Tester, J. W., Thermochemical biofuel production in hydrothermal media: A review of sub- and supercritical water technologies. *Energy Environ. Sci.* 2008, *1*, 32-65.

- [13] Lu, X. W.; Pellechia, P. J.; Flora, J. R. V.; Berge, N. D., Influence of reaction time and temperature on product formation and characteristics associated with the hydrothermal carbonization of cellulose. *Bioresour. Technol.* 2013, *138*, 180-190.
- [14] Pińkowska, H.; Wolak, P.; Złocińska, A., Hydrothermal decomposition of xylan as a model substance for plant biomass waste-Hydrothermolysis in subcritical water. *Biomass Bioenerg.* 2011, *35*, 3902-3912.
- [15] Marion, C.; Anne, L. S.; Dominique, D.; Jean-Michel, L.; Frédérique, H. P.; François, C.; Cyril, A., Thermogravimetric analysis as a new method to determine the lignocellulosic composition of biomass. *Biomass Bioenerg.* 2012, *35*, 298-307.
- [16] Yokoyama, T.; Kadla, J. F.; Chang, H. M., Microanalytical method for the characterization of fiber components and morphology of woody plants. *J. Agri. Food Chem.* 2002, *50*, 1040-1044.
- [17] Friedl, A.; Padouvas, E.; Rotter, H.; Varmuza, K., Prediction of heating values of biomass fuel from elemental composition. *Anal. Chim. Acta* 2005, *554*, 191-198.
- [18] Lynam, J. G.; Coronella, C. J.; Yan, W.; Reza, M. T.; Vasquez, V. R., Acetic acid and lithium chloride effects on hydrothermal carbonization of lignocellulosic biomass. *Bioresour. Technol.* 2011, *102*, 6192-6199.
- [19] Yan, W.; Hastings, J. T.; Acharjee, T. C.; Coronella, C. J.; Vasquez, V. R., Mass and energy balances of wet torrefaction of lignocellulosic biomass. *Energy Fuels* 2010, *24*, 4738-4742.
- [20] Xu, C. B.; Lad, N. D., Production of heavy oils with high caloric values by direct liquefaction of woody biomass in sub/near-critical water. *Energy Fuels* 2008, *22*, 635-642.
- [21] Jiang, X. X.; Ellis, N.; Zhong, Z. P., Fuel properties of bio-oil/bio-diesel mixture characterized by TG, FTIR and ¹H NMR. *Korean J. Chem. Eng.* 2011, *28*, 133-137.
- [22] Fogassy, G.; Thegarid, N.; Toussaint, G.; Veen, A. C.; Schuurman, Y.; Mirodatos, C., Biomass derived feedstock co-processing with vacuum gas oil for second-generation fuel production in FCC units. *Appl. Catal. B-Environ.* 2010, *96*, 476-485.
- [23] Venderbosch, R. H.; Ardiyanti, A. R.; Wildschut, J.; Oasmaa, A.; Heeres, H. J., Stabilization of biomass-derived pyrolysis oils. *J. Chem. Technol. Biotechnol.* 2010, *85*, 674-686.
- [24] Channiwala, S. A.; Parikh, P. P., A unified correlation for estimating HHV of solid, liquid and gaseous fuels. *Fuel* 2001, *81*, 1051-1063.
- [25] Prins, M. J.; Ptasinski, K. J.; Janssen, F. J. J. G., Torrefaction of wood Part 2. Analysis of products. *J. Anal. Appl. Pyrol.* 2006, *77*, 35-40.

[26] Ben, B. X.; Ragauskas, A. J., Torrefaction of loblolly pine. *Green Chem.* 2012, *14*, 72-76.

[27] Acharjee, T. C.; Coronella, T. C.; Vasquez, V. R., Effect of thermal pretreatment on equilibrium moisture content of lignocellulosic biomass. *Bioresour. Technol.* 2011,*102*, 4849-4854.